A Doctor Thesis

博士論文

Integrated Optimization of Guidance Navigation and Control Strategy for Deep Space Exploration via Stochastic Trajectory Optimization Approach

(確率的軌道最適化を用いた深宇宙探査における
航法誘導制御方策の統合的最適化)

by

Kota Kakihara

柿原浩太

Submitted to

the Graduate School of Engineering, the University of Tokyo

in Partial Fulfillment of the Requirements

for the Degree of Doctor of Philosophy

in Aeronautics and Astronautics

Thesis Supervisor: Ryu Funase　船瀬龍

Associate Professor of Aeronautics and Astronautics

ABSTRACT

In deep space exploration with micro/nano-spacecraft, the relatively high cost of trajectory correction and orbit determination is an important issue. In this study, a method is proposed to optimize the scheduling of the trajectory correction and the orbit determination in an integrated manner to minimize the amount of control required for trajectory correction. The problem is formulated by using the stochastic trajectory optimization technique. The stochastic trajectory optimization problem is converted into a deterministic optimization problem by parameterizing the probability distribution, and the optimization is solved numerically. The coupling effect between the true and estimated values of the state is considered, and both of them are defined together as augmented state values. The probability distribution of the augmented state is parameterized, and the propagation of the parameters is formulated. It is shown that the parameters depend on the trajectory correction time and the orbit determination time. The objective function and constraints are evaluated from those parameters, and the trajectory correction time and orbit determination time are optimized. The errors of uncertainty propagation methods were evaluated in the dynamics of two-body and circular restricted three-body problems. The optimization problem was solved for the Hohmann transfer trajectory in the two-body problem and the nominal trajectory of the micro-deep space probe PROCYON in a more realistic problem. These numerical simulations show the validity of the proposed method.

Acknowledgements

I am deeply grateful to the many people who have supported me in the pursuit of this research.

I would like to express my sincere gratitude to my supervisor, Professor Ryu Funase, for his advice in meetings, lectures, and other places during the course of my research. He gave me so much of his precious time as a supervisor in our university and as a project manager of EQUULEUS mission. Without his help, I would not have been able to complete my research.

I would like to express my sincere gratitude to Professor Shinichi Nakasuka for his many ideas in the laboratory lectures and meetings. He not only gave me advice on my research, but also taught me how to live as a human being.

I owe my deepest gratitude to Professor Naoya Ozaki. He gave me a lot of advice on my research, how to write and proofread my papers and thesis. He gave me a lot of insight into the motivation behind this research. Thank you very much.

I am grateful to my mates, Nobuhiro Funabiki, Ryohei Takahashi, Akihiro Ishikawa, Kanta Yanagida, and Shuhei Matsushita, in our laboratory for the many conversations and the friendly competition. I wouldn't have made it through the doctoral program without them.

I want to thank all staff and members of our laboratory for taking time out of their busy nano-satellite projects to allow me to concentrate on my research. I also want to thank Takuya Chikazawa for the heavy discussion on our research.

I would like to offer my special thanks to all members of ArkEdge Space Inc. for their support of my research.

I owe a very important debt to my family for taking care of me while my student

life. Thank you for raising me until now.

Finally, I would like to show my special appreciation to Nao Tomori and Momo Asakura for their emotional support.

This work was supported by JSPS KAKENHI Grant Number 19J22430.

Contents

List of Figures

List of Tables

Nomenclature

$\boldsymbol{\mu}$	mean of Gaussian distribution
$\boldsymbol{\theta}$	parameters of probability distribution
$\boldsymbol{\varepsilon}$	observation noise vector
$\boldsymbol{C}$	constraint function
$\boldsymbol{F}(\cdot)$	dynamics propagation function
$\boldsymbol{G}(\cdot)$	observation function
$\boldsymbol{R}$	position vector
$\boldsymbol{r}$	linearized position vector
$\boldsymbol{U}$	control vector
$\boldsymbol{u}$	linearized control vector
$\boldsymbol{V}$	velocity vector
$\boldsymbol{X}$	true state vector
$\boldsymbol{x}$	linearized true state vector
$\boldsymbol{Y}$	observation vector
$\boldsymbol{y}$	linearized observation vector
$\boldsymbol{Z}$	augmented state vector

$\delta \boldsymbol{U}$ control error vector

$\delta \boldsymbol{w}$ dynamics noise vector

Γ coefficient from dynamics noise to state vector

$\mathbb{E}[\cdot]$ Expected value

$\mathbb{V}[\cdot]$ Variance

μ gravitational parameter

Φ state transition matrix

Σ covariance matrix of Gaussian distribution

$\widehat{\boldsymbol{X}}$ estimated state vector

$\widehat{\boldsymbol{x}}$ linearized estimated state vector

B coefficient from control vector to state vecor

I identity matrix

i index number

$M(\cdot)$ control law function

N total number

O zero matrix

P state covariance matrix for Kalman Filter

$P(\cdot)$ probability function

$p(\cdot)$ probability distribution function

Q covariance matrix of dynamics error

R covariance matrix of observation error

S covariance matrix of control error

t time

Superscripts

$-$ just before control or orbit determination

$*$ related to reference or nominal trajectory

T transpose of matrix

Subscripts

0 related to initial time

f related to final time

i related to ith time

k related to kth trajectory correction or its time

l related to lth orbit determination or its time

$l(k)$ related to orbit determination just before kth trajectory correction

Chapter 1

Introduction

That's one small step for [a] man,

one giant leap for mankind.

Neil Armstrong

1.1 Background

With the development of micro/nano-satellite technology, deep space exploration missions using micro/nano-spacecraft have been proposed in recent years. In 2014, the world's first micro-deep space probe, PRoximate Object Close flYby with Optical Navigation (PROCYON), was launched with Hayabusa-2, demonstrating deep space exploration with micro-deep space probes.[1] In 2018, Mars Cube One (MarCO), which is the world's first deep-space CubeSat, was launched with Insight.[2] The Artemis program plans to launch as many as 10 CubeSats into deep space.[3]-[9] In the future, deep space exploration using micro deep space probes is expected to be carried out at low cost and high frequency.

There are two important issues in the trajectory problem of micro deep space missions (of course, these issues are also important for some deep space missions using large spacecraft): the first is the high importance of trajectory correction maneuvers (TCMs), and the second is the cost of orbit determination.

As for the first issue, the portion of TCMs in ΔV budget is relatively large for micro deep space missions. Nominal trajectories requiring little control and long time

of flight are often chosen such as low-energy transfer orbits for micro deep space missions because micro spacecraft do not have high orbit control capability. In addition, this is because micro/nano-spacecraft are often launched with large spacecraft to reduce launch costs and indirect trajectories are often chosen to reach the destination. For such trajectories, the ratio of fuel required for trajectory correction is relatively high compared to the fuel required for the nominal orbit control, and reduction of fuel for TCMs is significant.

The second issue is related to the cost of operation. In order to guide the trajectory of a spacecraft with high accuracy, it is necessary to improve the accuracy of orbit determination. In order to improve the accuracy of orbit determination, it is required to use a high-precision orbit determination method such as Delta Differential One-way Range (DDOR), or to increase the number of orbit determination. However, using a highly accurate orbit determination method or increasing the number of orbit determination will lead to an increase in the cost of operation. Therefore, with a fixed number of orbit determination, it is necessary to increase the number of orbit determination times when high-precision orbit determination is required and to decrease the number instead when it is not required.

Furthermore, the current technology used for deep space orbit navigation is based on radio navigation, which is heavily dependent on deep space ground stations such as Deep Space Network and Misasa Deep Space Station. The cost of using deep-space ground stations is high and the same for micro/nano-spacecraft as for large spacecraft, and thus operating them in the same way as large spacecraft would be a major impediment to cost reduction. Normally, the operation timing of deep space probes is heuristically determined, and few studies have focused on the optimization of orbit determination operations. In order to reduce the cost of navigation, unnecessary operations should be avoided and orbit determination operations should be performed at efficient times.

In addition, these two problems are deeply related. If the accuracy of the orbit determination is insufficient, the guidance accuracy of the TCM will deteriorate, and extra TCM must be performed to correct it. In order to minimize the fuel used for

TCM while satisfying the required guidance accuracy, it is necessary not only to optimize the TCM but also to optimize the orbit determination strategy.

In this study, an integrated optimization method for TCM and orbit determination is proposed in order to minimize the fuel required for TCM while maintaining the required guidance accuracy. The optimization method is based on the stochastic trajectory optimization technique, which has attracted much attention in recent years, and takes into account the probability distribution of state quantities. In order to optimize the orbit determination, a novel stochastic trajectory optimization framework that can take into account the orbit determination error, which is not often considered in the field of stochastic trajectory optimization, is also proposed. The concept of the method used in this study can be applied not only to the integrated optimization of TCM and orbit determination, but also to the integrated trajectory optimization of guidance, navigation, and control, including nominal trajectory design.

1.2 Related Work

1.2.1 Related Work of Trajectory Correction Optimization

As for the optimization of trajectory correction, research that optimizes the time of TCM has been done for a long time. Breakwell (1960) and Breakwell (1962) proposed a method for calculating the optimal trajectory correction maneuver time analytically called the Spacing Rule. [10][11] Kawaguchi and Matsuo (1996) proposed the Extended Spacing Rule, which is an extension of the Breakwell's Spacing Rule, and it showed that there are regions where Breakwell's method can be applied and regions where a new rule is required.[12] By using Spacing Rule, the optimal TCM timings are easily computed by analytical equations. In these studies, however, various approximations are used to derive analytical solutions, and the solution of them is different from the true optimal solution.

Serban, et al. (2002) and Gomez, Marcote, and Masdemont (2005) developed optimal TCM for transfer trajectories from Earth to libration orbits.[13][14] They used the trajectory optimization approach for designing TCMs. However, they consider

initial insertion error only and cannot handle other errors like orbit determination error and dynamical disturbances.

Formulations in the previous studies are not modern stochastic trajectory optimization, and they cannot handle numerical optimization that takes into account probabilistic distributions of uncertainties and constraints about state quantity. Kakihara et al. (2020) proposed a method to numerically optimize the trajectory correction time, but the formulation regarding the orbit determination error is not yet complete.[15]

1.2.2 Related Work of Orbit Determination Optimization

Not much research has been done on the optimization of orbit determination, and it is a field that has only begun to be studied with the advent of the micro/nano-satellite era. Gentile et al. (2019) proposed a method to optimize the orbit determination method and timing using the genetic algorithm to solve this problem. [16] However, in the previous study, only the optimization of orbit determination is considered, and it is not the optimization in conjunction with trajectory control.

1.2.3 Related Work of Stochastic Trajectory Optimization

In recent years, the study of stochastic trajectory optimization considering uncertainty has attracted much attention.[18]-[23] In stochastic trajectory optimization, unlike conventional deterministic trajectory design, uncertainties are taken into account like orbit insertion error, dynamics disturbances, and orbit determination error. The method of stochastic trajectory optimization can be used to efficiently design robust trajectories even in such uncertain situations. The state and control quantities of the trajectory are treated as random variables, and their probability distributions and means are used as objective functions and constraints for the optimization. These problems can be converted into deterministic optimization problems by parameterizing the probability distribution and solved numerically.

Ozaki, Campagnola, and Funase (2020) proposes robust trajectory optimization in non-linear system using stochastic trajectory optimization theory.[18] The constrained

stochastic trajectory optimization problem is converted into the deterministic trajectory optimization problem and solved by common trajectory optimization methods like Differential Dynamic Programming. Oguri and McMahon (2021) and Ridderhof, Pilipovsky, and Tsiotras (2020) also propose methods to design robust guidance strategies under uncertainty.[19][20][21] In these researches, the problems are formulated by the stochastic optimal control approach with chance constraints and solved by convex optimization. However, all of the researches do not consider orbit determination error and cannot handle it adequately.

Zavoli and Federici (2021) proposes a robust trajectory design method using reinforcement learning and considers orbit determination error.[22] In the study, however, the formulation of uncertainties is simplified and the applicability of that formulation is limited.

Greco, Campagnola, and Vasile (2020) introduces belief space into stochastic trajectory optimization.[23] Belief space is a posterior probability of state vector and represents orbit determination uncertainty. The method in the research can handle orbit determination error adequately, but it requires the Monte Carlo simulations to express belief space and much computational cost.

1.3 Proposed Method

In this study, the problem of optimizing the trajectory correction is extended to the problem of optimizing the orbit determination as well. There has been no such study that has taken both of these factors into account in optimization, and solving the problem is the novelty of this research.

The problem is formulated as a stochastic trajectory optimization problem, where the expected value of ΔV required for TCM and the guidance accuracy at the final time are expressed as a function of TCM time and orbit determination time. Orbit insertion error, dynamics error, control error, and orbit determination error are considered as uncertainties. To handle the orbit determination error, both the true and estimated values of the state quantities are considered and treated as augmented state quantities.

The probability distributions of the state and control quantities are parameterized, and the parameters of the state and control at any time can be calculated from the initial values of them, the parameters of the uncertainties, the TCM time, and the orbit determination time. The objective function and constraints are calculated from the parameters of the probability distribution at each time, and the relationship with the TCM time and orbit determination time is expressed. The formulated optimization problem is optimized numerically using mathematical programming techniques.

Chapter 2

Optimization of Trajectory Correction Maneuver

Then promise me. Swear you'll come back. We will meet again. I know it.

Nao Tomori (Charlotte)

In deep space exploration, the trajectory of a spacecraft is planned before launch. After launch, however, the actual orbit deviates from the nominal trajectory due to orbit injection errors, orbit control errors, and external disturbances. Trajectory correction maneuver (TCM) is often performed to correct this deviation and return the trajectory to the nominal trajectory.

The size of the control required for TCM is determined by the sensitivity of the control to the orbital state and the degree of deviation from the desired trajectory. The sensitivity of the control depends on the nature of the dynamics itself as a function of time. The deviation from the desired trajectory is a value that can be controlled in stochastic trajectory design, but it also depends on the strategy of TCM. Therefore, by optimizing the TCM strategy, it is possible to minimize the fuel required for TCM.

In this chapter, TCM is formulated, the factors that affect its magnitude are discussed, and a quantitative discussion on the optimization of the TCM is provided.

2.1 Formulation of Trajectory Correction Maneuver and Guidance Accuracy

In this study, the Fixed Time-of-Arrival (FTA) Guidance is discussed as a method of TCM, which is controlled to aim at the nominal position at a fixed final time.[11]

$$B\boldsymbol{U}_k = \boldsymbol{F}_{k,f}\left(\boldsymbol{X}_f^* - B\delta\boldsymbol{V}_f\right) - \widehat{\boldsymbol{X}_k^-}. \tag{2.1}$$

Linearizing this around the nominal trajectory leads to the following equation

$$\boldsymbol{u}_k = -\Phi_{rv,f,k}^{-1}\Phi_{rr,f,k}\widehat{\boldsymbol{r}_k^-} - \widehat{\boldsymbol{v}_k^-} \tag{2.2}$$

$$= -\begin{bmatrix} \Phi_{rv,f,k}^{-1}\Phi_{rr,f,k} & I \end{bmatrix}\widehat{\boldsymbol{x}_k^-} \tag{2.3}$$

$$\Phi_{f,k} = \begin{bmatrix} \Phi_{rr,f,k} & \Phi_{rv,f,k} \\ \Phi_{vr,f,k} & \Phi_{vv,f,k} \end{bmatrix}. \tag{2.4}$$

Therefore, it is the sensitivity of the control, $\begin{bmatrix} \Phi_{rv,f,k}^{-1}\Phi_{rr,f,k} & I \end{bmatrix}$, and the deviation from the nominal trajectory, $\widehat{\boldsymbol{x}_k^-}$, that affect the magnitude of the TCM. The amount of control can be reduced if TCM is performed at a timing with large control sensitivity or if the deviation of the trajectory at the TCM time can be reduced.

In addition, if the true state after TCM is propagated until the final time,

$$\boldsymbol{x}_f = \Phi_{f,k}\left(\boldsymbol{x}_k^- + B\boldsymbol{u}_k + B\delta u_k\right) + \Gamma\delta\boldsymbol{w}_{f,k} \tag{2.5}$$

$$= \Phi_{f,k}\left((\boldsymbol{x}_k^- - \widehat{\boldsymbol{x}_k^-}) + (\widehat{\boldsymbol{x}_k^-} + B\boldsymbol{u}_k) + B\delta u_k\right) + \Gamma\delta\boldsymbol{w}_{f,k} \tag{2.6}$$

$$= \Phi_{f,k}\left((\boldsymbol{x}_k^- - \widehat{\boldsymbol{x}_k^-}) + B\delta u_k\right) + \Gamma\delta\boldsymbol{w}_{f,k} + \begin{bmatrix} O \\ \left(\Phi_{vr,f,k} - \Phi_{vv,f,k}\Phi_{rv,f,k}^{-1}\Phi_{rr,f,k}\right)\widehat{\boldsymbol{r}_k^-} \end{bmatrix}. \tag{2.7}$$

Therefore, it is the sensitivity of the dynamics, $\Phi_{f,k}$, the orbit determination error at the TCM time, $\boldsymbol{x}_k^- - \widehat{\boldsymbol{x}_k^-}$, the control error, $B\delta u_k$, and the disturbance until the final

time, $\Gamma\delta\boldsymbol{w}_{f,k}$, that affect the guidance accuracy at the final time. In order to improve the guidance accuracy of position at the final time, the orbit determination and control errors should be reduced, or the time between the TCM time and the final time should be shortened to reduce the sensitivity and disturbance of the dynamics.

2.2 Effect of Trajectory Correction Maneuver Timing

Depending on the timing of the TCM, the expected value of the required ΔV and the guidance accuracy will change. Usually, TCM is performed multiple times, but for simplicity, a single TCM is discussed first.

In general, although it depends on the dynamics, the earlier the time is, the greater the sensitivity of the control to the state at the final time. For example, the state transition matrix of constant velocity linear motion is

$$\Phi_{f,k} = \begin{bmatrix} I & \left(t_f - t_k\right) I \\ O & I \end{bmatrix}, \tag{2.8}$$

and TCM is calculated from the equation as follows.

$$\boldsymbol{u}_k = -\begin{bmatrix} \frac{1}{t_f - t_k} I & I \end{bmatrix} \widehat{\boldsymbol{x}_k^-}. \tag{2.9}$$

Therefore, the expected value of ΔV required for TCM can be reduced by performing TCM at an earlier time when the sensitivity of the control to the state at the final time is larger, and vice versa. In addition, since the initial launch error increases with time because of dynamics and perturbations, the expected value of ΔV required for the TCM can be reduced by performing the TCM at an earlier timing for canceling the state deviations of the initial error.

The guidance accuracy at the final time, however, becomes worse when the TCM is performed earlier. Due to the estimation error of the state used to plan the TCM and the control error of the TCM, the trajectory still deviates from the nominal position at

the final time even after the TCM is performed. This deviation increases with time as a property of dynamics, and disturbances accumulate with time (Eq. (2.7)). Therefore, if TCM is performed earlier, the guidance accuracy at the final time becomes lower.

Based on the above discussion, there is a trade-off between the guidance accuracy at the final time and the ΔV required for TCM, and the TCM time must be determined to minimize the required ΔV while satisfying the guidance requirement at the final time.

The same discussion can be made when multiple TCMs are performed. When performing a TCM that cancels out the error left by the previous TCM, performing the TCM at an earlier time can reduce the ΔV required for that. However, if the TCM is performed earlier, the error that cancels out in the next TCM will increase and the ΔV required for the next TCM will become larger. Therefore, when performing multiple TCMs, there is a trade-off between the ΔV of one TCM and the ΔV of the next TCM, and the time of each TCM must be determined to minimize the sum of the all. The guidance accuracy at the final time depends on the last TCM, and the last TCM must be planned at a time that satisfies the guidance accuracy at the final time.

2.2.1 Spacing Rule

The Spacing Rule has been studied for a long time in TCM optimization.[10][11][12] In these studies, the accuracy of orbit determination is assumed to be constant, and only the optimization of the TCM time is considered for simplicity. By using the spacing rule, the relationship between the optimal TCM times can be expressed as a simple ratio, which makes it possible to easily determine the optimal TCM time.

However, Spacing Rule is a theory from a time when stochastic trajectory optimization and numerical optimization were not developed enough, and as mentioned above, it does not take into account the optimization of orbit determination, various approximations are made to solve it analytically, and it does not take into account the probability distribution. In this study, the optimization of TCM is formulated in the framework of modern stochastic trajectory optimization, which enables us to solve

problems where Spacing Rule cannot be applied.

2.3 Effect of Orbit Determination Accuracy

From Eq. (2.7), it can be seen that the orbit determination error has a significant effect on the guidance accuracy at the final time. The effect of orbit determination error on the magnitude of TCM is also discussed when multiple TCMs are performed. Equation (2.3) can be transformed as follows.

$$\boldsymbol{u}_{k+1} = -\begin{bmatrix} \Phi^{-1}_{rv,f,k+1}\Phi_{rr,f,k+1} & I \end{bmatrix}\widehat{\boldsymbol{x}^-_{k+1}} \tag{2.10}$$

$$= -\begin{bmatrix} \Phi^{-1}_{rv,f,k+1}\Phi_{rr,f,k+1} & I \end{bmatrix}(\widehat{\boldsymbol{x}^-_{k+1}} - \boldsymbol{x}^-_{k+1} + \boldsymbol{x}^-_{k+1}) \tag{2.11}$$

$$= -\begin{bmatrix} \Phi^{-1}_{rv,f,k+1}\Phi_{rr,f,k+1} & I \end{bmatrix}(\widehat{\boldsymbol{x}^-_{k+1}} - \boldsymbol{x}^-_{k+1} + \Phi_{k+1,k}\left((\boldsymbol{x}^-_k - \widehat{\boldsymbol{x}^-_k}) + (\widehat{\boldsymbol{x}^-_k} + B\boldsymbol{u}_k) + B\delta u_k\right) + \Gamma\delta\boldsymbol{w}_{k+1,k}). \tag{2.12}$$

In the equations,

$$\begin{bmatrix} \Phi^{-1}_{rv,f,k+1}\Phi_{rr,f,k+1} & I \end{bmatrix}\Phi_{k+1,k}\,(\widehat{\boldsymbol{x}^-_k} + B\boldsymbol{u}_k) \tag{2.13}$$

$$=\Phi^{-1}_{rv,f,k+1}\begin{bmatrix} \Phi_{rr,f,k+1} & \Phi_{rv,f,k+1} \end{bmatrix}\Phi_{k+1,k}\begin{bmatrix} I \\ \Phi^{-1}_{rv,k+1,k}\Phi_{rr,f,k} \end{bmatrix}\widehat{\boldsymbol{r}^-_k} \tag{2.14}$$

$$=\Phi^{-1}_{rv,f,k+1}\begin{bmatrix} \Phi_{rr,f,k+1} & \Phi_{rv,f,k+1} \end{bmatrix}\begin{bmatrix} \Phi_{rr,k+1,k} - \Phi_{rv,k+1,k}\Phi^{-1}_{rv,f,k}\Phi_{rr,f,k} \\ \Phi_{vr,k+1,k} - \Phi_{vv,k+1,k}\Phi^{-1}_{rv,f,k}\Phi_{rr,f,k} \end{bmatrix}\widehat{\boldsymbol{r}^-_k} \tag{2.15}$$

$$=\Phi^{-1}_{rv,f,k+1}\left(\Phi_{rr,f,k} - \Phi_{rv,f,k}\Phi^{-1}_{rv,f,k}\Phi_{rr,f,k}\right)\widehat{\boldsymbol{r}^-_k} \tag{2.16}$$

$$=\boldsymbol{0}. \tag{2.17}$$

.

The transformation of the last equation is from the propoerty of state transitiom

matrix,

$$\Phi_{f,k} = \Phi_{f,k+1}\Phi_{k+1,k} \tag{2.18}$$

$$\Phi_{rr,f,k} = \Phi_{rr,f,k+1}\Phi_{rr,k+1,k} + \Phi_{rv,f,k+1}\Phi_{vr,k+1,k} \tag{2.19}$$

$$\Phi_{rv,f,k} = \Phi_{rr,f,k+1}\Phi_{vr,k+1,k} + \Phi_{rv,f,k+1}\Phi_{vv,k+1,k}. \tag{2.20}$$

Finally, the formulation of TCM is as follows.

$$\boldsymbol{u}_{k+1} = -\begin{bmatrix} \Phi_{rv,f,k+1}^{-1}\Phi_{rr,f,k+1} & I \end{bmatrix}\left(-\left(\boldsymbol{x}_{k+1}^{-} - \widehat{\boldsymbol{x}}_{k+1}^{-}\right) + \Phi_{k+1,k}\left(\left(\boldsymbol{x}_{k}^{-} - \widehat{\boldsymbol{x}}_{k}^{-}\right) + B\boldsymbol{\delta u}_k\right) + \Gamma\boldsymbol{\delta w}_{k+1,k}\right). \tag{2.21}$$

From the formulation of TCM, it can be seen that there is an increase in the control due to the orbit determination error at TCM, $\boldsymbol{x}_{k+1}^{-} - \widehat{\boldsymbol{x}}_{k+1}^{-}$. In addition, the trajectory deviation caused by the orbit determination error at the previous TCM time and control error, $\Phi_{k+1,k}\left(\left(\boldsymbol{x}_{k}^{-} - \widehat{\boldsymbol{x}}_{k}^{-}\right) + B\boldsymbol{\delta u}_k\right)$, increases the TCM control at the next time. Therefore, in order to reduce the ΔV required for TCM, it is necessary to improve the orbit determination accuracy at the TCM time.

In order to reduce the orbit determination error, it is necessary to use an observation method with high accuracy such as Delta Differential One-way Range (DDOR) measurement or to perform orbit determination multiple times. In addition, the accuracy of orbit determination may vary depending on the timing as a property of dynamics and observation methods. Therefore, it is desirable to reduce the orbit determination error by optimizing the timing of the orbit determination within the range of resources to reduce the ΔV of TCM.

2.4 Integrated Optimization of Trajectory Correction Maneuver Timing and Orbit Determination Accuracy

From Eq. (2.7), the guidance accuracy at the final time is determined by the orbit determination accuracy at the time of the last TCM and the disturbance that accumulates between that time and the final time. If the orbit determination accuracy can be improved, the magnitude of the disturbance, i.e. the time between the last TCM time and the final time, can be increased. Thereby, the sensitivity of the control at the last TCM time can be extended, and the required ΔV can be reduced. In the case other than the last TCM, if the orbit determination accuracy is high, the portion of the trajectory deviation to be canceled in the next TCM that comes from the orbit determination error can be reduced, and the TCM time can be advanced to reduce the ΔV required for that TCM. Therefore, if the orbit determination accuracy can be improved, it will be possible to reduce the ΔV required for the TCM by both the effect of the sensitivity of dynamics and the effect of the orbit determination accuracy itself. The above discussion shows that in TCM optimization, both TCM time and orbit determination accuracy have a significant effect on the ΔV and guidance accuracy required for TCM, and both of them need to be optimized in an integrated manner. Especially in the case of missions where the cost of orbit determination is limited, a major issue is how much resource of orbit determination to allocate to which timing.

Chapter 3

Stochastic Trajectory Optimization Problems

God does not play dice with the universe.

Albert Einstein

In this chapter, stochastic trajectory optimization is explained. First, an ordinary deterministic trajectory optimization problem is formulated, and then a stochastic trajectory optimization problem is formulated by defining the state and control quantities as stochastic processes. A method of solving the stochastic trajectory optimization problem by converting it into a deterministic trajectory optimization problem by parameterizing the probability distribution is introduced, and issues to be considered in the formulation of the problem in this study are discussed.

3.1 Deterministic Trajectory Optimization Problems

Although there are various expressions for the deterministic trajectory optimization problem depending on the assumptions of the problem, the deterministic trajectory optimization problem with fixed initial time, final time, initial state quantity, and final state quantity in the discrete-time dynamical system can be expressed by the following equation.

$$\underset{\boldsymbol{M}_i}{\text{minimize}} \quad \sum_{i}^{N_i} J_i\left(\boldsymbol{X}_i,\ \boldsymbol{U}_i\right) \tag{3.1}$$

$$\text{subject to} \quad \boldsymbol{X}_i = \boldsymbol{F}_{i,i-1}\left(\boldsymbol{X}_{i-1}\right) + B\boldsymbol{U}_{i-1} \tag{3.2}$$

$$\boldsymbol{U}_i = \boldsymbol{M}_i\left(\boldsymbol{X}_i^{-}\right) \tag{3.3}$$

$$\boldsymbol{X}_0 = \overline{\boldsymbol{X}_0} \tag{3.4}$$

$$\boldsymbol{X}_f = \overline{\boldsymbol{X}_f} \tag{3.5}$$

$$\boldsymbol{C}_i\left(\boldsymbol{X}_i,\ \boldsymbol{U}_i\right) \leq \boldsymbol{0}. \tag{3.6}$$

Equation 3.1 represents the objective function, which is the sum of the cost functions at each time. Equation 3.2 represents the transition of the state quantity due to dynamics and control. Equation 3.3 represents the control strategy based on state quantities, which consists of feed-forward control, which is a function of time only, and feed-back control based on time and state quantities. Equations 3.4 and 3.5 represent the initial and final values of the state quantity, respectively. Equation 3.6 shows the constraints of the state and control quantities at each time.

Although many methods have been proposed to solve the deterministic trajectory optimization problem, such as the direct method, indirect method, shooting method, collocation method, etc., it is basically converted into a numerical optimization problem and solved using numerical optimization methods.

3.2 Stochastic Trajectory Optimization Problems

It is necessary to solve stochastic trajectory optimization problems in order to account for uncertainties in state quantities, control errors, stochastic disturbances, etc. In the stochastic trajectory optimization problem, the state and control quantities are defined as stochastic processes, and the state and control quantities at each time are random variables.

3.2.1 Stochastic Trajectory Optimization Problems with Perfect Information

When the information of the state quantity to be used for feedback control is completely known, the stochastic trajectory optimization problem can be expressed by the following equation.

$$\underset{\boldsymbol{M}_i}{\text{minimize}} \quad E\left[\sum_{i}^{N_i} J_i\left(\boldsymbol{X}_i,\ \boldsymbol{U}_i\right)\right] \tag{3.7}$$

$$\text{subject to} \quad \boldsymbol{X}_i = \boldsymbol{F}_{i,i-1}\left(\boldsymbol{X}_{i-1}\right) + B\left(\boldsymbol{U}_{i-1} + \delta\boldsymbol{U}_i\right) + \Gamma\delta\boldsymbol{w}_{i,i-1} \tag{3.8}$$

$$\boldsymbol{U}_i = \boldsymbol{M}_i\left(\boldsymbol{X}_i^-\right) \tag{3.9}$$

$$p\left(\boldsymbol{X}_0\right) = p\left(\overline{\boldsymbol{X}_0}\right) \tag{3.10}$$

$$P\left(\boldsymbol{C}_i\left(\boldsymbol{X}_i,\ \boldsymbol{U}_i\right) \leq \boldsymbol{0}\right) \geq 1 - \Delta_i. \tag{3.11}$$

Equation 3.7 represents the objective function, which is expressed as the expected value of the sum of the cost functions at each time. Equation 3.8 represents the transition of state quantities due to dynamics, control, and stochastic disturbances. Equation 3.9 represents a control strategy similar to the deterministic trajectory optimization problem. Equation 3.10 shows the initial distribution of the state quantities. Equation 3.11 shows the constraints on the state and control quantities at each time. In stochastic trajectory optimization problems, these constraints are expressed as chance constraints.[17][19]

3.2.2 Stochastic Trajectory Optimization Problems with Imperfect Information

In the real situation, the information on the state quantity used for feedback control will never be completely known, and the control will be based on the estimated value. In this case, Equation 2.9 is changed as follows to control based on the estimated value.

$$\boldsymbol{U}_i = \boldsymbol{M}_i\left(\widehat{\boldsymbol{X}_i^-}\right). \tag{3.12}$$

Various methods to obtain the estimated values have been studied, and batch filters and Kalman filters are often used.[30] In addition, there is an error between the estimated state value and the true state value, and the estimation error changes the control quantity and affects the uncertainty of the true state value. How to deal with the estimation error is a major issue in stochastic trajectory optimization. In this study, this problem is solved by introducing an augmented state quantity that combines the true state value and the estimated state value.

3.2.3 Solving Method of Stochastic Trajectory Optimization Problems

Like the deterministic trajectory optimization problem, the stochastic trajectory optimization problem also needs to be converted into a numerical optimization problem and solved using a numerical optimization method. Various methods have been proposed to solve the problem, but the most common method is to parameterize the probability distribution of state and control quantities and convert the problem into a deterministic trajectory optimization problem with respect to the parameters. Once the deterministic trajectory optimization problem for the parameters of the probability distribution is formulated, it can be solved using numerical optimization methods similar to those used for ordinary deterministic trajectory optimization problems.

Parameterization of the probability distribution is done by approximating the probability distribution of the state and control quantities represented by a certain parameter, as follows.

$$p(\boldsymbol{X}) \approx f_X(\boldsymbol{X}, \boldsymbol{\theta}_X) \tag{3.13}$$

$$p(\boldsymbol{U}) \approx f_U(\boldsymbol{U}, \boldsymbol{\theta}_U). \tag{3.14}$$

This makes it possible to express the probability distributions of the state and control quantities at each time as parameters rather than functions. Various methods have been proposed for parameterizing probability distributions and propagating these parameters.

The probability distribution is parameterized and the deterministic trajectory op-

timization problem with respect to it is expressed by the following equations.

$$\underset{\boldsymbol{M}_i}{\text{minimize}} \quad \sum_{i}^{N_i} \mathscr{J}_i\left(\boldsymbol{\theta}_{X,i},\ \boldsymbol{\theta}_{U,i}\right) \tag{3.15}$$

$$\text{subject to} \quad \boldsymbol{\theta}_{X,i} = \mathscr{F}_{i,i-1}\left(\boldsymbol{\theta}_{X,i-1}\right) \tag{3.16}$$

$$\boldsymbol{\theta}_{U,i} = \mathscr{M}_i\left(\boldsymbol{\theta}_{X,i}^{-}\right) \tag{3.17}$$

$$\boldsymbol{\theta}_{X,0} = \overline{\boldsymbol{\theta}}_{X,0} \tag{3.18}$$

$$\mathscr{C}_i\left(\boldsymbol{\theta}_{X,i},\ \boldsymbol{\theta}_{U,i}\right) \leq \mathbf{0}. \tag{3.19}$$

Equation 3.15 is the objective function transformed into a function of the parameters of the probability distribution. Equation 3.16 is the propagation equation of the parameters of the probability distribution of the state quantity. Equation 3.17 is a formula for obtaining the probability distribution of a control quantity by using the parameters of the probability distribution of the state quantity and the control strategy. Equation 3.18 is the initial value of the parameter of the probability distribution of the state quantity. Equation 3.19 is the chance constraint converted to a function of the parameters of the probability distribution.

3.3 Formulation of Problem

In this section, the optimization problem to be solved in this study is formulated. The problem of optimizing the TCM time and orbit determination time is solved so as to minimize the expected value of ΔV required for TCMs while satisfying the required guidance accuracy at the final time. Uncertainties to be considered include orbit insertion error, orbit determination error, control error, and dynamics error, whereby state and control quantities are considered as stochastic processes.

The optimization problem is described in terms of stochastic trajectory optimization. The expected value of ΔV required for trajectory correction is minimized. The propagation of the probability distribution of the augmented state, which is a combi-

nation of the true and estimated state, is considered. Constraints on the augmented states and optimization variables are placed as chance constraints. The optimization variables are the trajectory correction maneuver time t_k and the orbit determination time t_l. Therefore, the optimization problem to be solved in this study is as follows.

$$\underset{t_k \in \mathcal{T}_k,\ t_l \in \mathcal{T}_l}{\text{minimize}} \quad E\left[\sum_{k}^{N_k} \|\boldsymbol{U}_k + \delta \boldsymbol{U}_k\|_2\right] \tag{3.20}$$

$$\text{subject to} \quad p(\boldsymbol{Z}_i) = \mathcal{F}_{i,i-1}\left(p\left(\boldsymbol{Z}_{i-1}\right)\right) \tag{3.21}$$

$$p\left(\boldsymbol{Z}_0\right) = p_0\left(\boldsymbol{Z}_0\right) \tag{3.22}$$

$$p\left(\boldsymbol{U}_k\right) = \mathcal{M}_k\left(p\left(\boldsymbol{Z}_k^-\right)\right) \tag{3.23}$$

$$P\left(\boldsymbol{C}_i\left(\boldsymbol{Z}_i\right) \leq \boldsymbol{0}\right) \geq 1 - \Delta_i \qquad t_i \in \mathcal{T} \tag{3.24}$$

$$\boldsymbol{C}\left(t_k,\ t_l\right) \leq \boldsymbol{0}, \tag{3.25}$$

where $\mathcal{F}$ is an operator of time propagation of $p\left(\boldsymbol{Z}\right)$ derived from $\boldsymbol{F}$, $\mathcal{M}$ is an operator calculating $p\left(\boldsymbol{U}_k\right)$ from $p\left(\boldsymbol{Z}_k^-\right)$ derived from $\boldsymbol{M}$, and $\mathcal{T}$ is a possible range of time.

It is difficult to solve this optimization problem directly considering the probability, and thus it is necessary to formulate the problem to be optimized numerically. In this research, the probability distribution of the state quantity is parameterized by the Gaussian approximation method or the Monte Carlo method. By formulating the propagation equation of the augmented state, the propagation of the probability distribution can be derived. The probability distribution of the control is also parameterized in the same way, and its parameters are calculated from the control law and the probability distribution of the state. The chance constraint on the state quantity is also formulated so that it can be calculated from the parameters of the probability distribution of the state. With this formulation, the objective function and all constraints can be calculated as a function of the trajectory correction time and orbit determination time, and optimization can be performed using numerical optimization algorithms.

3.4 Issues to Solve Stochastic Trajectory Optimization Problems

From the formulation in the previous section, the following issues exist in order to solve stochastic trajectory optimization problems, and they need to be formulated appropriately for the problem so that they can be solved as numerical optimization problems. The formulation of issues in this study will be explained in detail in Chapter 4.

1. Formulation of estimation of state and handling of estimation errors
2. Parameterization of probability distributions of state quantities, control quantities, and uncertainties
3. Propagation of parameters of probability distributions of state quantities
4. Computation of parameters of probability distributions of control quantities
5. Calculation of objective function based on parameters of the probability distribution of state and control quantities
6. Formulation of chance constraints
7. Selection of numerical optimization method

Chapter 4

Formulation of Optimization Problem

He who would learn to fly one day
must first learn to stand and walk
and run and climb and dance; one
cannot fly into flying.

Friedrich Wilhelm Nietzsche

In this chapter, the optimization problem presented in the previous chapter is formulated. The probability distribution of state and control is parameterized. The objective function and constraints of the optimization problem are formulated as functions of the parameters of the probability distribution of state and the control variables, and the stochastic optimization problem is converted into the deterministic optimization problem to be solved by numerical optimization algorithms.

4.1 Propagation of State

This section describes how the probability distributions of the true and estimated state quantities of a spacecraft are propagated under uncertainty such as errors in dynamics, control, and observation. Under the uncertainty, the state quantities related to the trajectory of the spacecraft can be considered as a stochastic process, and if the probability distribution can be calculated, it is possible to calculate the accuracy of the trajectory guidance required for the success of the mission and the expected value of the ΔV required for the trajectory correction.

There are two types of state quantities: the true state, which we cannot know, and the estimated state, which can be estimated by orbit determination. The former is related to the success or failure of the mission, but we can only use the latter for orbit control. These state quantities are considered to influence each other and are coupled. Figure4.1 shows the coupling between the true state and the estimated state The true state performs motions according to the natural dynamics, and the trajectory control that affects the true state is planned according to the estimated state. On the other hand, the estimated state is transitioned by an estimation algorithm such as the Kalman filter and updated based on the observables generated from the true state. Therefore, except in special problem settings, these cannot be considered separately. In this research, the problem using augmented state quantities is formulated, which are a combination of these two. The concept of augmented state is often used in linear covariance analysis of rendezvous problems, where the dynamics is linear, but in this study, the formulation is applicable to nonlinear dynamics problems and stochastic trajectory optimization.[25]-[28]

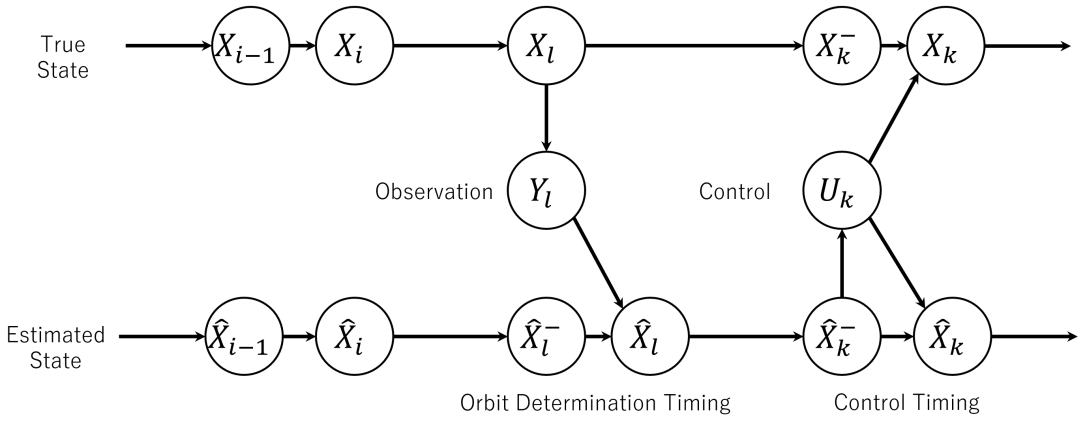

Figure 4.1: Coupling between the true state and the estimated state.

When the algorithms for trajectory correction and orbit determination are fixed, the formulation of the propagation of augmented state quantities makes it possible to calculate the probability distribution of state quantities at all times from the probability distribution of the initial state and the timing of trajectory correction and orbit determination.

4.1.1 Stochastic Differential Equation

In this study, it is assumed that the motion of the spacecraft follows a stochastic differential equation. The stochastic differential equation is expressed by the following equation.[29]

$$d\boldsymbol{X} = \boldsymbol{F}(\boldsymbol{X}, t)\, dt + \boldsymbol{\Gamma}(\boldsymbol{X}, t)\, dw. \tag{4.1}$$

It is difficult to obtain analytical solutions for nonlinear stochastic differential equations.

Solutions to ordinary differential equations, which ignores the Brownian motion term, can be obtained by numerical integration or mathematical analysis. The solution of nonlinear ordinary differential equation,

$$d\boldsymbol{X} = \boldsymbol{F}(\boldsymbol{X}, t)\, dt, \tag{4.2}$$

is

$$\boldsymbol{X} = \boldsymbol{F}_{t,t_0}(\boldsymbol{X}_{t_0}). \tag{4.3}$$

In addition, the solution of linear stochastic differential equations can be solved analytically. The solution to the linear stochastic differential equation with linearization around a reference trajectory and assumption of $\boldsymbol{\Gamma}(\boldsymbol{X}, t) = \boldsymbol{\Gamma}$,

$$d\boldsymbol{x} = A(t)\, \boldsymbol{x} dt + \boldsymbol{\Gamma} dw, \tag{4.4}$$

is as follows

$$\boldsymbol{x} = \Phi_{t,t_0} \boldsymbol{x}_0 + \Gamma \delta \boldsymbol{w}_{t,t_0}, \tag{4.5}$$

where $\delta \boldsymbol{w}_{t,t_0}$ is a random variable that follows a Gaussian distribution,

$$\delta \boldsymbol{w}_{t,t_0} \sim \mathcal{N}(\boldsymbol{0}, Q_{t,t_0}) \tag{4.6}$$

$$Q_{t,t_0} = \int_{t_0}^{\mathsf{T}} \Phi_{t,\tau} Q \Phi_{t,\tau}^{\mathsf{T}} d\tau \tag{4.7}$$

$$Q = \boldsymbol{\Gamma}\boldsymbol{\Gamma}^{\mathsf{T}}. \tag{4.8}$$

Actually $\Gamma = I$, and it is unnecessary for representation, but it is left in for compatibility with common expressions.

As mentioned above, it is difficult to obtain analytical solutions to nonlinear stochastic differential equations, and the computation becomes complicated when the coupling between the disturbance term and the dynamics is considered. In this study, therefore, the solution of the nonlinear ordinary differential equation, that is the dynamics without the Brownian motion term, plus the disturbance term obtained as the solution of the linear stochastic differential equation, is treated as an approximation of the solution of the nonlinear stochastic differential equation.[19]

$$\boldsymbol{X} = \boldsymbol{F}_{t,t_0}(\boldsymbol{X}_{t_0}) + \Gamma \delta \boldsymbol{w}_{t,t_0}. \tag{4.9}$$

4.1.2 Control and Control Error

In this study, the control is assumed to be an impulsive feedback control based on an estimated state value.

$$\boldsymbol{U}_k = \boldsymbol{M}_k\left(\widehat{\boldsymbol{X}_k^-}\right). \tag{4.10}$$

For modeling of control error, Gate's model has been proposed.[40][41] In this study, the following model consisting of two types of control error is considered for simplicity: one that is constant regardless of the magnitude of control, and one that is proportional to the magnitude of control.

$$\delta \boldsymbol{U}_k \sim \mathcal{N}\left(\boldsymbol{0}, S_{0,k} + c^2 \boldsymbol{U}_k \boldsymbol{U}_k^{\mathsf{T}}\right), \tag{4.11}$$

where $S_{0,k}$ is the fixed control error and c is the coefficient of proportional control error.

4.1.3 Propagation of True States

First, the propagation of the true state is discussed. It is assumed that the true state is propagated according to the dynamics and stochastic disturbances.

$$\boldsymbol{X}_i = \boldsymbol{F}_{i,i-1}\left(\boldsymbol{X}_{i-1}\right) + \Gamma \delta \boldsymbol{w}_{i,i-1}. \tag{4.12}$$

At the timing of the trajectory correction, the control is added based on the estimated state at orbit determination timing t_l propagated to the current time. Considering the control law and the control error, the propagation of the true state can be expressed as follows.

$$\boldsymbol{X}_k = \boldsymbol{F}_{k,l(k)}\left(\boldsymbol{X}_{l(k)}\right) + B\left(\boldsymbol{U}_k + \delta \boldsymbol{U}_k\right) + \Gamma \delta \boldsymbol{w}_{k,l(k)} \tag{4.13}$$

$$\boldsymbol{U}_k = \boldsymbol{M}_k\left(\widehat{\boldsymbol{X}}_k^-\right) \tag{4.14}$$

$$= \boldsymbol{M}_k\left(\boldsymbol{F}_{k,l(k)}\left(\widehat{\boldsymbol{X}}_{l(k)}\right)\right). \tag{4.15}$$

At the timing of the orbit determination, the true state is not affected by it, and thus the propagation is the same as Eq. (4.12).

$$\boldsymbol{X}_l = \boldsymbol{F}_{l,l-1}\left(\boldsymbol{X}_{l-1}\right) + \Gamma \delta \boldsymbol{w}_{l,l-1}. \tag{4.16}$$

4.1.4 Propagation of Estimated States

In this study, an estimated state value is defined as a conditional expectation about the observed value of a state quantity. Using Bayesian estimation, the estimated value is

expressed as a random variable with conditional probability about the observed value.

$$\widehat{\boldsymbol{X}} \sim p\left(\boldsymbol{X} \mid \{\boldsymbol{Y}_1 ... \boldsymbol{Y}_l\}\right). \tag{4.17}$$

The feedback control law treated in this research does not use all the information of the probability distribution, but defines one estimated value and performs control based on that estimated value. In this case, an estimate that minimizes the mean square of the estimation error is used generally, which is the conditional expectation of the observed value of the state quantity.

$$\widehat{\boldsymbol{X}} = \mathbb{E}\left[\boldsymbol{X} \mid \{\boldsymbol{Y}_1 ... \boldsymbol{Y}_l\}\right]. \tag{4.18}$$

The Kalman filter is an algorithm that can compute the conditional expectation of the observed values of state variables in a sequential manner.[30] In this study, the Extended Kalman Filter (EKF) is adopted, which is extended to nonlinearity, as a method to compute the estimated values. It is also possible to use other estimation algorithms like Unscented Kalman Filter (UKF).[31]-[33]

$$\widehat{\boldsymbol{X}}_i = \boldsymbol{F}_{i,i-1}\left(\widehat{\boldsymbol{X}}_{i-1}\right) \tag{4.19}$$

$$P_i = \Phi_{i,i-1} P_{i-1} \Phi_{i,i-1}^{\mathsf{T}} + \Gamma Q_{i,i-1} \Gamma^{\mathsf{T}} \tag{4.20}$$

$$\Phi_{i,i-1} = \left.\frac{\partial \boldsymbol{F}_{i,i-1}}{\partial \boldsymbol{X}_{i-1}}\right|_{\widehat{\boldsymbol{X}}_{i-1}}. \tag{4.21}$$

At the timing of the trajectory correction, the control is added, and the control error is taken into account for the propagation of P.

$$\widehat{\boldsymbol{X}}_k = \boldsymbol{F}_{k,l(k)}\left(\widehat{\boldsymbol{X}}_{l(k)}\right) + B\boldsymbol{U}_k \tag{4.22}$$

$$P_k = \Phi_{k,l(k)} P_{l(k)} \Phi_{k,l(k)}^{\mathsf{T}} + B S_k B + \Gamma Q_{k,l(k)} \Gamma^{\mathsf{T}} \tag{4.23}$$

$$\Phi_{k,l(k)} = \left.\frac{\partial \boldsymbol{F}_{k,l(k)}}{\partial \boldsymbol{X}_{l(k)}}\right|_{\widehat{\boldsymbol{X}}_{l(k)}}. \tag{4.24}$$

At the timing of the orbit determination, the observation update is performed based on the observation generated from the true state and the observation error.

$$\widehat{\boldsymbol{X}}_l = \boldsymbol{F}_{l,l-1}\left(\widehat{\boldsymbol{X}}_{l-1}\right) + K_l\left(\boldsymbol{Y}_l - \widehat{\boldsymbol{Y}}_l\right) \tag{4.25}$$

$$\boldsymbol{Y}_l = \boldsymbol{G}\left(\boldsymbol{X}_l\right) + \boldsymbol{\varepsilon}_l \tag{4.26}$$

$$\widehat{\boldsymbol{Y}}_l = \boldsymbol{G}\left(\widehat{\boldsymbol{X}}_l\right) \tag{4.27}$$

$$K_l = P_{l|l-1}H_l^{\mathsf{T}}\left(H_l P_{l|l-1}H_l^{\mathsf{T}} + R_l\right)^{-1} \tag{4.28}$$

$$H_l = \left.\frac{\partial \boldsymbol{G}}{\partial \boldsymbol{X}_l}\right|_{\boldsymbol{F}_{l,l-1}\left(\widehat{\boldsymbol{X}}_{l-1}\right)} \tag{4.29}$$

$$P_{l|l-1} = \Phi_{l,l-1}P_{l-1}\Phi_{l,l-1}^{\mathsf{T}} + \Gamma Q_{l,l-1}\Gamma^{\mathsf{T}} \tag{4.30}$$

$$P_l = \left(I - K_l H_l\right)P_{l|l-1}. \tag{4.31}$$

4.1.5 Propagation of Augmented States

The discussion in the previous section shows that the propagation of the true state value and the estimated state value are coupled to each other. These couplings cannot be ignored except in special situations where the Separation Principle is valid. Therefore, the propagation of the augmented state is considered, which combines the true state value and the estimated value state together.

$$\boldsymbol{Z} = \begin{bmatrix} \boldsymbol{X} \\ \widehat{\boldsymbol{X}} \end{bmatrix} \tag{4.32}$$

In fact, the covariance matrix in the EKF is also a quantity that should be treated as an augmented state. However, since the covariance matrix of the Kalman filter in linear dynamics is not a variable that can be distributed as a quantity that depends on the true state, the estimated state (mean), or observed value, it is not included in the augmented state when using the Gaussian approximation method described later. In this case, the covariance matrix is calculated around the nominal trajectory, and is treated as a quantity independent of the true or estimated state. If Monte Carlo approximation is used for propagation, the covariance matrix can be calculated at

each point.

From Eqs. (4.12) to (4.31) the propagation equation of the augmented state is

$$\begin{bmatrix} \boldsymbol{X}_i \\ \widehat{\boldsymbol{X}}_i \end{bmatrix} = \begin{bmatrix} \boldsymbol{F}_{i,i-1}\left(\boldsymbol{X}_{i-1}\right) + \Gamma\delta\boldsymbol{w}_{i,i-1} \\ \boldsymbol{F}_{i,i-1}\left(\widehat{\boldsymbol{X}}_{i-1}\right) \end{bmatrix} \tag{4.33}$$

$$P_i = \Phi_{i,i-1} P_{i-1} \Phi_{i,i-1}^{\mathsf{T}} + \Gamma Q_{i,i-1} \Gamma^{\mathsf{T}}. \tag{4.34}$$

At the timing of the trajectory correction,

$$\begin{bmatrix} \boldsymbol{X}_k \\ \widehat{\boldsymbol{X}}_k \end{bmatrix}, = \begin{bmatrix} \boldsymbol{F}_{k,l(k)}\left(\boldsymbol{X}_{l(k)}\right) + \Gamma\delta\boldsymbol{w}_{k,l(k)} + B\left(\boldsymbol{U}_k + \delta\boldsymbol{U}_k\right) \\ \boldsymbol{F}_{k,l(k)}\left(\widehat{\boldsymbol{X}}_{l(k)}\right) + B\boldsymbol{U}_k \end{bmatrix} \tag{4.35}$$

$$\boldsymbol{U}_k = \boldsymbol{M}_k\left(\boldsymbol{F}_{k,l(k)}\left(\widehat{\boldsymbol{X}}_{l(k)}\right)\right) \tag{4.36}$$

$$P_k = \Phi_{k,l(k)} P_{l(k)} \Phi_{k,l(k)}^{\mathsf{T}} + B S_k B + \Gamma Q_{k,l(k)} \Gamma^{\mathsf{T}} \tag{4.37}$$

and at the timing of the orbit determination,

$$\begin{bmatrix} \boldsymbol{X}_l \\ \widehat{\boldsymbol{X}}_l \end{bmatrix} = \begin{bmatrix} \boldsymbol{F}_{l,l-1}\left(\boldsymbol{X}_{l-1}\right) + \Gamma\delta\boldsymbol{w}_{l,l-1} \\ \boldsymbol{F}_{l,l-1}\left(\widehat{\boldsymbol{X}}_{l-1}\right) + K_l\left(\boldsymbol{Y}_l - \widehat{\boldsymbol{Y}}_l\right) \end{bmatrix} \tag{4.38}$$

$$\boldsymbol{Y}_l = \boldsymbol{G}\left(\boldsymbol{X}_l\right) + \boldsymbol{\varepsilon}_l \tag{4.39}$$

$$\widehat{\boldsymbol{Y}}_l = \boldsymbol{G}\left(\widehat{\boldsymbol{X}}_l\right) \tag{4.40}$$

$$K_l = P_{l|l-1} H_l^{\mathsf{T}} \left(H_l P_{l|l-1} H_l^{\mathsf{T}} + R_l\right)^{-1} \tag{4.41}$$

$$P_{l|l-1} = \Phi_{l,l-1} P_{l-1} \Phi_{l,l-1}^{\mathsf{T}} + \Gamma Q_{l,l-1} \Gamma^{\mathsf{T}} \tag{4.42}$$

$$P_l = \left(I - K_l H_l\right) P_{l|l-1}. \tag{4.43}$$

4.1.6 Propagation of Targeting States

In this section, targeting states $\boldsymbol{X}'$ is proposed, which are not directly related to the optimization formulation but are useful for the quantitative analysis of TCM. The propagation equation of targeting states is as follows.

The targeting states are propagated by state equation without stochastic distur-

bance,

$$\boldsymbol{X}'_i = \boldsymbol{F}_{i,i-1}\left(\boldsymbol{X}'_{i-1}\right). \tag{4.44}$$

At the timing of the trajectory correction, the targeting state value is initialized by the estimated state value,

$$\boldsymbol{X}'_k = \widehat{\boldsymbol{X}}_k. \tag{4.45}$$

When the FTA Guidance introduced in Chapter 2 is adopted for the TCM control law, the propagated position of the targeting states until the final time coincides with the position of the nominal trajectory.

$$\boldsymbol{F}_{f,i}\left(\boldsymbol{X}'_i\right) = \boldsymbol{X}^*_f - B\delta\boldsymbol{V}_f. \tag{4.46}$$

Therefore, the difference between the true state and the targeting state is an indication of the guidance error, especially when the propagation is done after the last TCM until the final time, which is consistent with the final guidance error. The difference between the true state and the targeting state corresponds to the orbit determination error and control error at the TCM time, and increases thereafter as the characteristics of the dynamics and disturbance accumulation.

The difference between the estimated state and the targeting state is directly related to the magnitude of the TCM. Considering the linearized system as in Chapter 2, the following equation shows that the TCM is affine to the difference between the estimated state and the targeting state.

$$\boldsymbol{u}_k = -\begin{bmatrix} \Phi_{rv,f,k}^{-1}\Phi_{rr,f,k} & I \end{bmatrix}\widehat{\boldsymbol{x}_k^-} \tag{4.47}$$

$$= -\begin{bmatrix} \Phi_{rv,f,k}^{-1}\Phi_{rr,f,k} & I \end{bmatrix}(\widehat{\boldsymbol{x}_k^-} - \boldsymbol{x}_k'^- + \boldsymbol{x}_k'^-) \tag{4.48}$$

$$= -\begin{bmatrix} \Phi_{rv,f,k}^{-1}\Phi_{rr,f,k} & I \end{bmatrix}(\widehat{\boldsymbol{x}_k^-} - \boldsymbol{x}_k'^- + \Phi_{k,k-1}\widehat{\boldsymbol{x}}_{k-1}) \tag{4.49}$$

$$= -\begin{bmatrix} \Phi_{rv,f,k}^{-1}\Phi_{rr,f,k} & I \end{bmatrix}(\widehat{\boldsymbol{x}_k^-} - \boldsymbol{x}_k'^-)\,. \tag{4.50}$$

Therefore, the difference between the estimated state and the targeting state is an approximate amount of the size of the TCM when the TCM is planned at that time. If the orbit determination error is ignored, the difference between the true state and the targeting state also corresponds to it. This means that the TCM except for the first TCM is planned to cancel out the error accumulated after the previous TCM. Since the orbit determination error depends on the timing or method of the orbit determination, the difference between the true state and the targeting state is a quantity that is not affected by it. Thus, the difference between the true state and the targeting state can be treated as an indication when analyzing the effect of uncertainties except for orbit determination error on the magnitude of TCM.

Of course, the targeting state is coupled with the true state and the estimated state, so when performing analysis using the targeting state, it is necessary to add the targeting state to the augmented state for propagation.

4.2 Parameterization of Probability Distributions

With the presence of uncertainty, the true state and the estimated state become random variables. There are various methods for parameterization of the probability distribution of the augmented state $p(\boldsymbol{Z})$. Although any formulation method can be used in this study, the two most commonly used methods for parameterization of the probability distributions are the Gaussian approximation method and the Monte Carlo method.

4.2.1 Gaussian Approximation Method

The Gaussian approximation regards the probability distribution at each time as a Gaussian distribution. The parameters are the mean $\boldsymbol{\mu}$ and covariance matrix Σ.

$$\boldsymbol{Z} \sim \mathcal{N}(\boldsymbol{\mu}_{\boldsymbol{Z}}, \Sigma_{\boldsymbol{Z}}) \tag{4.51}$$

$$p(\boldsymbol{Z}) \approx \frac{\exp\left(-\frac{1}{2}(\boldsymbol{Z}-\boldsymbol{\mu}_{\boldsymbol{Z}})^{\mathsf{T}}{\Sigma_{\boldsymbol{Z}}}^{-1}(\boldsymbol{Z}-\boldsymbol{\mu}_{\boldsymbol{Z}})\right)}{\sqrt{(2\pi)^d|\Sigma_{\boldsymbol{Z}}|}} \tag{4.52}$$

$$\boldsymbol{\theta}_{Z_i} = \left[\boldsymbol{\mu}_{\boldsymbol{Z}_i}\ \Sigma_{\boldsymbol{Z}_i}\right], \tag{4.53}$$

where d is the dimension of agumented state vector.

The Gaussian approximation method is a very popular method due to its ease of theoretical handling. However, since the Gaussianity is lost due to the propagation of the probability distribution under nonlinear dynamics, there is a problem that the approximation accuracy deteriorates for problems with strong nonlinearity.

4.2.2 Monte Carlo method

The Monte Carlo method is a method of approximating a probability distribution as a collection of particles $\boldsymbol{Z}^{(n)}$. The parameters are the state vectors of the particles $\boldsymbol{Z}^{(n)}$.

$$p(\boldsymbol{Z}) \approx \frac{1}{N}\sum_{n=1}^{N}\delta\left(\boldsymbol{Z}-\boldsymbol{Z}^{(n)}\right) \tag{4.54}$$

$$\boldsymbol{\theta}_{Z_i} = \left[\boldsymbol{Z}_i^{(1)}\ \boldsymbol{Z}_i^{(2)}\ \cdots\ \boldsymbol{Z}_i^{(N)}\right], \tag{4.55}$$

where $\delta(\cdot)$ is the Dirac delta distribution.

Since this method directly approximates the probability distribution, it can be applied to general probability distributions other than the Gaussian distribution.

4.3 Formulation of Uncertainty Propagation

By using methods introduced in the previous section, the propagation of the parameters of the probability distribution can be formulated with their initial values as follows.

$$\boldsymbol{\theta}_{Z_i} = \mathscr{F}_{i,i-1}\left(\boldsymbol{\theta}_{Z_{i-1}}\right) \tag{4.56}$$

$$\boldsymbol{\theta}_{Z_0} = \bar{\boldsymbol{\theta}}_{Z_0}, \tag{4.57}$$

where $\mathscr{F}$ is a function of time propagation of $\boldsymbol{\theta}_Z$ derived from $\boldsymbol{F}$ and $\bar{\boldsymbol{\theta}}_{Z_0}$ is the initial value of $\boldsymbol{\theta}_{Z_0}$.

4.3.1 Gaussian Approximation Method

Linear approximation is often used for propagation of $\boldsymbol{\mu}$ and Σ because of its short computation time. Unscented Transform or cubature rules, which are useful for highly nonlinear problems, can also be used.[31]-[34]

The propagation equations for the mean and covariance matrices in the linear approximation are as follows (see Appendix A). At the control time,

$$\boldsymbol{\mu}_{\boldsymbol{Z}_k} = \begin{bmatrix} I & C_k \\ O & I + C_k \end{bmatrix} \begin{bmatrix} \Phi_{k,l(k)} & O \\ O & \Phi_{k,l(k)} \end{bmatrix} \boldsymbol{\mu}_{\boldsymbol{Z}_{l(k)}} \tag{4.58}$$

$$\begin{aligned} \Sigma_{\boldsymbol{Z}_k} = &\begin{bmatrix} I & C_k \\ O & I + C_k \end{bmatrix} \begin{bmatrix} \Phi_{k,l(k)} & O \\ O & \Phi_{k,l(k)} \end{bmatrix} \Sigma_{\boldsymbol{Z}_{l(k)}} \begin{bmatrix} \Phi_{k,l(k)} & O \\ O & \Phi_{k,l(k)} \end{bmatrix}^{\mathsf{T}} \begin{bmatrix} I & C_k \\ O & I + C_k \end{bmatrix}^{\mathsf{T}} \\ &+ \begin{bmatrix} B \\ O \end{bmatrix} S_k \begin{bmatrix} B \\ O \end{bmatrix}^{\mathsf{T}} + \begin{bmatrix} \Gamma \\ O \end{bmatrix} Q_{k,l(k)} \begin{bmatrix} \Gamma \\ O \end{bmatrix}^{\mathsf{T}} \end{aligned} \tag{4.59}$$

$$C_k = B \frac{\partial \boldsymbol{M}_k}{\partial \boldsymbol{X}_k}\bigg|_{\boldsymbol{F}_{k,l(k)}\left(\boldsymbol{X}^*_{l(k)}\right)}, \tag{4.60}$$

and at the orbit determination time,

$$\boldsymbol{\mu}_{\boldsymbol{Z}_l} = \begin{bmatrix} I & O \\ K_l H_l & I - K_l H_l \end{bmatrix} \begin{bmatrix} \Phi_{l,l-1} & O \\ O & \Phi_{l,l-1} \end{bmatrix} \boldsymbol{\mu}_{\boldsymbol{Z}_{l-1}} \tag{4.61}$$

$$\begin{aligned} \Sigma_{\boldsymbol{Z}_l} = & \begin{bmatrix} I & O \\ K_l H_l & I - K_l H_l \end{bmatrix} \begin{bmatrix} \Phi_{l,l-1} & O \\ O & \Phi_{l,l-1} \end{bmatrix} \Sigma_{\boldsymbol{Z}_{l-1}} \begin{bmatrix} \Phi_{l,l-1} & O \\ O & \Phi_{l,l-1} \end{bmatrix}^{\mathsf{T}} \begin{bmatrix} I & O \\ K_l H_l & I - K_l H_l \end{bmatrix}^{\mathsf{T}} \\ & + \begin{bmatrix} \Gamma \\ O \end{bmatrix} Q_{k,l(k)} \begin{bmatrix} \Gamma \\ O \end{bmatrix}^{\mathsf{T}} + \begin{bmatrix} O \\ K_l \end{bmatrix} R_l \begin{bmatrix} O \\ K_l \end{bmatrix}^{\mathsf{T}}. \end{aligned} \tag{4.62}$$

In the above equations, since the control error represented in the equation does not follow a Gaussian distribution, the following approximation is placed to perform the calculation.

$$\delta \boldsymbol{U}_k \sim \mathcal{N}(\boldsymbol{0}, S_k) \tag{4.63}$$

$$S_k = S_{0,k} + c^2 \Sigma_{\boldsymbol{U}_k} \tag{4.64}$$

$$= S_{0,k} + c^2 \left. \frac{\partial \boldsymbol{M}_k}{\partial \boldsymbol{X}_k} \right|_{\boldsymbol{F}_{k,l(k)}\left(\boldsymbol{X}^*_{l(k)}\right)} \begin{bmatrix} O & \Phi_{k,l(k)} \end{bmatrix} \Sigma_{\boldsymbol{Z}_{l(k)}} \begin{bmatrix} O & \Phi_{k,l(k)} \end{bmatrix}^{\mathsf{T}} \left. \frac{\partial \boldsymbol{M}_k}{\partial \boldsymbol{X}_k} \right|^{\mathsf{T}}_{\boldsymbol{F}_{k,l(k)}\left(\boldsymbol{X}^*_{l(k)}\right)}. \tag{4.65}$$

The accuracy becomes worse when the true probability distribution moves away from the Gaussian distribution due to the strong nonlinearity of the dynamics. However, when considering a problem such as the one in this study, in which the states are guided to a certain point, the probability distribution is often close to the Gaussian distribution, making it applicable to a wide range of problems.

4.3.2 Monte Carlo method

Each of the particles $\boldsymbol{Z}^{(n)}$ is propagated by state quantity propagation equations (Eqs. (4.12) to (4.31)). It requires a large number of particles to accurately approximate the probability distribution, and the computational cost is much higher than that of the Gaussian approximation method. In order to reduce the computational cost, instead

of using the equation for propagation of random variables, a method of propagation using a surrogate model such as Polynomial Chaos Expansion (PCE) or State Transition Tensor (STT) has been proposed.[35]-[39]

4.3.3 Initial Distribution

In this research, there are two ways of assuming the initial distribution depending on the phase of solving the problem. In this section, the Gaussian approximation method is used as an example for explanation.

$$\boldsymbol{Z}_0 \sim \mathcal{N}\left(\begin{bmatrix} \boldsymbol{\mu}_{X_0} \\ \boldsymbol{\mu}_{\widehat{X}_0} \end{bmatrix}, \begin{bmatrix} \Sigma_{X_0} & O \\ O & \Sigma_{\widehat{X}_0} \end{bmatrix}\right). \tag{4.66}$$

The first is the case where the optimization problem is solved before launch. In this case, the distributions of the true and the estimated state are assumed to follow the initial distribution according to the launch error, respectively.

$$\boldsymbol{\mu}_{X_0} = \boldsymbol{\mu}_{\widehat{X}_0} = \overline{\boldsymbol{\mu}}_0 \tag{4.67}$$

$$\Sigma_{X_0} = \Sigma_{\widehat{X}_0} = \overline{\Sigma}_0. \tag{4.68}$$

The second case is to optimize the problem again after the spacecraft is launched and the orbit determination is conducted. In this case, the initial estimated state is considered to be a non-distributed quantity that is uniquely determined by the outcome of the orbit determination. The initial true state is considered to be a quantity that is distributed according to the belief of the orbit determination result.

$$\boldsymbol{\mu}_{\boldsymbol{X}_0} = \boldsymbol{\mu}_{\widehat{\boldsymbol{X}}_0} = \widehat{\boldsymbol{X}}_0 \tag{4.69}$$

$$\Sigma_{\boldsymbol{X}_0} = P_0 \tag{4.70}$$

$$\Sigma_{\widehat{\boldsymbol{X}}_0} = O. \tag{4.71}$$

4.4 Computation of parameters of probability distributions of control

Like the state quantity, the probability distribution of control quantity can also be parameterized using Gaussian approximation or the Monte Carlo method. The parameters of the probability distribution are a function of the parameters of the probability distribution of the state quantity before control.

$$\boldsymbol{\theta}_{U_k} = \mathscr{M}_k\left(\boldsymbol{\theta}_{Z_k}^-\right), \tag{4.72}$$

where $\mathscr{M}$ is a function calculating $\boldsymbol{\theta}_{U_k}$ from $\boldsymbol{\theta}_{Z_k}^-$ derived from $\boldsymbol{M}$.

Although there are variations in the form of $\mathscr{M}$ depending on the parameterization method, the same method as uncertainty propagation described in the previous section can be used.

4.5 Objective Functions

The objective function (Eq. (3.20)) is the expected value of ΔV needed for the trajectory correction. Even if the Gaussian approximation method is used, the expected value of the 2-norm of the control vector cannot be calculated analytically from the parameters. Therefore, it is necessary to approximate the objective function, and there are two main possible methods to approximate the objective function.

4.5.1 Jensen's Inequality

When the probability distribution of the control quantity is given by the Gaussian approximation method, the upper bound on the objective function can be calculated by using Jensen's inequality, and this method uses that upper bound as the objective function.

Jensen's inequality holds for convex function $f(x)$,

$$f(\mathbb{E}[x]) \leq \mathbb{E}[f(x)]. \tag{4.73}$$

When $f(x) = x^2$ and $x = ||\boldsymbol{U}_k + \delta\boldsymbol{U}_k||_2$, this inequality become

$$(\mathbb{E}[||\boldsymbol{U}_k + \delta\boldsymbol{U}_k||_2])^2 \leq \mathbb{E}\left[(||\boldsymbol{U}_k + \delta\boldsymbol{U}_k||_2)^2\right] \tag{4.74}$$

$$\mathbb{E}[||\boldsymbol{U}_k + \delta\boldsymbol{U}_k||_2] \leq \sqrt{\mathbb{E}\left[(||\boldsymbol{U}_k + \delta\boldsymbol{U}_k||_2)^2\right]} = \sqrt{(||\mathbb{E}[\boldsymbol{U}_k + \delta\boldsymbol{U}_k]||_2)^2 + \mathrm{tr}(\mathbb{V}[\boldsymbol{U}_k + \delta\boldsymbol{U}_k])}. \tag{4.75}$$

Therefore, in this method, the right-hand side of the equation is regarded as a new objective function to be minimized. This objective function is computationally inexpensive and can be handled easily. It is a good method to obtain an approximate solution for the true optimization, but since it does not minimize the true objective function, a better calculation method is necessary to obtain the true optimal solution, as explained in the next section.

4.5.2 Monte Carlo method

Monte Carlo methods are used to directly approximate the true objective function. It can calculate the true objective function more accurately than the upper bound of Jensen's inequality.

$$\mathbb{E}[||\boldsymbol{U}_k + \delta\boldsymbol{U}_k||_2] \approx \frac{1}{N}\sum_{n=1}^{N} ||\boldsymbol{U}_k^{(n)} + \delta\boldsymbol{U}_k^{(n)}||_2. \tag{4.76}$$

For the Gaussian approximation method, the method is to generate samples from the probability distribution of $\boldsymbol{U}_k + \delta\boldsymbol{U}_k$ and to calculate the mean of the 2-norm of the values of the samples. This method requires a large number of samples to improve the accuracy, but even with a large number of samples, it can be computed relatively fast by parallel computing using graphical processing units.

When the Monte Carlo method is employed for propagating the probability distribution, it is possible to directly approximate the probability distribution of $\|\boldsymbol{U}_k + \delta\boldsymbol{U}_k\|_2$ and thus calculate the objective function.

4.6 Constraints

4.6.1 Chance Constraint on State

The chance constraint on state quantities is formulated as a function of the parameters of the probability distribution.

$$\boldsymbol{C}_Z\left(\boldsymbol{\theta}_{Z_i}\right) \leq \boldsymbol{0}. \tag{4.77}$$

The method of the formulation depends on the chance constraints themselves, and it is necessary for them to be formulated accordingly.

An example of a chance constraint is that the probability of a state quantity being within a certain region is greater than a certain value.[42]-[48]

$$P\left(\boldsymbol{X} \in S\right) \geq 1 - \Delta. \tag{4.78}$$

This chance constraint can be transformed into the following condition when $\boldsymbol{X}$ follows a Gaussian distribution, $\boldsymbol{X} \sim \mathcal{N}\left(\boldsymbol{\mu}_X, \Sigma_X\right)$, and S is affine to $\boldsymbol{X}$, $S = \{\boldsymbol{X} \mid \boldsymbol{a}^\mathsf{T}\boldsymbol{X} + b \leq 0\}$.

$$\boldsymbol{a}^\mathsf{T}\boldsymbol{\mu}_X + b + \Psi\left(1 - \Delta\right)\sqrt{\boldsymbol{a}^\mathsf{T}\Sigma_X\boldsymbol{a}} \leq 0. \tag{4.79}$$

where $\Psi(\cdot)$ is the inverse function of the standard Gaussian cumulative distribution function.

When the Monte Carlo method is adopted, the chance constraint is formulated that the percentage of particles that satisfy the constraint is larger than the threshold.

$$\sum_{n=1}^{N} \frac{\delta^{(n)}}{N} \geq 1 - \Delta \tag{4.80}$$

$$\delta^{(n)} = \begin{cases} 1 & \boldsymbol{X}^{(n)} \in S \\ 0 & otherwise \end{cases} \tag{4.81}$$

In addition to the single chance constraint, the joint chance constraint can also be considered.

$$P\left(\wedge_j \boldsymbol{X} \in S_j\right) \geq 1 - \Delta. \tag{4.82}$$

For all individual constraints, the following inequality is assumed.

$$P\left(\boldsymbol{X} \in S_j\right) \geq 1 - \Delta_j \tag{4.83}$$

$$\Leftrightarrow P\left(\boldsymbol{X} \notin S_j\right) \leq \Delta_j. \tag{4.84}$$

By using Boole's inequality,

$$P\left(\vee_j \boldsymbol{X} \notin S_j\right) \leq \sum_j P\left(\boldsymbol{X} \notin S_j\right) \leq \sum_j \Delta_j. \tag{4.85}$$

Therefore, if $\sum_j \Delta_j \leq \Delta$ holds,

$$P\left(\wedge_j \boldsymbol{X} \in S_j\right) = 1 - P\left(\vee_j \boldsymbol{X} \notin S_j\right) \geq 1 - \sum_j \Delta_j \geq 1 - \Delta. \tag{4.86}$$

4.6.2 Terminal Constraint on Final State

The constraint on the guidance accuracy for the state at the final time can be set in the chance constraint, but, in this study, it is assumed to be the condition on the mean and

the covariance matrix of the final state, referring to the Covariance Control.[42]

$$\mathbb{E}\left[\boldsymbol{X}_f\right] = X_f^* \tag{4.87}$$

$$\mathbb{V}\left[\boldsymbol{X}_f\right] \preceq \overline{\Sigma_{\boldsymbol{X}_f}} \tag{4.88}$$

4.6.3 Constraint on Optimization Variables

Examples of constraints about optimization variables, trajectory correction and orbit determination timings, are the minimum intervals between orbit determination timings and the fixed cut-off time of orbit determination before trajectory correction,

$$t_l - t_{l-1} \geq \delta t_{od} \tag{4.89}$$

$$t_k - t_{l(k)} = \delta t_{cf} \tag{4.90}$$

$$t_l \leq t_{l(k)} - \delta t_{\mathrm{od}} \text{ or } t_l \geq t_k + \delta t_{od}, \tag{4.91}$$

where δt_{od} is the minimal interval of the orbit determination. Equation (4.91) can be converted into the following equation of a nonlinear constraint.

$$\min\left(t_l - \left(\left(t_{l(k)} - \delta t_{\mathrm{od}}\right), t_k - t_l\right) \leq 0. \right. \tag{4.92}$$

4.7 Numerical Optimization Algorithm

In the formulation of this study, the numerical optimization algorithm to be used is constrained nonlinear programming. Sequential Quadratic Programming (SQP), Generalized Pattern Search (GPS), and Genetic Algorithm (GA) are used in the simulation of this study.[49]

SQP is an optimization method that solves quadratic programming subproblems iteratively. SQP requires that the objective function and the constraints are twice continuously differentiable. However, since the objective function in this research is discontinuous when the TCM timings change over the orbit determination timings because of an instant change of covariance matrix of Kalman Filter, SQP cannot handle

such a change of TCM timings.

GPS is an optimization method that does not require information on the gradient of the objective function. The objective function can be discontinuous and non-differentiable, and it can handle linear and non-linear constraints on the optimization variables. Because of the discontinuity of the objective function in this study, GPS can be suitable as the optimization method. However, GPS requires much computational time and function evaluation, it is not appropriate for optimizing local change of which SQP is good at optimization. Therefore, it seems that a combination of GPS and SQP would be a good idea.

In particular problems, GA can be useful in terms of global optimization. When the number of optimization variables is large, the calculation of GA takes a lot of time. In this study, since both the TCM time and the orbit determination time are optimized, the number of optimization variables is large, which makes the use of GA difficult. However, it is possible to reduce the number of optimization variables by, for example, assuming that the orbit determination time is placed with a fixed time interval just before the orbit determination, and using the number of orbit determination just before each TCM as the optimization variable instead of the orbit determination time. Since GA can also handle mixed-integer programming, applying GA to the optimization problem with the TCM time and the corresponding number of orbit determination can be considered.

4.8 Transcription of Deterministic Optimization Problem

In summary, the stochastic optimization problem (Eqs. (3.20) to (3.25)) can be transformed into the following deterministic optimization problem. This optimization problem is solved by using the numerical algorithm.

$$\underset{t_k \in \mathcal{T}_k,\ t_l \in \mathcal{T}_l}{\text{minimize}} \quad \frac{1}{N} \sum_{k}^{N_k} \sum_{n=1}^{N} \| \boldsymbol{U}_k^{(n)} + \delta \boldsymbol{U}_k^{(n)} \|_2 \tag{4.93}$$

$$\text{subject to} \quad \boldsymbol{\theta}_{Z_i} = \mathscr{F}_{i,i-1} \left(\boldsymbol{\theta}_{Z_{i-1}} \right) \tag{4.94}$$

$$\boldsymbol{\theta}_{Z_0} = \bar{\boldsymbol{\theta}}_{Z_0} \tag{4.95}$$

$$\boldsymbol{\theta}_{U_k} = \mathscr{M}_k \left(\boldsymbol{\theta}_{Z_k}^{-} \right) \tag{4.96}$$

$$\boldsymbol{C}_Z \left(\boldsymbol{\theta}_{Z_i} \right) \leq \mathbf{0} \qquad t_i \in \mathcal{T} \tag{4.97}$$

$$\boldsymbol{C} \left(t_k,\ t_l \right) \leq \mathbf{0}. \tag{4.98}$$

Chapter 5

Numerical Simulations

Knowledge is of no value unless you put it into practice.

Anton Chekhov

In this chapter, the validity of the proposed method was demonstrated by numerical simulations. First, the methods of uncertainty propagation were compared for various trajectories. Next, the optimization was performed for a simple problem of Hohmann Transfer trajectory in the two-body problem. Finally, the proposed method was applied to the real problem about the nominal trajectory of PROCYON.

5.1 Assumptions

The assumptions in the numerical simulation are explained in this section.

5.1.1 State Variables

In the numerical simulation of this study, the position and velocity of the spacecraft were considered as state quantities.

$$\boldsymbol{X} = \left[\boldsymbol{R}^{\mathsf{T}}\ \boldsymbol{V}^{\mathsf{T}}\right]^{\mathsf{T}} \tag{5.1}$$

$$\widehat{\boldsymbol{X}} = \left[\widehat{\boldsymbol{R}}^{\mathsf{T}}\ \widehat{\boldsymbol{V}}^{\mathsf{T}}\right]^{\mathsf{T}} \tag{5.2}$$

$$\boldsymbol{Z} = \left[\boldsymbol{X}^{\mathsf{T}}\ \widehat{\boldsymbol{X}}^{\mathsf{T}}\right]^{\mathsf{T}}. \tag{5.3}$$

5.1.2 Control Strategy

The control law for trajectory correction was FTA guidance law as stated in Chapter 2. The control was applied to the orbit determination value at the trajectory correction time, and the control was such that the position of the orbit determination value coincides with the position of the nominal trajectory when it was propagated to the final time.

5.1.3 Dynamics and Observation

The dynamics used in the numerical simulations were the two-body problem (TBP), the circular restricted three-body problem (CRTBP), and the n-body problem with ephemeris. MATLAB ode113 was used for propagation of the TBP and CRTBP, and jTOP propagator was used for propagation of the n-body problem.[50] In the n-body problem, solar radiation pressure was also taken into account.

The observational model is assumed to acquire the whole state quantities directly for simplicity's sake.

$$\boldsymbol{G}(\boldsymbol{X}_l) = \boldsymbol{X}_l. \tag{5.4}$$

5.1.4 Probability Distribution of Errors

The following Gaussian distribution was assumed for the initial state, dynamics, observation, and control errors. These errors were assumed to be independent of each other.

$$\boldsymbol{Z}_0 \sim \mathcal{N}\left(\begin{bmatrix} \boldsymbol{\mu}_{X_0} \\ \boldsymbol{\mu}_{\widehat{X}_0} \end{bmatrix}, \begin{bmatrix} \Sigma_{X_0} & O \\ O & \Sigma_{\widehat{X}_0} \end{bmatrix}\right) \tag{5.5}$$

$$\delta \boldsymbol{w}_{i,i-1} \sim \mathcal{N}(\boldsymbol{0}, Q_{i,i-1}) \tag{5.6}$$

$$\boldsymbol{\varepsilon}_l \sim \mathcal{N}(\boldsymbol{0}, R_l) \tag{5.7}$$

$$\delta \boldsymbol{U}_k \sim \mathcal{N}(\boldsymbol{0}, S_k). \tag{5.8}$$

5.1.5 Dynamics Error

The dynamics error was an equation that is a solution of a linear stochastic differential equation as discussed in Chapter 4. In the equation, the calculation of the time integral of the state transition matrix (STM) is complicated.

One approximation method is to divide the integration time and assume that the dynamics are time-invariant at that time.[21]

$$Q_{i,i-1} = \int_{t_{i-1}}^{t_i} \Phi_{t_i,\tau} Q \Phi_{t_i,\tau}^{\mathsf{T}} d\tau \tag{5.9}$$

$$= \sum_{j=0}^{N-1} \Phi_{t_i,t_{i,j+1}} \left(\int_{t_{i,j}}^{t_{i,j+1}} \Phi_{t_{i,j+1},\tau} Q \Phi_{t_{i,j+1},\tau}^{\mathsf{T}} d\tau \right) \Phi_{t_i,t_{i,j+1}}^{\mathsf{T}} \quad (t_{i,0} = t_{i-1}, t_{i,N} = t_i). \tag{5.10}$$

Between $t_{i,j}$ and $t_{i,j+1}$, the linearized dynamics is assumed as time-invariant,

$$d\boldsymbol{x} = A\boldsymbol{x}dt \tag{5.11}$$

$$\Phi_{t,\tau} = \exp\left(A\left(t-\tau\right)\right) \tag{5.12}$$

$$\Phi_{t,\tau}^{\mathsf{T}} = \exp\left(A^{\mathsf{T}}\left(t-\tau\right)\right) \tag{5.13}$$

$$A = A\left(t_{i,j}\right). \tag{5.14}$$

And here, we have the following theorem [52]

$$\exp\left(\begin{bmatrix} A & Q \\ O & -A^{\mathsf{T}} \end{bmatrix} t'\right) = \begin{bmatrix} \exp\left(At'\right) & \mathcal{G}\left(t'\right) \\ O & \exp\left(-A^{\mathsf{T}}t'\right) \end{bmatrix} \tag{5.15}$$

$$\mathcal{G}\left(t'\right) = \int_0^{t'} \exp\left(A\left(t'-s\right)\right) Q \exp\left(-A^{\mathsf{T}}s\right) ds, \tag{5.16}$$

and substituting $t' = t_{i,j+1} - t_{i,j}$ and $s = \tau - t_{i,j}$, then,

$$\mathcal{G}_j = \int_{t_{i,j}}^{t_{i,j+1}} \exp\left(A\left(t_{i,j+1} - \tau\right)\right) Q \exp\left(A^{\mathsf{T}}\left(t_{i,j} - \tau\right)\right) d\tau \tag{5.17}$$

$$= \int_{t_{i,j}}^{t_{i,j+1}} \Phi_{t_{i,j+1},\tau} Q \Phi_{t_{i,j},\tau}^{\mathsf{T}} d\tau, \tag{5.18}$$

and

$$\int_{t_{i,j}}^{t_{i,j+1}} \Phi_{t_{i,j+1},\tau} Q \Phi_{t_{i,j+1},\tau}^{\mathsf{T}} d\tau = \mathcal{G}_j \Phi_{t_{i,j+1},t_{i,j}}^{\mathsf{T}}. \tag{5.19}$$

Therefore, the dynamics error can be calculated as follows.

$$Q_{i,i-1} \approx \sum_{j=0}^{N-1} \Phi_{t_i,t_{i,j+1}} \left(\mathcal{G}_j \exp\left(A\left(t_{i,j}\right)^{\mathsf{T}}\left(t_{i,j+1} - t_{i,j}\right)\right)\right) \Phi_{t_i,t_{i,j+1}}^{\mathsf{T}}. \tag{5.20}$$

Another simple approximation method is that the STM of constant velocity linear motion is used instead of the exact STM.

$$\Phi_{i,\tau} \approx \begin{bmatrix} I & (t_i - \tau) I \\ 0 & I \end{bmatrix} \tag{5.21}$$

$$Q_{i,i-1} \approx \begin{bmatrix} \frac{1}{3}(t_i - t_{i-1})^3 Q' & \frac{1}{2}(t_i - t_{i-1})^2 Q' \\ \frac{1}{2}(t_i - t_{i-1})^2 Q' & (t_i - t_{i-1}) Q' \end{bmatrix} \tag{5.22}$$

$$Q = \begin{bmatrix} O & O \\ O & Q' \end{bmatrix}. \tag{5.23}$$

5.1.6 Constraints

The constraints on the final guidance accuracy, the trajectory correction time, and orbit determination time were the Eqs. (4.89), (4.90), and (4.92).

5.2 Numerical Simulations of Uncertainty Propagation

5.2.1 Conditions

Three different propagation methods were applied to the two trajectories, and the magnitudes of the mean and covariance of the state quantities and ΔV were evaluated and compared. The propagation methods were linear approximation, the Monte Carlo method with PCE (100,000 samples), and the ordinary Monte Carlo method (100,000 samples). The number of samples used for the evaluation of the objective function at the linear approximation method was 10,000,000. The two types of trajectories are shown in Table 5.1 and 5.2. Case 1 is a TBP with an Earth-Mars Hohmann transfer trajectory, and case 2 is a CRTBP of the Saturn-Titan system with a swing-by trajectory to Titan.

Table 5.1: Simulation parameter settings for case 1.

Variables	Values
$\boldsymbol{R}_0^*$, $\boldsymbol{\mu}_{\boldsymbol{R}_0}$, $\boldsymbol{\mu}_{\widehat{\boldsymbol{R}}_0}$	[0.00, -1.49e8, 0.00]$^\mathsf{T}$ km
$\boldsymbol{V}_0^*$, $\boldsymbol{\mu}_{\boldsymbol{V}_0}$, $\boldsymbol{\mu}_{\widehat{\boldsymbol{V}}_0}$	[0.00, 32.7, 0.00]$^\mathsf{T}$ km/s
dynamics	Two-Body
μ_{tbp}	1.327e11 km^3/s^2
t_f	258.9 days
$\Sigma_{\boldsymbol{R}_0}$, $\Sigma_{\widehat{\boldsymbol{R}}_0}$ (1σ)	1000 km
$\Sigma_{\boldsymbol{V}_0}$, $\Sigma_{\widehat{\boldsymbol{V}}_0}$ (1σ)	1.00e-3 km/s
N_k	4
t_k	[11.57 92.59 173.31 254.63] days
S_0 (1σ)	2.00e-5 km/s
Q (1σ)	1.26e-14 km^2/s^3
δt_{od}	7 days
$R_{\boldsymbol{R}}$ (1σ)	100.0 km
$R_{\boldsymbol{V}}$ (1σ)	1.00e-4 km/s

5.2.2 Results

The simulation results are shown in Figs. 5.1, 5.2, 5.3, and , 5.4 and Table 5.3 and 5.4. The ratio of the standard deviation of the position and velocity and the mean and standard deviation of ΔV are shown when compared to the usual Monte Carlo method.

Table 5.2: Simulation parameter settings for case 2.[51]

Variables	Values
$\boldsymbol{R}_0^*$, $\boldsymbol{\mu}_{\boldsymbol{R}_0}$, $\boldsymbol{\mu}_{\widehat{\boldsymbol{R}}_0}$	$[3.19e5,\ -6.97e5,\ -1.86e4]^\mathsf{T}$ km
$\boldsymbol{V}_0^*$, $\boldsymbol{\mu}_{\boldsymbol{V}_0}$, $\boldsymbol{\mu}_{\widehat{\boldsymbol{V}}_0}$	$[3.74,\ 3.47,\ -0.253]^\mathsf{T}$ km/s
dynamics	CRTBP
μ_{crtbp}	2.366e-4
t_f	19 days
$\Sigma_{\boldsymbol{R}_0}$, $\Sigma_{\widehat{\boldsymbol{R}}_0}$ (1σ)	100 km
$\Sigma_{\boldsymbol{V}_0}$, $\Sigma_{\widehat{\boldsymbol{V}}_0}$ (1σ)	1.00e-4 km/s
N_k	6
t_k	[4.0 6.8 9.6 12.4 15.2 18.0] days
S_0 (1σ)	2.00e-5 km/s
Q (1σ)	1.26e-14 km^2/s^3
δt_{od}	0.5 days
$R_{\boldsymbol{R}}$ (1σ)	100.0 km
$R_{\boldsymbol{V}}$ (1σ)	1.00e-6 km/s

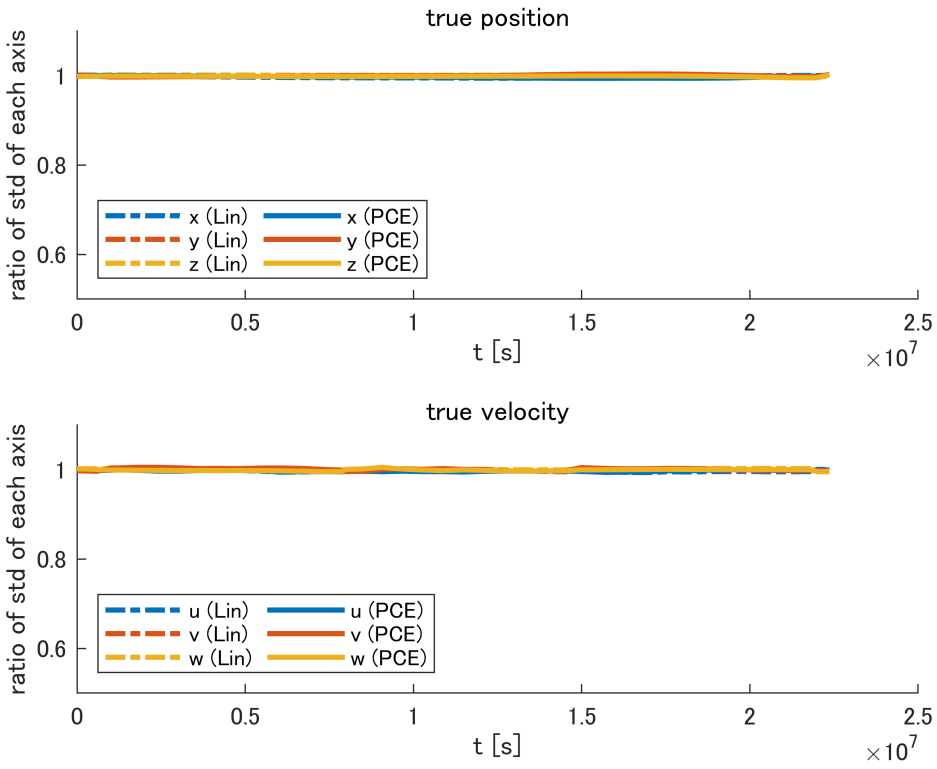

Figure 5.1: Ratio of the standard deviation of true position and velocity compared to normal Monte Carlo at case 1.

Table 5.3: Ratio of ΔV mean compared with Monte Carlo of case 2.

Method	TCM1	TCM2	TCM3	TCM4
Lin	0.9992	0.9957	0.9996	0.9981
PCE	0.9977	0.9974	0.9994	0.9973

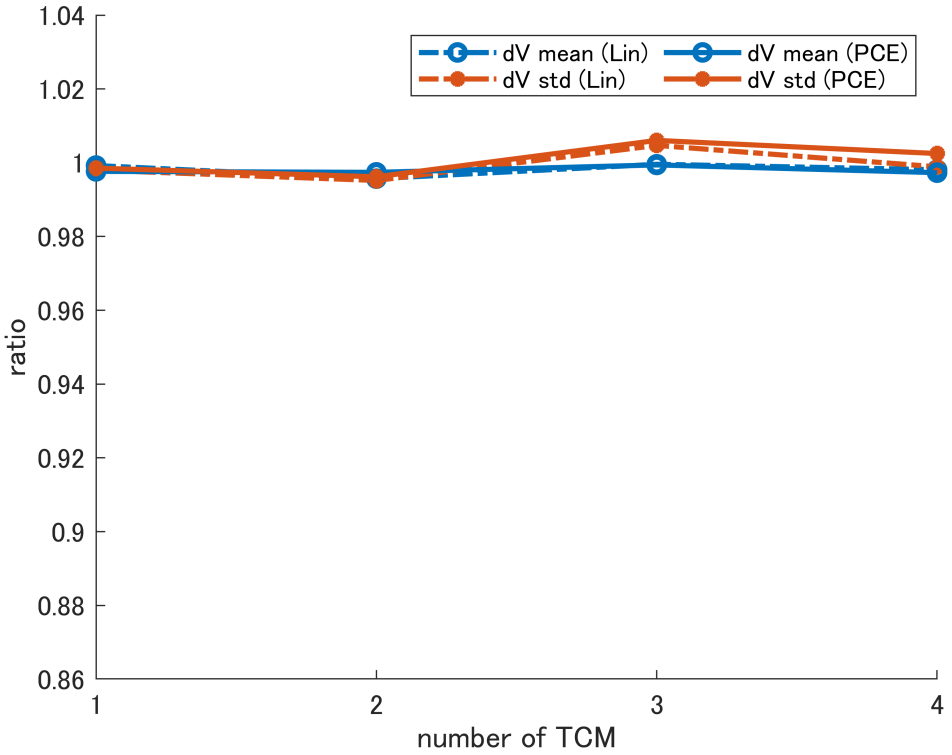

Figure 5.2: Ratio of the mean and standard deviation of ΔV compared to normal Monte Carlo at case 1.

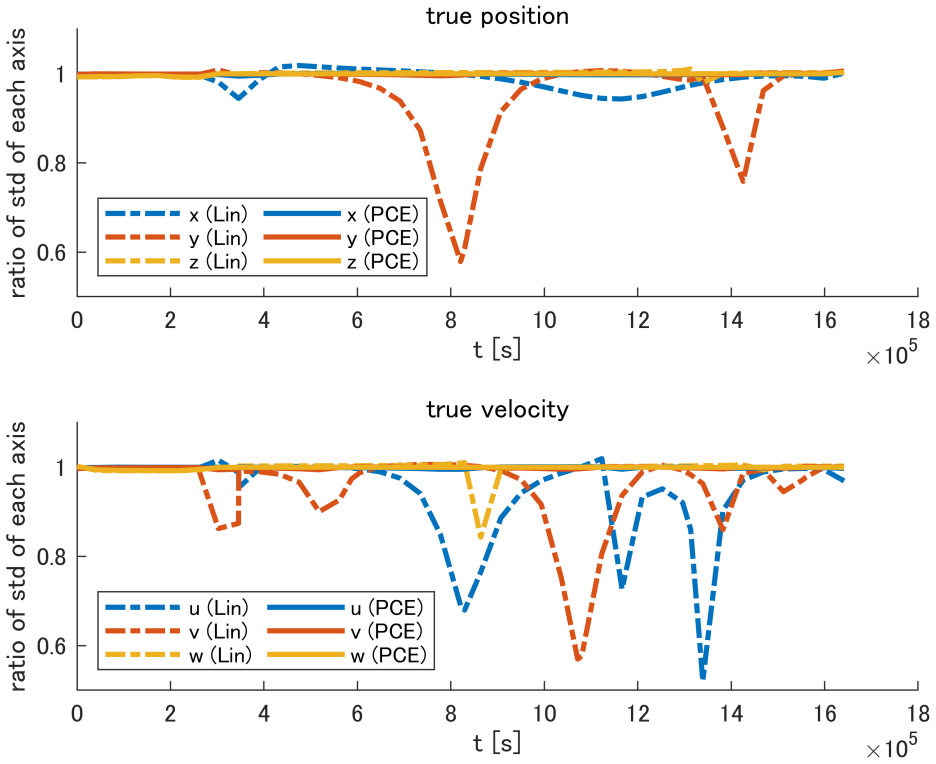

Figure 5.3: Ratio of the standard deviation of true position and velocity compared to normal Monte Carlo at case 2.

Table 5.4: Ratio of ΔV mean compared with Monte Carlo of case 2.

Method	TCM1	TCM2	TCM3	TCM4	TCM5	TCM6
Lin	0.9650	0.9987	0.9993	0.9994	0.9921	0.9987
PCE	0.9977	0.9989	0.9998	0.9997	0.9982	0.9990

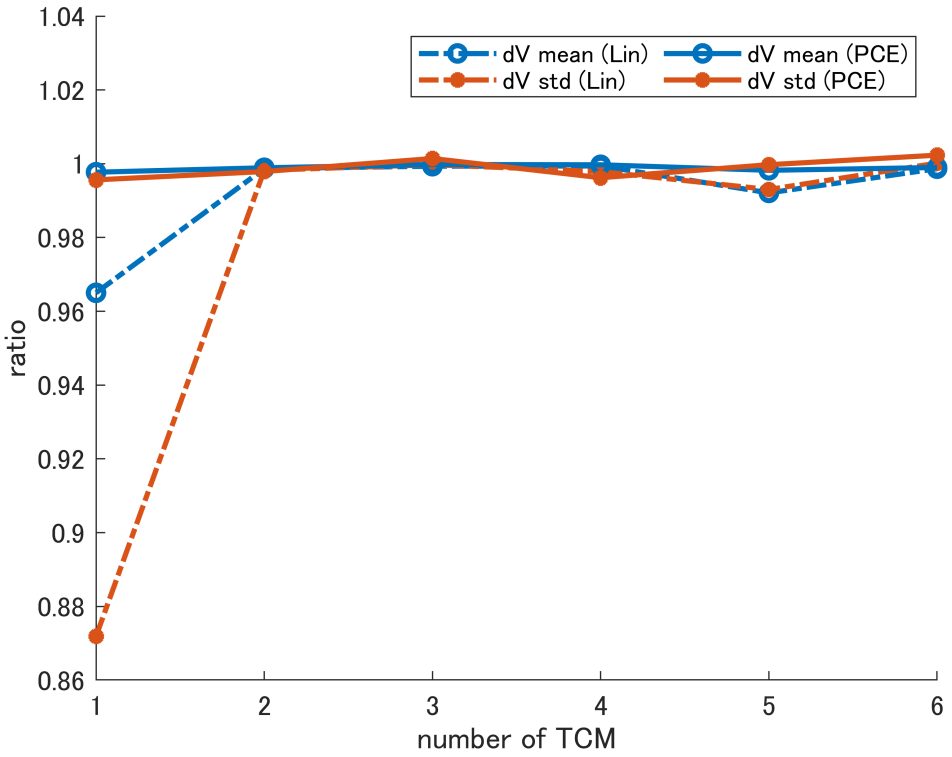

Figure 5.4: Ratio of the mean and standard deviation of ΔV compared to normal Monte Carlo at case 2.

5.2.3 Discussion

The simulation results show that for the TBP (case 1), there was almost no difference between the linear approximation and the PCE, and both results were in good agreement with the usual Monte Carlo method and their difference were less than 1%. The reason for the small error is that the two-body problem is weakly nonlinear, and the deviation of state was sufficiently small for the scale of the trajectory.

For the CRTBP (case 2), the error in the linear approximation was quite large for position and velocity, while the error of PCE was sufficiently small. As for ΔV, while the error for the first time was large in the linear approximation, it was as small as PCE after the second time. The reason why the error of ΔV was smaller than that of the state is that the error of the state in the direction of the maximum principal axis,

which has a large impact on the error of ΔV, was smaller than that in other principal axes.

The reason why the error of the first ΔV was large and became small after the second ΔV is thought to be that at the time of the first ΔV, the error increased due to the swing-by and the distribution of the state and control deviated greatly from the Gaussian distribution, but after the second ΔV, the distribution became closer to the Gaussian distribution because later TCMs was planned to cancel relatively small errors of dynamics error, orbit determination error, and control error as discussed in Chapter 2. Figure 5.5 shows the distribution of the control at the time of the first and sixth TCM for the normal Monte Carlo method. As shown in Fig. 5.5, at the time of the first TCM, the distribution deviated from the Gaussian distribution.

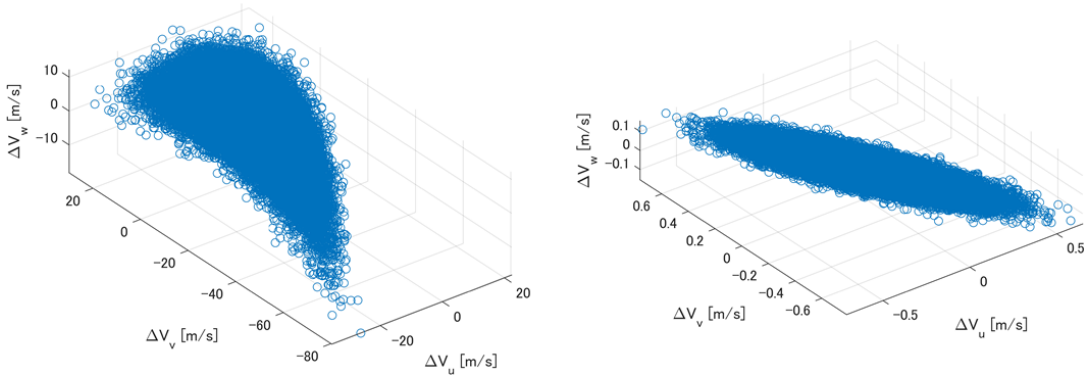

Figure 5.5: Result of normal Monte Carlo simulation of case 2. The left and right figure show the control vector of the first and sixth control, respectively.

These results indicate that a highly accurate approximation method is necessary for trajectories with strong nonlinearity, such as swing-by trajectories in the CRTBP. However, because of the effect that the TCMs prevent deviation of trajectory, a linear approximation would be sufficient for a wide range of problems.

5.3 Numerical Simulations of Optimization Case 1: Two-Body Problem

As an example of optimization simulation, a simple case of a two-body problem was solved. First, various methods of the optimization algorithm were tested and com-

pared. Next, a sensitivity analysis was performed to investigate the effects of varying various uncertainty parameters on the optimization variables and objective function.

5.3.1 Conditions

The table 5.5 shows the simulation parameters. The optimization method is shown in Table 5.6.

Table 5.5: Simulation parameter settings for optimization case 1.

Variables	Values
$\boldsymbol{R}_0^*$, $\boldsymbol{\mu}_{\boldsymbol{R}_0}$, $\boldsymbol{\mu}_{\widehat{\boldsymbol{R}}_0}$	[0.00, -1.49e8, 0.00]$^\mathsf{T}$ km
$\boldsymbol{V}_0^*$, $\boldsymbol{\mu}_{\boldsymbol{V}_0}$, $\boldsymbol{\mu}_{\widehat{\boldsymbol{V}}_0}$	[0.00, 32.7, 0.00]$^\mathsf{T}$ km/s
dynamics	Two-Body
μ_{tbp}	1.327e11 km^3/s^2
t_f	258.9 days
$\Sigma_{\boldsymbol{R}_0}$, $\Sigma_{\widehat{\boldsymbol{R}}_0}$ (1σ)	1000 km
$\Sigma_{\boldsymbol{V}_0}$, $\Sigma_{\widehat{\boldsymbol{V}}_0}$ (1σ)	1.00e-3 km/s
N_k	6
N_l	18
$\delta R_{\mathrm{th},f}$	120 km
S_0 (1σ)	2.00e-5 km/s
c	0.01
Q (1σ)	1.26e-14 km^2/s^3
$R_{\boldsymbol{R}}$ (1σ)	100.0 km
$R_{\boldsymbol{V}}$ (1σ)	1.00e-4 km/s

Table 5.6: Optimization Methods.

Opt. Method No.	Algorithm	Opt. Variables	Remarks
1	SQP	t_k	t_l is fixed.
2	GPS	t_k	t_l is fixed.
3	SQP	t_k and t_l	
4	GPS	t_k and t_l	
5	GPS and SQP	t_k and t_l	
6	SQP	t_k	$N_{od,k}$ is fixed.
7	GA	t_k and $N_{od,k}$	
8	SQP	t_k and $N_{od,k}$	$N_{od,k}$ is changed in outer loop.

In optimization methods 1 and 2, only the TCM time was optimized. Optimization methods 3, 4, and 5 optimize both TCM time and orbit determination time. In optimization method 5, optimization was done by GPS and then by SQP. In optimization method 6, only the TCM time was optimized, assuming that it was optimal for the orbit determination time to come just before the TCM time. In this method, the number

of orbit determination to be performed just before each TCM was fixed. Optimization methods 7 and 8 optimize the TCM time and the number of orbit determination immediately before each TCM. In optimization method 7, both of them were combined and optimized by GA. In optimization method 8, the optimization was divided into an outer loop that changes the number of orbit determination and an inner loop that optimizes the TCM time. The inner loop was consistent with the optimization method 6.

In all cases, Jensen's inequality was used as the objective function of the optimization to speed up the computation, and the Monte Carlo method (10,000,000 samples) was used in the evaluation of the optimal solution.

5.3.2 Results

Figure 5.6 shows the TCM time in each optimization result. Figure 5.7 and Table 5.7 show the ΔV required for TCM in each case.

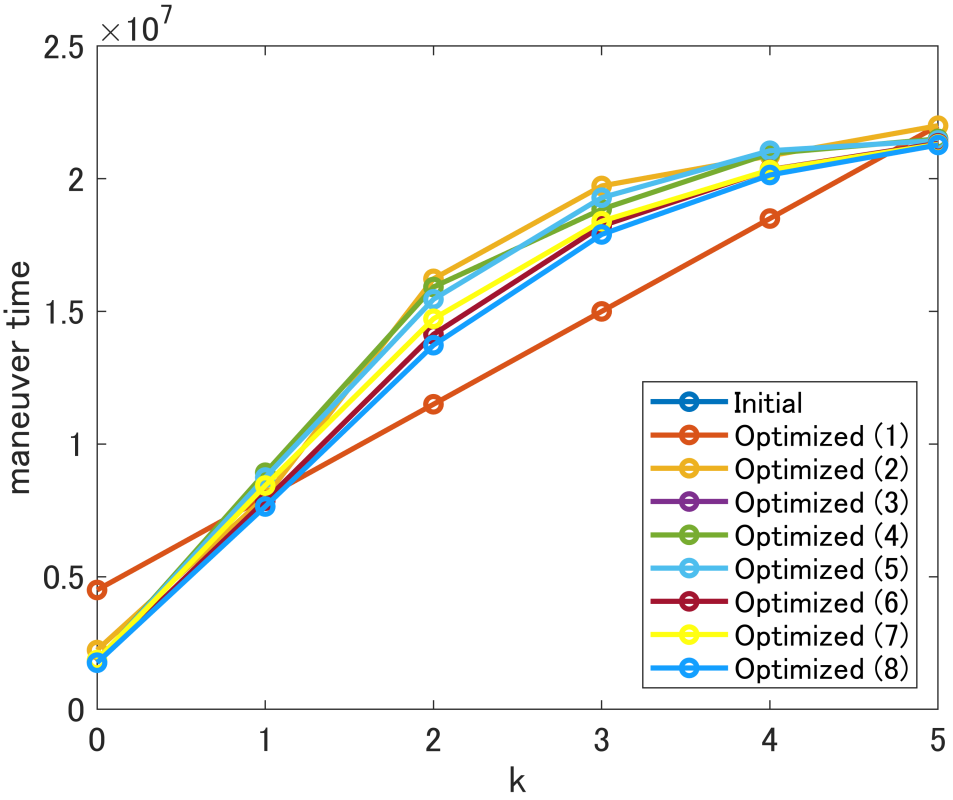

Figure 5.6: TCM timing of optimization results.

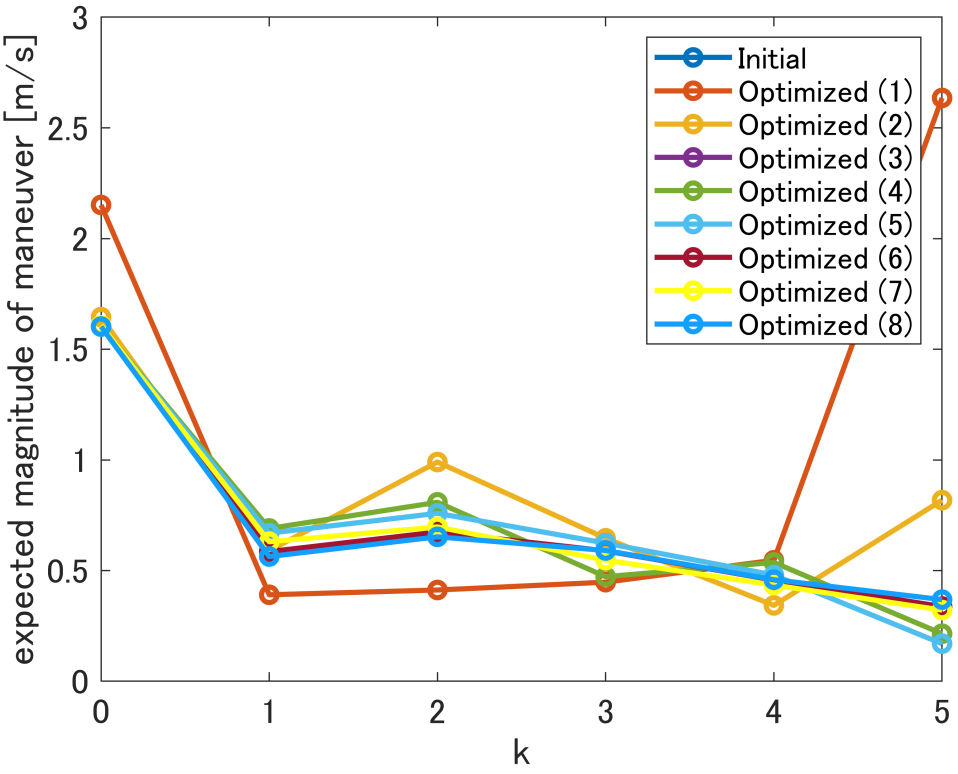

Figure 5.7: Expected value of ΔV of optimization results.

Table 5.7: Expected value of ΔV of optimization results [m/s].

Opt. Method No.	TCM1	TCM2	TCM3	TCM4	TCM5	TCM6	Total
1	2.1518	0.3908	0.4123	0.4477	0.5466	2.6351	6.5842
2	1.6451	0.5902	0.9904	0.6461	0.3429	0.8182	5.0329
3	1.6028	0.5855	0.6744	0.5893	0.4572	0.3375	4.2467
4	1.6019	0.6904	0.8085	0.4725	0.5368	0.2148	4.3250
5	1.6032	0.6691	0.7588	0.6240	0.4800	0.1698	4.3049
6	1.6028	0.5857	0.6743	0.5892	0.4572	0.3375	4.2467
7	1.6079	0.6303	0.6972	0.5470	0.4345	0.3216	4.2385
8	1.6025	0.5636	0.6524	0.5908	0.4589	0.3688	4.2371

5.3.3 Discussion

As for the TCM times, the overall trend was similar except for case 1. In those cases, TCM1 to cancel the initial error and TCM6 to satisfy the terminal constraint were almost the same time. This indicates that although the large TCM1 was done at a time with large sensitivity and TCM6 was done at a time that satisfies the terminal constraint, the other TCMs have various local solutions that are similar but different in the balance of ΔV required for each TCM.

For optimization of TCM time only (case 1 and 2), GPS performed better than SQP. This is because SQP assumes the second-order differentiability of the objective function and the constraints on the TCM time and orbit determination time prevent the TCM time from changing beyond the orbit determination time. In contrast, since GPS can be applied to discontinuous objective functions, it was possible to change the TCM time beyond the orbit determination time and to search for a better solution that cannot be explored by SQP.

From the optimization results, it is found that the objective function can be significantly reduced by optimizing not only the TCM time but also the orbit determination time. This is evidence that the orbit determination accuracy has a significant impact on the size of the TCM.

In cases 3, 4, and 5, the solution using only SQP performed better. The difference between the case using only SQP and the case using both GPS and SQP is that in the former case, the number of orbit determination between TCM times does not change, while in the latter case, it may change. The reason why the former gave better results can be attributed to the fact that under the conditions of the present simulation, the SQP case happened to have a better distribution of orbit determination times in the initial solution, while the GPS case converged to a solution with a worse distribution of orbit determination times. Therefore, the superiority of these methods depends on the initial value, and it is difficult to make a general discussion. It is suggested that the use of GPS does not necessarily lead to a good solution in terms of varying the allocation of the number of orbit determination.

In cases 3, 4, and 5, almost all of the orbit determination were performed just before the TCM time. This is because it is more efficient to collect the orbit determination just before the TCM in order to reduce the navigation error at the TCM time. This result supports the assumption that the orbit determination time is placed just before the TCM time in cases 6, 7, and 8. Also, the results of case 3 and case 6 are consistent.

Among cases 6, 7 and 8, case 8 gave the best results. In case 7, due to the nature of GA, the solution is dominated by stochastic factors such as initial population and mu-

tation, and there is a possibility that the global minimum cannot be reached. In case 8, since the search for the number of orbit determination is a strategy that changes in the local direction, there is also a possibility that the global minimum cannot be reached depending on the problem, but the best results were obtained under the simulation conditions. The difference between the two cases is quite small and is not considered to be a major problem in practical use. However, these methods assume that the orbit determination time is placed just before the TCM time, and it cannot be easily applied when considering problems that place constraints on state deviations and orbit determination errors in the middle of the trajectory. It is better to use optimization methods such as case 3 and case 5 for such problems.

5.3.4 Sensitivity Analysis on Orbit Insertion Error

Conditions

In order to perform sensitivity analysis on the orbit insertion error, simulations using the optimization method 8 were performed by varying the orbit insertion error. The conditions other than the initial error were the same as in the table, with $\Sigma_{\boldsymbol{R}_0}$ set to 800 km, 600 km, 400 km, 200 km, and 100 km, and $\Sigma_{\boldsymbol{V}_0}$ set to 0.8 m/s, 0.6 m/s, 0.4 m/s, 0.2 m/s, and 0.1 m/s. In all cases, Jensen's inequality was used as the objective function of the optimization to speed up the computation, and the Monte Carlo method (10,000,000 samples) was used in the evaluation of the optimal solution.

Results

Figures 5.8 and 5.9 show the TCM time in each optimization result. Figures 5.10 and 5.11 and Table 5.8 show the ΔV required for TCM in each case. Table 5.9 shows the number of orbit determination for each TCM.

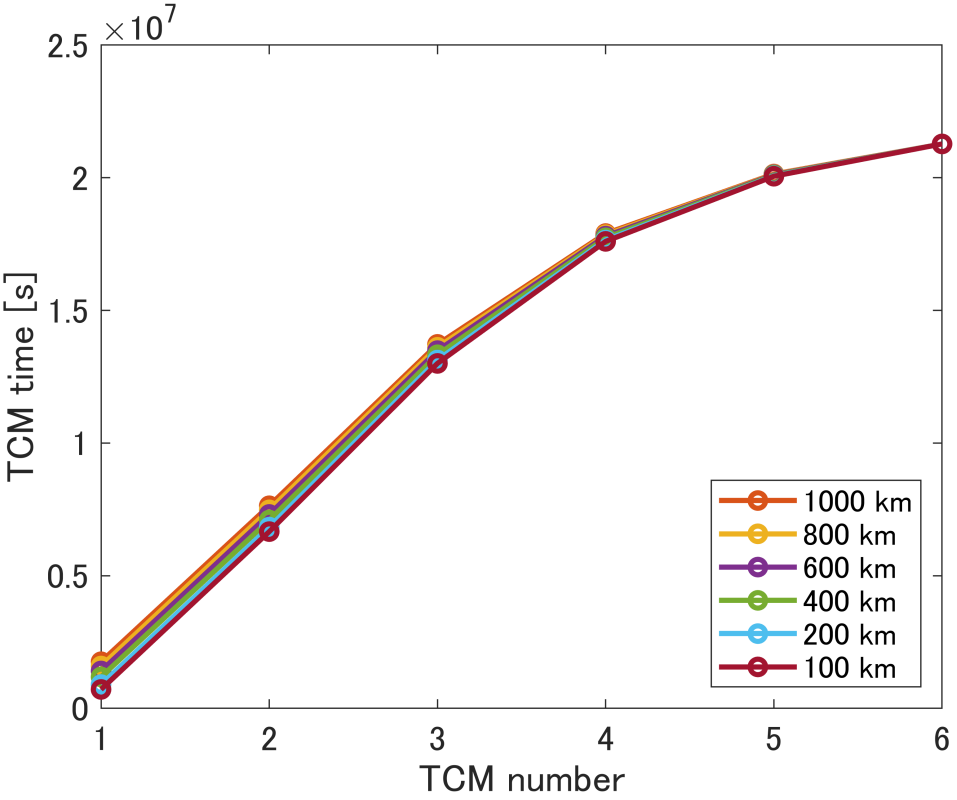

Figure 5.8: TCM timing of optimization results when initial position error was changed.

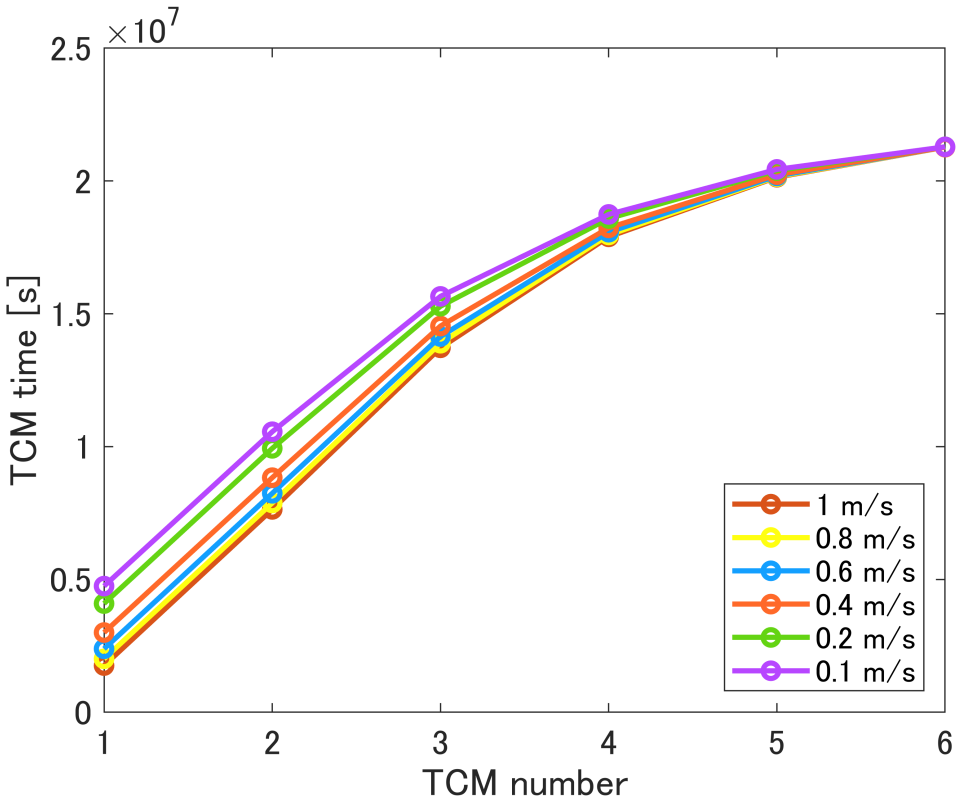

Figure 5.9: TCM timing of optimization results when initial velocity error was changed.

Table 5.8: Expected value of ΔV of optimization results when initial error was changed [m/s].

$\Sigma_{\boldsymbol{R}_0}$ and $\Sigma_{\boldsymbol{V}_0}$	TCM1	TCM2	TCM3	TCM4	TCM5	TCM6	Total
1000km, 1m/s	1.6025	0.5636	0.6524	0.5908	0.4589	0.3688	4.2371
800km, 1m/s	1.5443	0.5632	0.6547	0.5966	0.4637	0.3726	4.1950
600km, 1m/s	1.4852	0.5627	0.6568	0.6027	0.4687	0.3763	4.1523
400km, 1m/s	1.4243	0.5619	0.6592	0.6101	0.4748	0.3808	4.1111
200km, 1m/s	1.3598	0.5613	0.6621	0.6196	0.4826	0.3867	4.0720
100km, 1m/s	1.3261	0.5610	0.6638	0.6256	0.4877	0.3904	4.0545
1000km, 0.8m/s	1.3507	0.5645	0.6495	0.5828	0.4525	0.3643	3.9644
1000km, 0.6m/s	1.1065	0.5661	0.6442	0.5705	0.4425	0.3568	3.6866
1000km, 0.4m/s	0.8822	0.5687	0.6346	0.5507	0.4265	0.3451	3.4078
1000km, 0.2m/s	0.7173	0.5788	0.6187	0.5196	0.4064	0.3046	3.1453
1000km, 0.1m/s	0.6778	0.5817	0.6039	0.5000	0.3910	0.2924	3.0469

Discussion

Table 5.9 shows that the initial error has little effect on the orbit determination strategy.

Figure 5.8 shows that when the initial error of the position becomes small, the

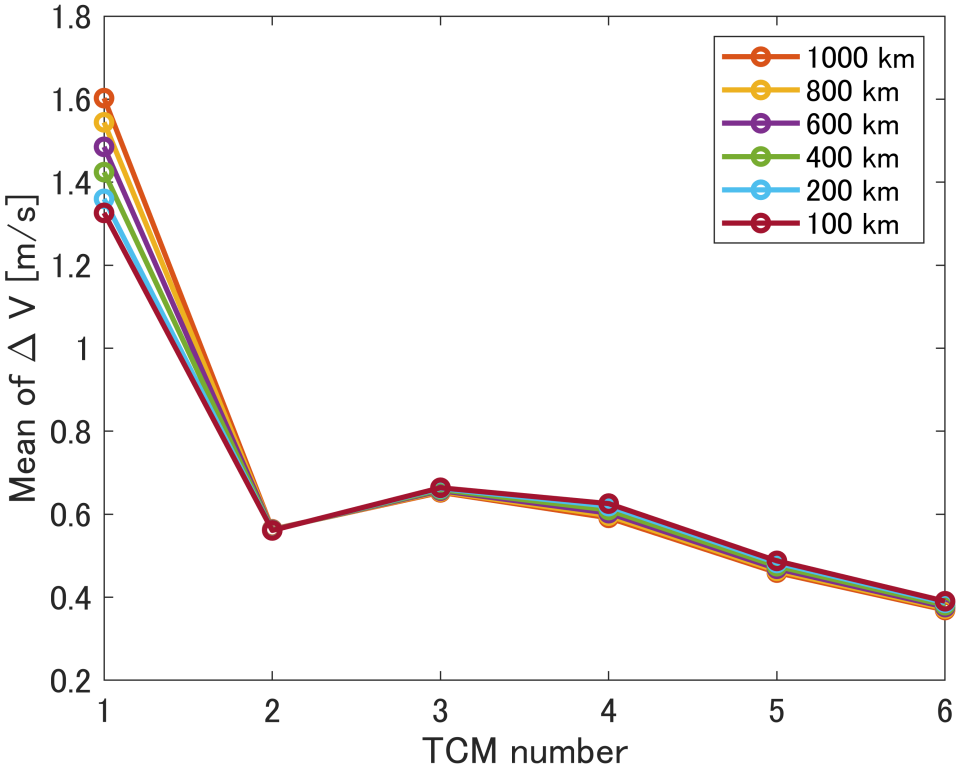

Figure 5.10: Expected value of ΔV of optimization results when initial position error was changed.

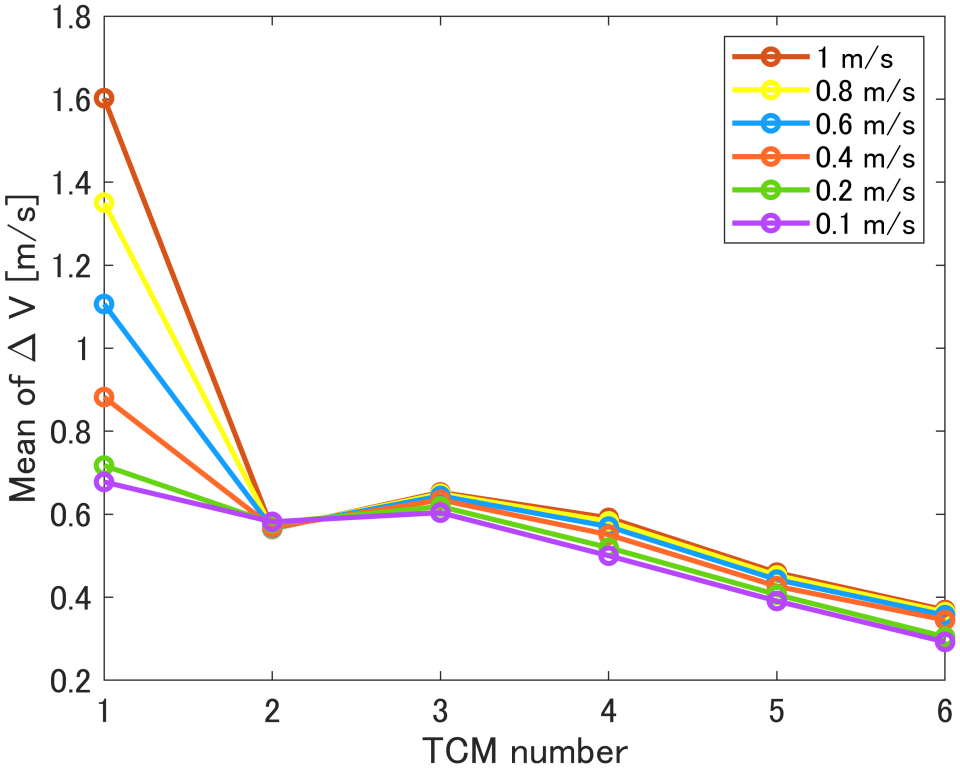

Figure 5.11: Expected value of ΔV of optimization results when initial velocity error was changed.

Table 5.9: Number of orbit determination of optimization results when initial error was changed.

$\Sigma_{\boldsymbol{R}_0}$ and $\Sigma_{\boldsymbol{V}_0}$	TCM1	TCM2	TCM3	TCM4	TCM5	TCM6
1000km, 1m/s	3	2	2	3	3	5
800km, 1m/s	3	2	2	3	3	5
600km, 1m/s	3	2	2	3	3	5
400km, 1m/s	3	2	2	3	3	5
200km, 1m/s	3	2	2	3	3	5
100km, 1m/s	3	2	2	3	3	5
1000km, 0.8m/s	3	2	2	3	3	5
1000km, 0.6m/s	3	2	2	3	3	5
1000km, 0.4m/s	3	2	2	3	3	5
1000km, 0.2m/s	3	2	2	3	4	4
1000km, 0.1m/s	3	2	2	3	4	4

TCM time is brought forward. This is probably because the effect of the dynamics error in TCM1 becomes relatively larger as the initial error becomes smaller, and the time of TCM1 is moved forward to make TCM1 as small as possible. By bringing forward TCM1, TCM2 and subsequent TCMs are also brought forward, increasing the time interval between TCMs and thus increasing the ΔV of TCM2 and subsequent TCMs. However, since the effect of reducing the size of TCM1 is greater than that effect, the optimal strategy is to move TCM1 forward.

In contrast, as the initial error in the velocity becomes smaller, the TCM time is pushed back overall in Fig. 5.9. This is because the effect of the smaller initial error of velocity is considerably larger than the effect of the dynamics error in TCM1, and the strategy is to delay the overall TCM to make it smaller after TCM2.

From the above, it is found that the initial error has little effect on the strategy for orbit determination, and the optimal strategy for TCM time is different due to the difference in sensitivity between position and velocity in the initial error. The contrasting strategies may be determined by the magnitude of the impact of the initial error on TCM1.

5.3.5 Sensitivity Analysis on Dynamics Error

Conditions

In order to perform sensitivity analysis on the dynamics error, simulations using the optimization method 8 were performed by varying the dynamics error. The conditions other than the dynamics error were the same as in the table, with Q set to 3.15e-15km^2/s^3, 2.02e-15km^2/s^3, 1.14e-15km^2/s^3, 5.05e-16km^2/s^3, and 1.26e-16km^2/s^3. In all cases, Jensen's inequality was used as the objective function of the optimization to speed up the computation, and Monte Carlo method (10,000,000 samples) was used in the evaluation of the optimal solution.

Results

Figure 5.12 shows the TCM time in each optimization result. Figure 5.13 and Table 5.10 show the ΔV required for TCM in each case. Table 5.11 shows the number of orbit determination for each TCM.

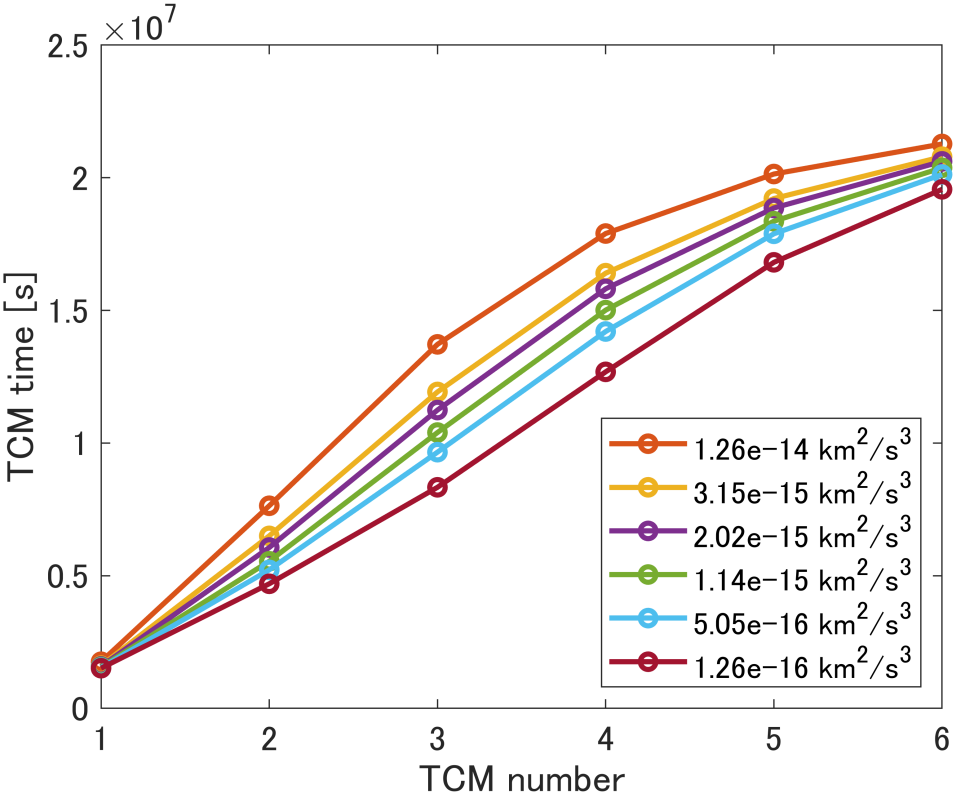

Figure 5.12: TCM timing of optimization results when dynamics error was changed.

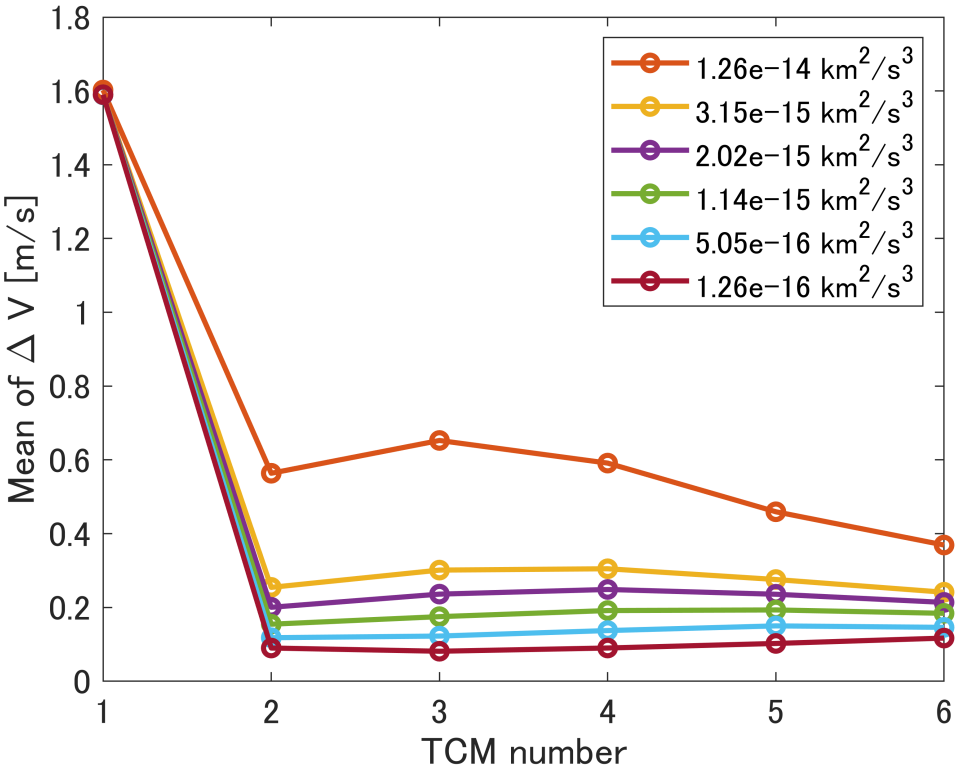

Figure 5.13: Expected value of ΔV of optimization results when dynamics error was changed.

Table 5.10: Expected value of ΔV of optimization results when dynamics error was changed [m/s].

Q	TCM1	TCM2	TCM3	TCM4	TCM5	TCM6	Total
1.26e-14km^2/s^3	1.6025	0.5636	0.6524	0.5908	0.4589	0.3688	4.2371
3.15e-15km^2/s^3	1.5903	0.2545	0.3013	0.3050	0.2758	0.2413	2.9683
2.02e-15km^2/s^3	1.5896	0.2005	0.2362	0.2488	0.2359	0.2138	2.7248
1.14e-15km^2/s^3	1.5894	0.1547	0.1752	0.1917	0.1933	0.1842	2.4884
5.05e-16km^2/s^3	1.5895	0.1181	0.1225	0.1374	0.1501	0.1461	2.2638
1.26e-16km^2/s^3	1.5901	0.0901	0.0814	0.0902	0.1025	0.1171	2.0713

Table 5.11: Number of orbit determination of optimization results when dynamics error was changed.

Q	TCM1	TCM2	TCM3	TCM4	TCM5	TCM6
1.26e-14km^2/s^3	3	2	2	3	3	5
3.15e-15km^2/s^3	4	2	2	2	3	5
2.02e-15km^2/s^3	4	2	2	2	3	5
1.14e-15km^2/s^3	4	2	2	2	3	5
5.05e-16km^2/s^3	5	2	2	2	3	4
1.26e-16km^2/s^3	6	2	2	2	2	4

Discussion

Figure 5.12 shows that TCM6 can be brought forward due to the smaller dynamics error. Correspondingly, TCM2 to TCM5 are also brought forward. As the dynamics error becomes smaller, the error accumulated between each TCM becomes smaller, and the ΔV required for each TCM, except for TCM1, is greatly reduced. The impact of the decrease in the dynamics error is small for TCM1 because the initial error has a large impact.

Since the influence of TCM1 in the whole becomes relatively larger as the dynamics error becomes smaller, the strategy of orbit determination is to concentrate the orbit determination just before TCM1 so that the orbit determination error at TCM1 becomes smaller.

5.3.6 Sensitivity Analysis on Observation Error

Conditions

In order to perform sensitivity analysis on the observation error, simulations using the optimization method 8 were performed by varying the observation error. The conditions other than the observation error were the same as in the table, with R_R set to 80 km, 60 km, 40 km, 20 km, and 10 km, and R_V set to 0.08 m/s, 0.06 m/s, 0.04 m/s, 0.02 m/s, and 0.01 m/s. In all cases, Jensen's inequality was used as the objective function of the optimization to speed up the computation, and the Monte Carlo method (10,000,000 samples) was used in the evaluation of the optimal solution.

Results

Figures 5.14 and 5.15 show the TCM time in each optimization result. Figures 5.16 and 5.17 and Table 5.12 show the ΔV required for TCM in each case. Table 5.13 shows the number of orbit determination for each TCM.

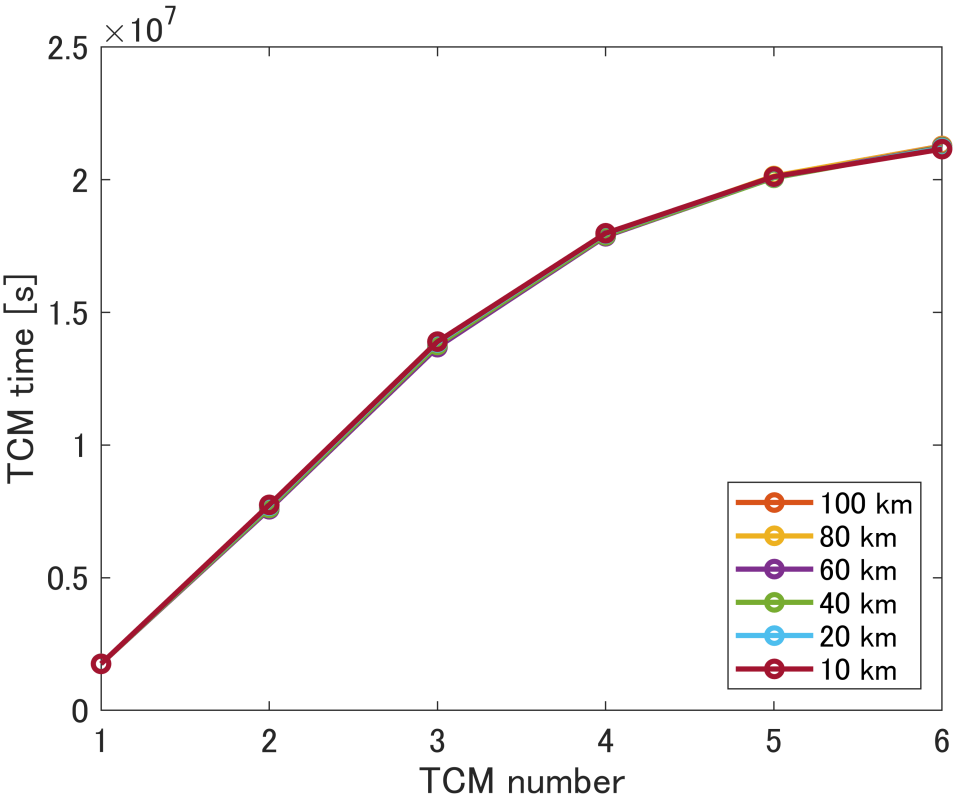

Figure 5.14: TCM timing of optimization results when observation error about position was changed.

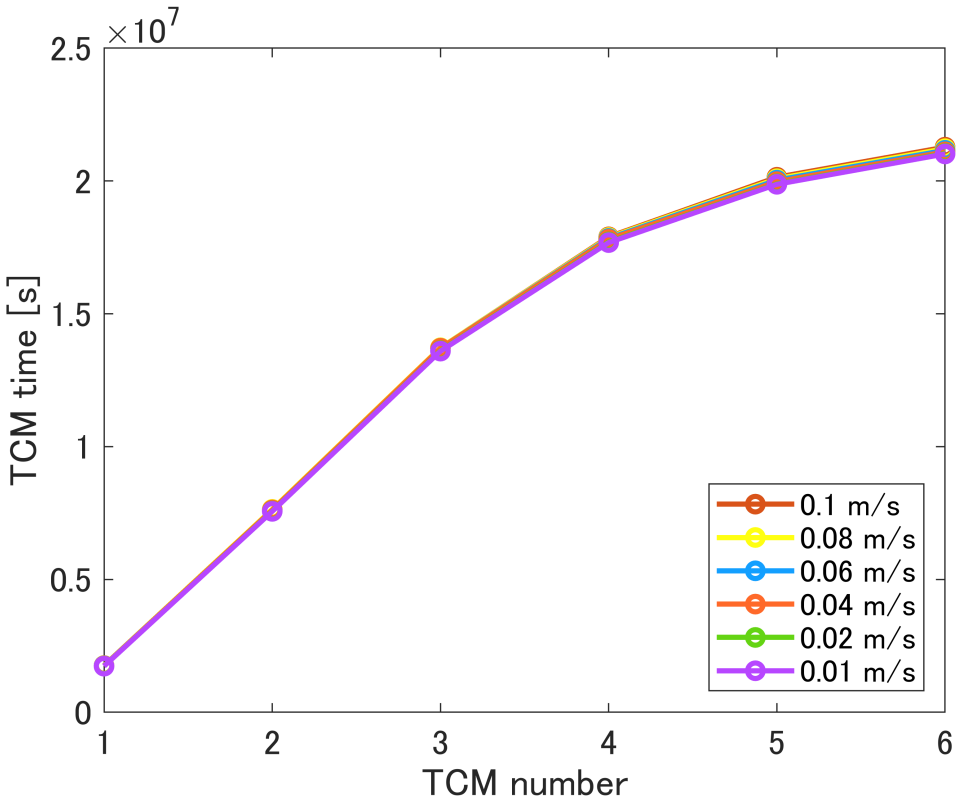

Figure 5.15: TCM timing of optimization results when observation error about velocity was changed.

Table 5.12: Expected value of ΔV of optimization results when observation error was changed [m/s].

R_R and R_V	TCM1	TCM2	TCM3	TCM4	TCM5	TCM6	Total
100km, 0.1m/s	1.6025	0.5636	0.6524	0.5908	0.4589	0.3688	4.2371
80km, 0.1m/s	1.6025	0.5628	0.6596	0.5849	0.4534	0.3606	4.2239
60km, 0.1m/s	1.6024	0.5582	0.6556	0.5823	0.4486	0.3616	4.2087
40km, 0.1m/s	1.6024	0.5648	0.6541	0.5775	0.4412	0.3531	4.1931
20km, 0.1m/s	1.6022	0.5674	0.6558	0.5760	0.4370	0.3312	4.1696
10km, 0.1m/s	1.6021	0.5671	0.6535	0.5712	0.4322	0.3131	4.1393
100km, 0.08m/s	1.6023	0.5601	0.6466	0.5777	0.4417	0.3487	4.1772
100km, 0.06m/s	1.6025	0.5572	0.6416	0.5664	0.4284	0.3248	4.1208
100km, 0.04m/s	1.6024	0.5541	0.6360	0.5550	0.4137	0.3115	4.0728
100km, 0.02m/s	1.6024	0.5478	0.6279	0.5455	0.4079	0.3040	4.0355
100km, 0.01m/s	1.6024	0.5463	0.6254	0.5430	0.4060	0.2990	4.0221

Discussion

As the observation error about the position becomes smaller, the error caused by the orbit determination error in the guidance accuracy at the final time can be made

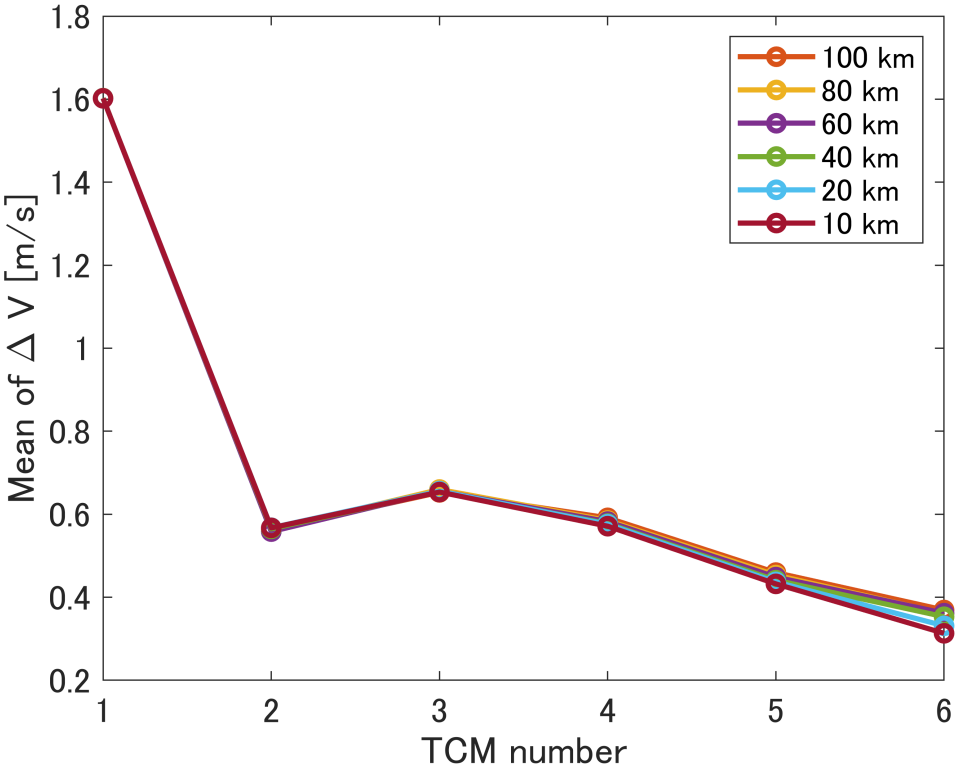

Figure 5.16: Expected value of ΔV of optimization results when observation error about position was changed.

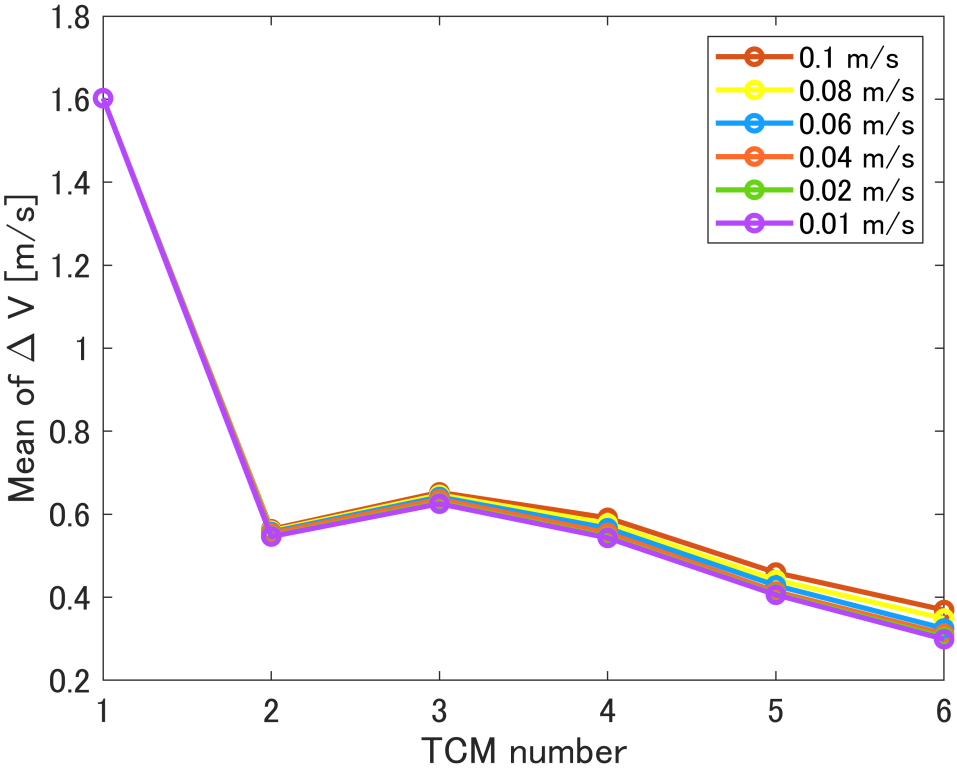

Figure 5.17: Expected value of ΔV of optimization results when observation error about velocity was changed.

Table 5.13: Number of orbit determination of optimization results when observation error was changed.

R_R and R_V	TCM1	TCM2	TCM3	TCM4	TCM5	TCM6
100km, 0.1m/s	3	2	2	3	3	5
80km, 0.1m/s	3	2	3	3	3	4
60km, 0.1m/s	3	2	3	3	3	4
40km, 0.1m/s	3	3	3	3	3	3
20km, 0.1m/s	4	3	3	3	3	2
10km, 0.1m/s	4	3	3	3	3	2
100km, 0.08m/s	3	2	2	3	3	5
100km, 0.06m/s	2	2	2	3	4	5
100km, 0.04m/s	2	2	2	3	4	5
100km, 0.02m/s	2	1	2	2	5	6
100km, 0.01m/s	2	1	1	2	6	6

smaller. Therefore, the TCM6 can be brought forward due to the smaller observation error in position, which results in a smaller TCM6. Since the effect on the guidance accuracy is reduced, the concentration of orbit determination on TCM6 is reduced, and it is thought that orbit determination is performed evenly. It can also be seen that the magnitude of TCM4 to TCM6 is reduced as the orbit determination error becomes smaller.

When the observation error related to velocity is changed, the guidance accuracy at the final time is not improved much, and rather the orbit determination is concentrated just before TCM5 and TCM6. It is thought that the improvement in the accuracy of the orbit determination with respect to velocity reduces the number of orbit determination required in the first half of the TCM, and the strategy of concentrating the orbit determination just before later TCMs is applied in order to accelerate the time of TCM6.

For the cases changing observation error, the strategy of TCM was the same for both the improvement of position error and velocity error, but the difference was observed in the strategy of orbit determination. It is interesting to note that the strategy is different for position error and velocity error as in the case of initial error, but the difference is in the strategy of TCM for initial error, while the difference is in the strategy of orbit determination for observation error. The reason for this difference may be that the initial error has a large impact on TCM1, while the observation error

has a large impact on the guidance accuracy and the TCM6 to achieve it. Of course, this is because the initial error is canceled out by TCM1 and affects the TCM strategy, while the observation error has a direct effect on the orbit determination accuracy.

5.3.7 Sensitivity Analysis on Control Error

Conditions

In order to perform sensitivity analysis on the control error, simulations using the optimization method 8 were performed by varying the control error. The conditions other than the control error were the same as in the table, with fixed error set to 1e-5km/s, 8e-6km/s, 6e-6km/s, 4e-6km/s, and 2e-6km/s, and proportional error coefficient set to 0.008, 0.006, 0.004, 0.002, and 0.001. In all cases, Jensen's inequality was used as the objective function of the optimization to speed up the computation, and the Monte Carlo method (10,000,000 samples) was used in the evaluation of the optimal solution.

Results

Figures 5.18 and 5.19 show the TCM time in each optimization result. Figures 5.20 and 5.21 and Table 5.14 show the ΔV required for TCM in each case. Table 5.15 shows the number of orbit determination for each TCM.

Table 5.14: Expected value of ΔV of optimization results when control error was changed [m/s].

S	TCM1	TCM2	TCM3	TCM4	TCM5	TCM6	Total
2e-5km/s, 0.01	1.6025	0.5636	0.6524	0.5908	0.4589	0.3688	4.2371
1e-5km/s, 0.01	1.6023	0.5616	0.6502	0.5871	0.4531	0.3608	4.2152
8e-6km/s, 0.01	1.6022	0.5613	0.6500	0.5866	0.4524	0.3598	4.2123
6e-6km/s, 0.01	1.6022	0.5612	0.6497	0.5682	0.4518	0.3590	4.2101
4e-6km/s, 0.01	1.6022	0.5610	0.6496	0.5860	0.4515	0.3584	4.2085
2e-6km/s, 0.01	1.6022	0.5609	0.6495	0.5858	0.4511	0.3580	4.2075
2e-5km/s, 0.008	1.6025	0.5637	0.6526	0.5911	0.4592	0.3691	4.2383
2e-5km/s, 0.006	1.6025	0.5636	0.6525	0.5910	0.4591	0.3690	4.2378
2e-5km/s, 0.004	1.6025	0.5636	0.6525	0.5909	0.4590	0.3689	4.2374
2e-5km/s, 0.002	1.6025	0.5636	0.6524	0.5908	0.4590	0.3689	4.2371
2e-5km/s, 0.001	1.6025	0.5636	0.6524	0.5908	0.4589	0.3688	4.2371

Discussion

From the results, it can be seen that the control error has little effect on the objective function, TCM, and orbit determination strategy under the conditions of the present

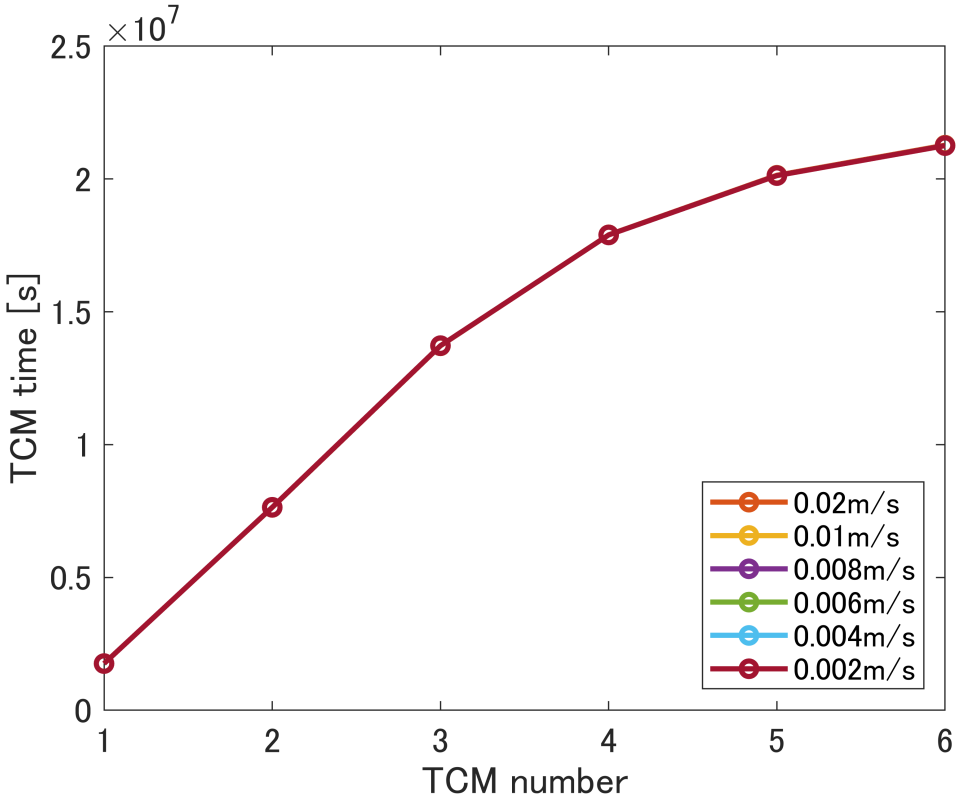

Figure 5.18: TCM timing of optimization results when fixed control error was changed.

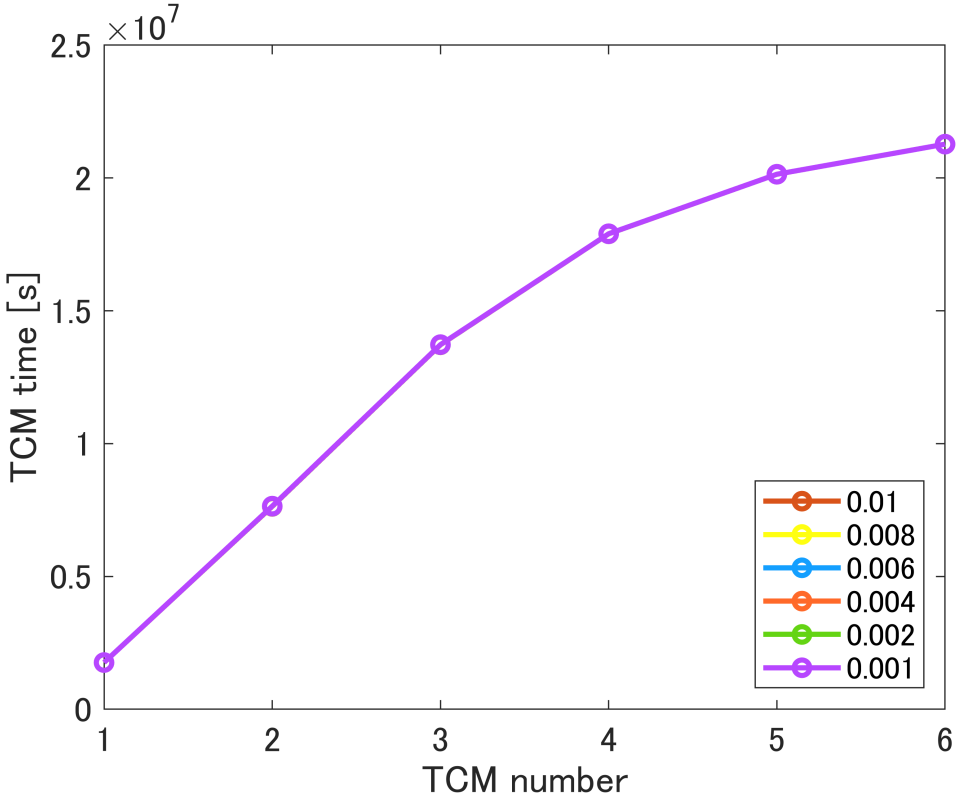

Figure 5.19: TCM timing of optimization results when proportional control error was changed.

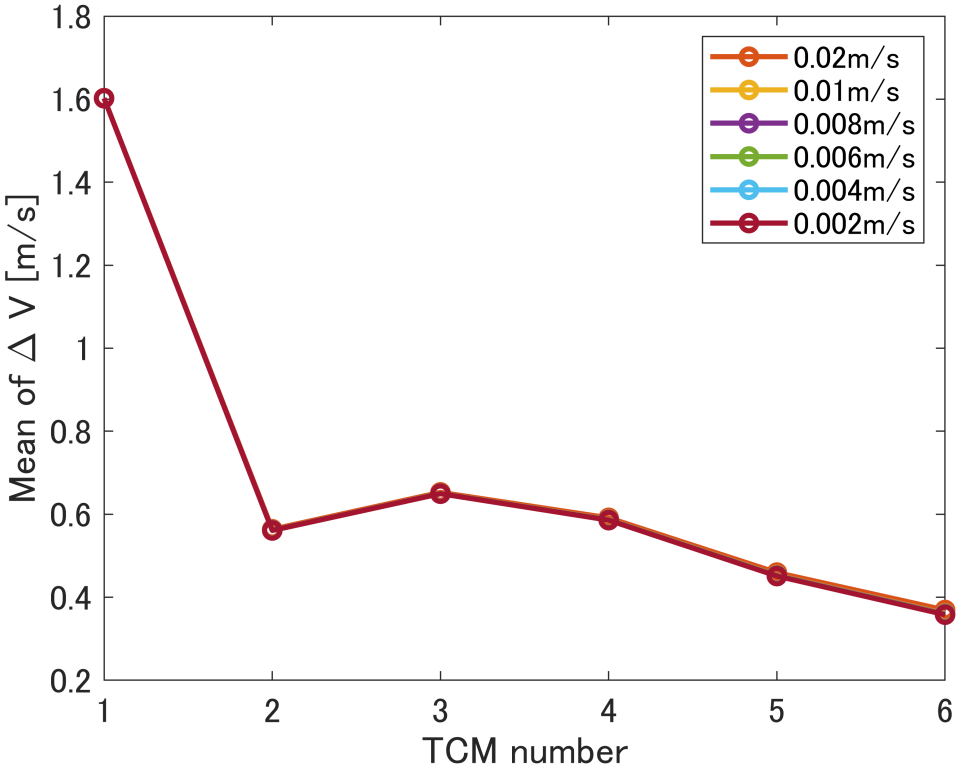

Figure 5.20: Expected value of ΔV of optimization results when fixed control error was changed.

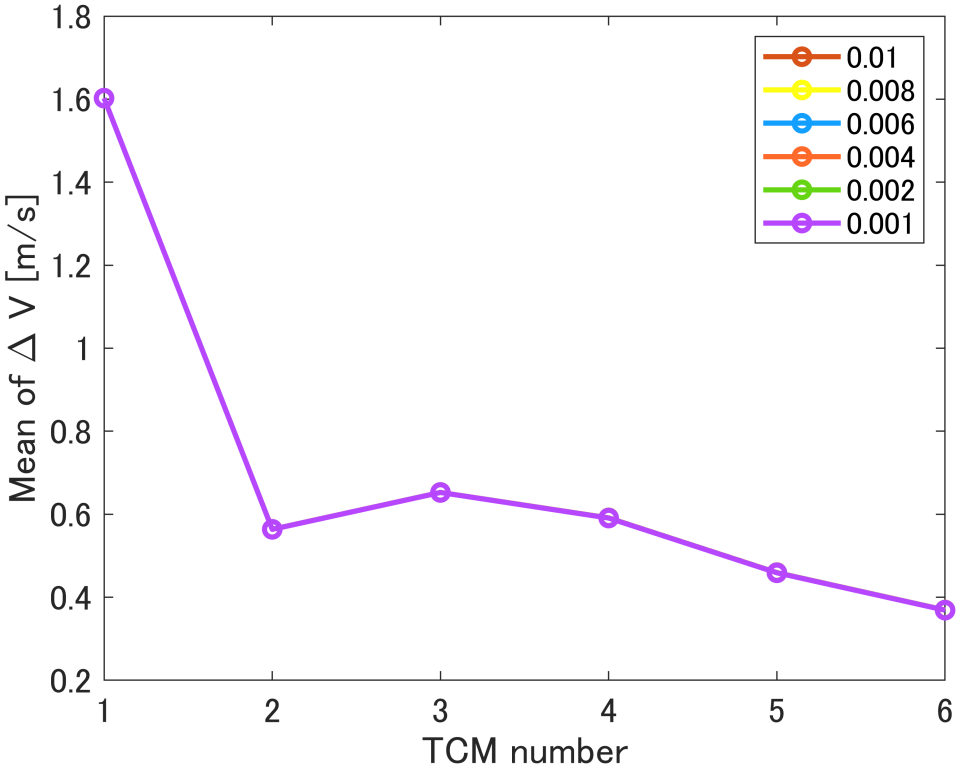

Figure 5.21: Expected value of ΔV of optimization results when proportional control error was changed.

Table 5.15: Number of orbit determination of optimization results when control error was changed.

S	TCM1	TCM2	TCM3	TCM4	TCM5	TCM6
2e-5km/s, 0.01	3	2	2	3	3	5
1e-5km/s, 0.01	3	2	2	3	3	5
8e-6km/s, 0.01	3	2	2	3	3	5
6e-6km/s, 0.01	3	2	2	3	3	5
4e-6km/s, 0.01	3	2	2	3	3	5
2e-6km/s, 0.01	3	2	2	3	3	5
2e-5km/s, 0.008	3	2	2	3	3	5
2e-5km/s, 0.006	3	2	2	3	3	5
2e-5km/s, 0.004	3	2	2	3	3	5
2e-5km/s, 0.002	3	2	2	3	3	5
2e-5km/s, 0.001	3	2	2	3	3	5

simulation. This is probably because in the nominal case, there is almost no effect of control error on the objective function, and even if it is changed, there is little effect on the whole. However, in the case where a controller with a large control error is used, the increase in TCM due to the control error cannot be ignored and is expected to become important.

5.3.8 Sensitivity Analysis on Guidance Accuracy

Conditions

In order to perform sensitivity analysis on the guidance accuracy, simulations using the optimization method 8 were performed by varying the final state constraint. The conditions other than the final state constraint were the same as in the table, with the final state constraint set to 200km, 400km, 600km, 800km, and 1000km. In all cases, Jensen's inequality was used as the objective function of the optimization to speed up the computation, and the Monte Carlo method (10,000,000 samples) was used in the evaluation of the optimal solution.

Results

Figure 5.22 shows the TCM time in each optimization result. Figure 5.23 and Table 5.16 show the ΔV required for TCM in each case. Table 5.17 shows the number of orbit determination for each TCM.

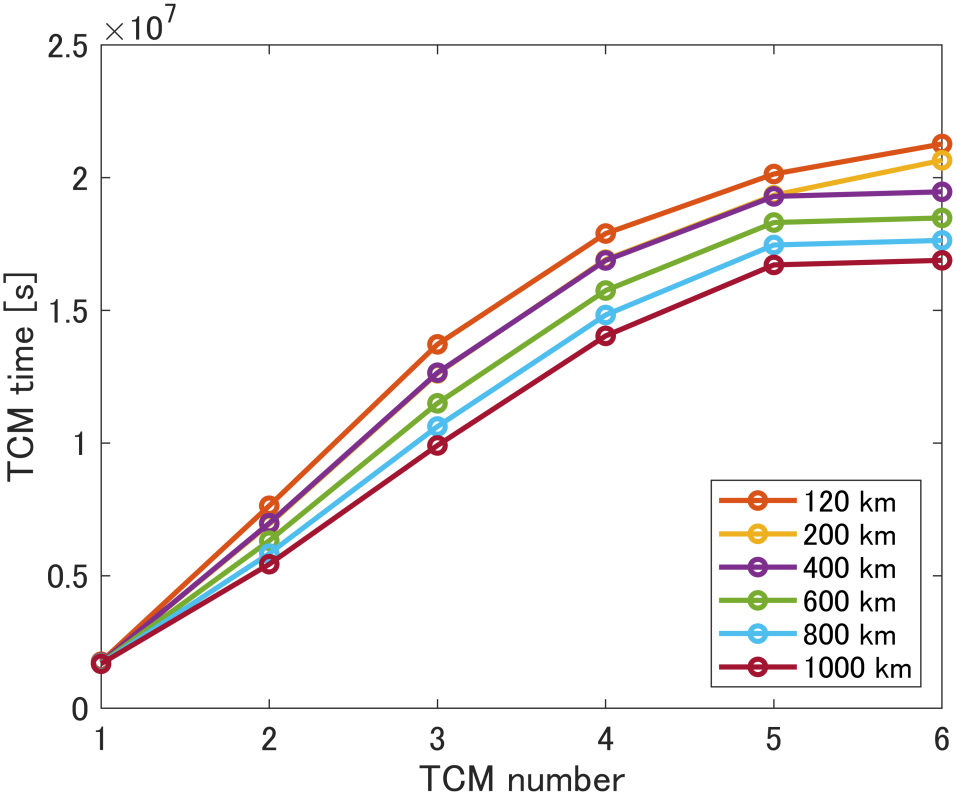

Figure 5.22: TCM timing of optimization results when final state constraint was changed.

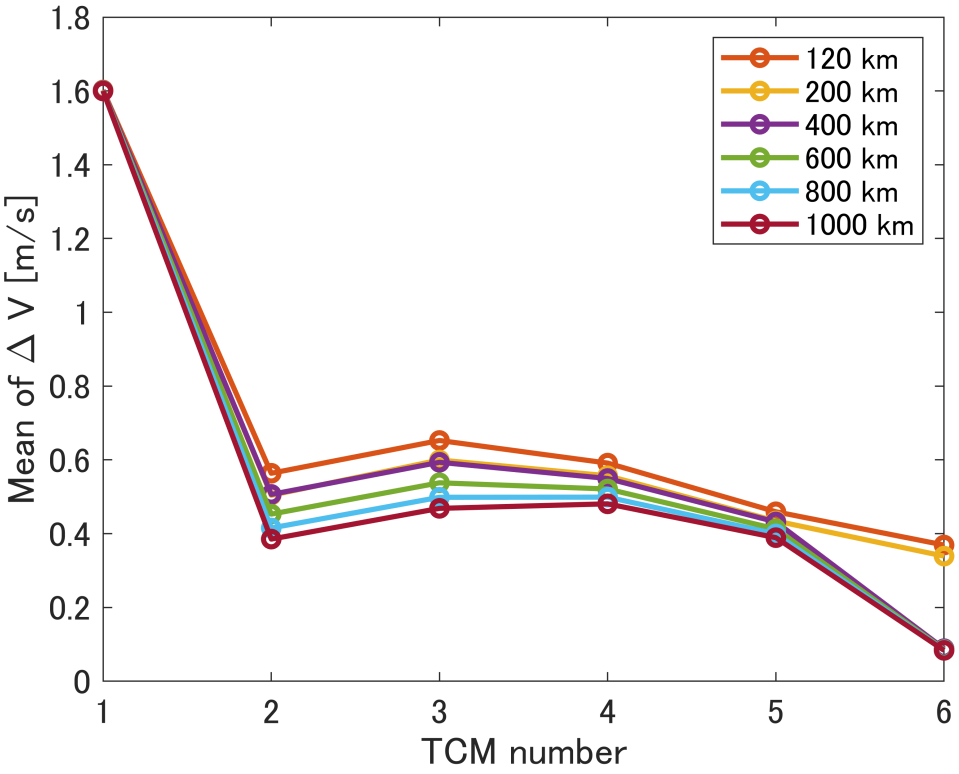

Figure 5.23: Expected value of ΔV of optimization results when final state constraint was changed.

Table 5.16: Expected value of ΔV of optimization results when final state constraint was changed [m/s].

$\delta R_{\mathrm{th},f}$	TCM1	TCM2	TCM3	TCM4	TCM5	TCM6	Total
120km	1.6025	0.5636	0.6524	0.5908	0.4589	0.3688	4.2371
200km	1.6015	0.5040	0.5997	0.5569	0.4345	0.3391	4.0358
400km	1.6011	0.5065	0.5935	0.5496	0.4319	0.0884	3.7710
600km	1.6004	0.4531	0.5379	0.5211	0.4129	0.0859	3.6113
800km	1.6001	0.4154	0.4987	0.4991	0.3995	0.0845	3.4973
1000km	1.5999	0.3853	0.4686	0.4809	0.3892	0.0837	3.4077

Discussion

From the results, it can be seen that TCM6 can be brought forward significantly due to the relaxation of the terminal constraint. In the case of 400 km or more, TCM5 and TCM6 are performed consecutively, indicating that TCM6 is no longer necessary. By bringing forward TCM6, TCM2 to TCM5 can also be brought forward, leading to a decrease in ΔV for each TCM. However, since the main factor for TCM1 is the

Table 5.17: Number of orbit determination of optimization results when final state constraint was changed.

$\delta R_{\mathrm{th},f}$	TCM1	TCM2	TCM3	TCM4	TCM5	TCM6
120km	3	2	2	3	3	5
200km	3	2	3	3	3	4
400km	4	3	3	3	4	1
600km	4	3	3	3	4	1
800km	4	3	3	3	4	1
1000km	4	3	3	3	4	1

initial error, the effect on TCM1 is hardly seen. In addition, the number of orbit determination used in TCM6 appears to decrease as the final constraint is relaxed, but since TCM5 and TCM6 are integrated in the case of 400 km or more, the strategy seems to be to make orbit determination evenly when TCM6 is excluded.

5.3.9 Sensitivity Analysis on Total Orbit Determination Number

Conditions

In order to perform sensitivity analysis on the total orbit determination number, simulations using the optimization method 8 were performed by varying the total orbit determination number. The conditions other than the final state constraint were the same as in the table, with the total orbit determination numbers set to 12, 18, 24, and 30. In all cases, Jensen's inequality was used as the objective function of the optimization to speed up the computation, and the Monte Carlo method (10,000,000 samples) was used in the evaluation of the optimal solution.

Results

Figure 5.24 shows expected value of ΔV of optimization results with respect to the total number of orbit determination.

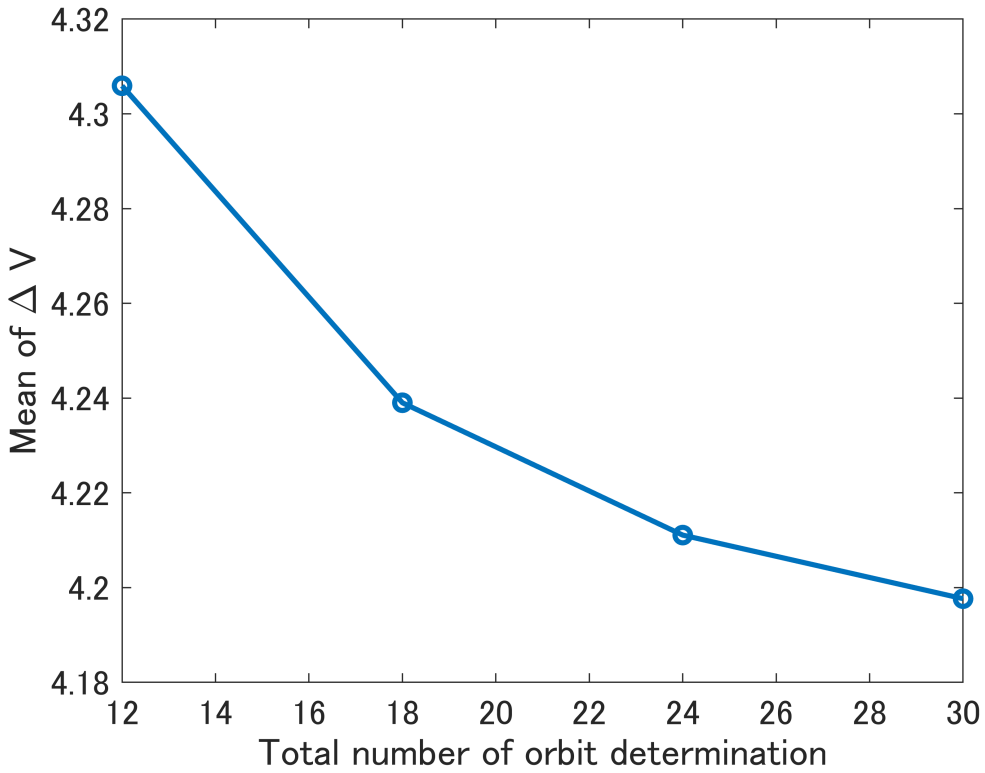

Figure 5.24: Expected value of ΔV of optimization results when total orbit determination number was changed.

Discussion

From the results, it can be seen that there is a trade-off between the total number of orbit determination and the ΔV required for TCM. This is because the more the total number of orbit determination is increased, the smaller the orbit determination error during TCM becomes, and the deviations that need to be corrected in TCM decrease. Although the total number of orbit determination cannot be changed in the optimization formulation of this study, it can be changed outside the optimization, and useful information about trade-offs against ΔV can be provided to mission designers.

5.3.10 Difference between Objective Functions

Conditions

The simulations so far in this section have used Jensen's inequality as the objective function in order to reduce computational cost. In order to check the difference between the Jensen's inequality and the Monte Carlo method, the problem was optimized using the Monte Carlo method as the objective function. In this simulation, the initial guess was the result of optimization case 8.

Results

Figure 5.25 and 5.26 show expected value of ΔV and TCM time of optimization results. The expected value of ΔV was 4.267 m/s for the Jensen's inequality case and 4.2404 m/s for the Monte Carlo method case.

Discussion

The results show that using the Monte Carlo method as the objective function gives a better solution because the actual optimization problem is not solved when Jensen's inequality is used as the objective function. As for the TCM time, the time for TCM6 remains the same, but the time for TCM is shifted backward when using the Monte Carlo method compared to when using Jensen's inequality with TCM1-3 increasing instead of TCM4-6 decreased. However, the difference between results was not large,

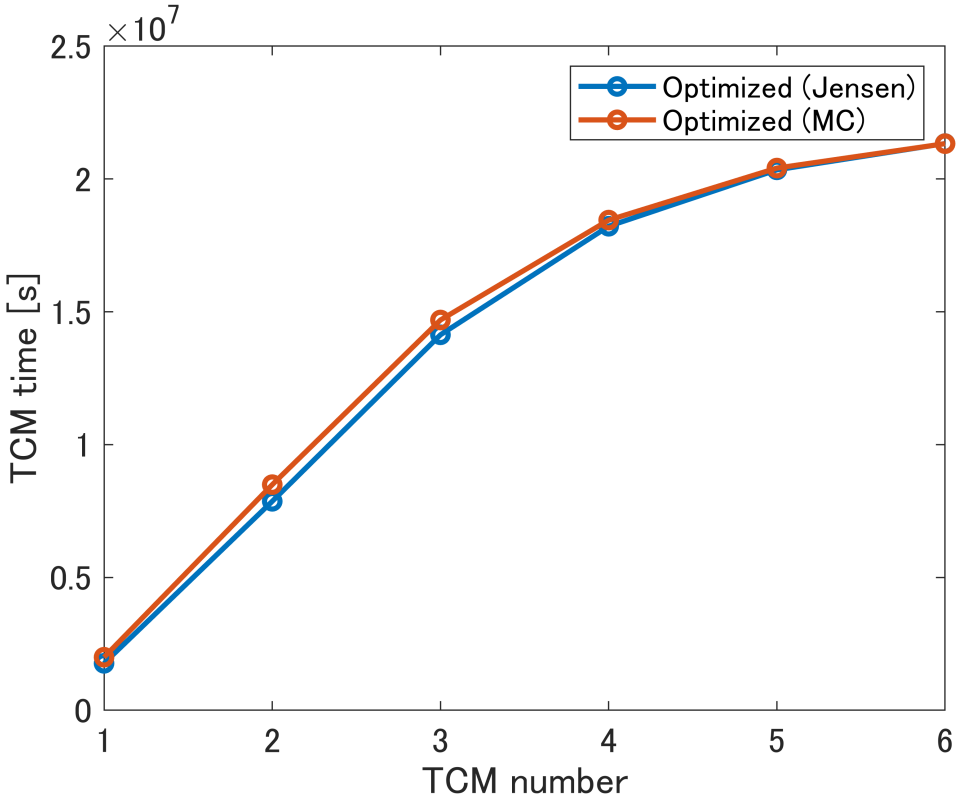

Figure 5.25: TCM timing of optimization results when the objective function was changed.

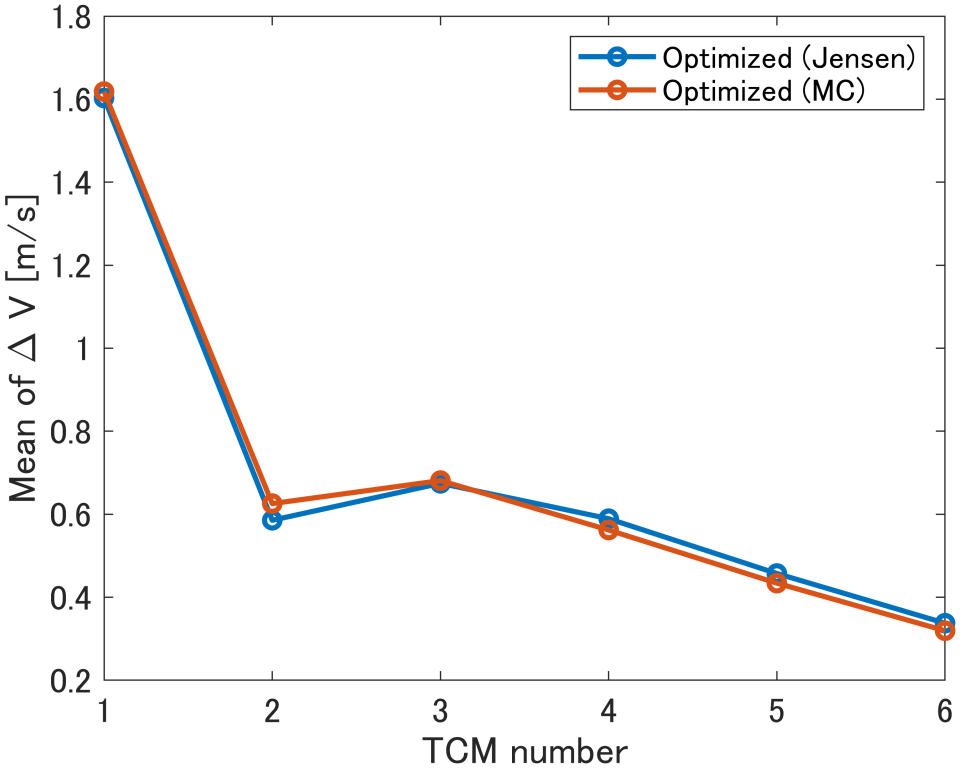

Figure 5.26: Expected value of ΔV of optimization results when the objective function was changed.

and it may be a good strategy to use Jensen's inequality to reduce the computation time and search for a wide range of solutions, and then re-optimize using the Monte Carlo method.

5.3.11 Overall Discussion

From the sensitivity analysis, it is found that the magnitude of the various uncertainties has a significant effect on the ΔV required for the TCM, the guidance accuracy at the final time, the optimal TCM time, and the number of orbit determination. It is also found that the each uncertainty complexly affects TCMs and the effect is different depending on the role of the TCM, i.e., whether the TCM is used to cancel the initial error, to cancel various errors during the TCM, or to ensure the final guidance accuracy.

The fact that the various uncertainties also have a significant impact on the orbit determination strategy suggests the importance of optimization of orbit determination, which has not received much attention so far. The integrated optimization of TCM and orbit determination strategy, focusing on such various uncertainties, cannot be handled by the conventional method called Spacing Rule, and is a problem that can be solved by using the proposed method in this study.

5.4 Numerical Simulations of Optimization Case 2: PROCYON Trajectory

The optimization of the trajectory correction time and orbit determination time for the nominal orbit of PROCYON was performed as an example of optimization.[50]

5.4.1 Conditions

The simulation conditions are shown in Table 5.18. The gravity of the Sun, Earth, Moon, and Mars and solar radiation pressure were considered as dynamics. The coordinate system was ECJ2000 and the center was the Solar System barycenter.

Table 5.18: Simulation parameter settings for the optimization at PROCYON nominal trajectory.

Variables	Values
$\boldsymbol{R}_0^*$, $\boldsymbol{\mu}_{\boldsymbol{R}_0}$, $\boldsymbol{\mu}_{\widehat{\boldsymbol{R}}_0}$	[-5.68e6, 1.52e8, -6.75e6]$^\mathsf{T}$ km
$\boldsymbol{V}_0^*$, $\boldsymbol{\mu}_{\boldsymbol{V}_0}$, $\boldsymbol{\mu}_{\widehat{\boldsymbol{V}}_0}$	[-29.0, 1.20, -3.32]$^\mathsf{T}$ km/s
dynamics	gravity of 4 bodies and SRP
t_0	2014 Dec. 25 09 : 45 : 00
t_f	2016 May 12 18 : 29 : 49
$\Sigma_{\boldsymbol{R}_0}$, $\Sigma_{\widehat{\boldsymbol{R}}_0}$ (1σ)	1000 km
$\Sigma_{\boldsymbol{V}_0}$, $\Sigma_{\widehat{\boldsymbol{V}}_0}$ (1σ)	1.00e-4 km/s
N_k	6
N_l	39
$\delta R_{\mathrm{th},f}$	110 km
S (1σ)	2.00e-5 km/s
Q (1σ)	1.26e-14 km^2/s^3
$R_{\boldsymbol{R}}$ (1σ)	100.0 km
$R_{\boldsymbol{V}}$ (1σ)	1.00e-4 km/s

The trajectory of PROCYON is shown in the Fig. 5.27. After departing from the Earth, the nominal trajectory is controlled by ion thrusters for the first 6.5 months, and then after that, PROCYON performs an Earth gravity assist at an altitude of about 500,000 km. The spacecraft arrives at the asteroid about five months after the Earth gravity assist.[50]

In this optimization, trajectory correction was planned for the ballistic trajectory from the end of the control by ion thruster to the final time, and the time of TCM was optimized. Orbit determination was available for the entire period of the trajec-

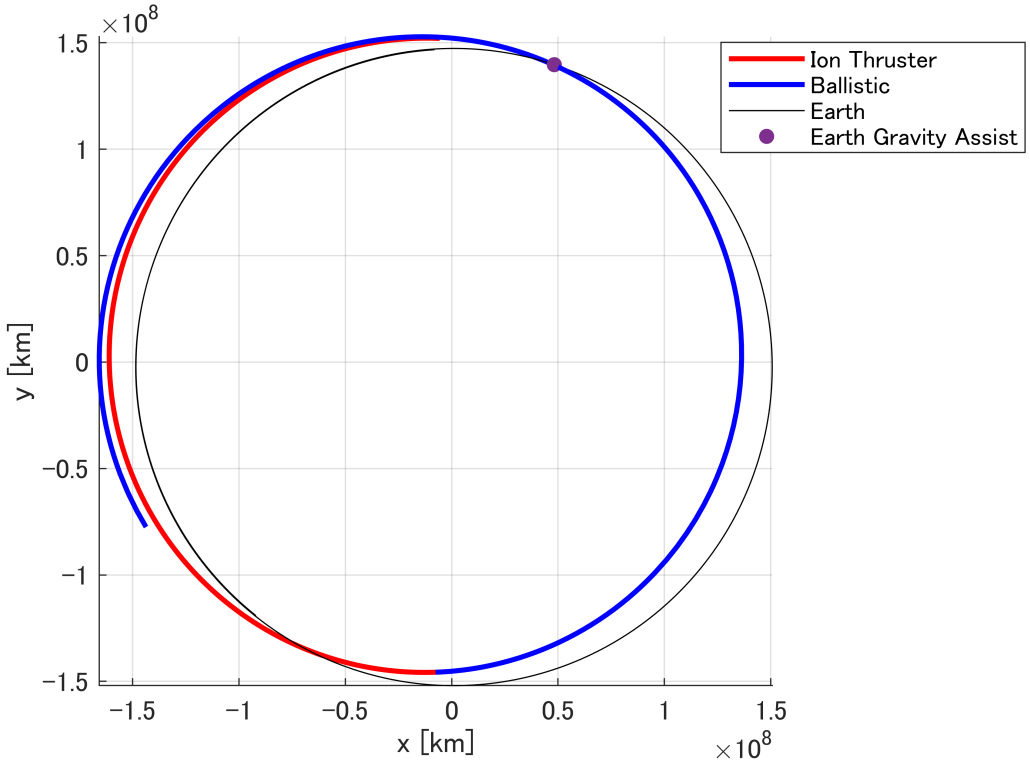

Figure 5.27: PROCYON nominal trajectory.

tory, and optimization of the timings of orbit determination was performed as well. The number of trajectory correction and orbit determination was constant. One orbit determination was always performed one day before the trajectory correction.

Optimization of trajectory correction time only and optimization of both trajectory correction time and orbit determination time were performed and compared. SQP and GPS were used for optimization algorithms, and the results were compared. Uncertainty propagation was done by linear approximation, and the number of samples used for the evaluation of the objective function was 10,000,000. Using the solution of the optimization, the approximation error was calculated from the ratio of the results of the linear approximation to those of the normal Monte Carlo method (9,000 samples).

5.4.2 Results

Figure 5.28 illustrates the trajectory correction and orbit determination time before and after optimization. Also shown in the Fig. 5.29 are the mean of ΔV for each trajectory correction before and after optimization. Figure 5.30 shows the cumulative

distribution function of the total ΔV for each optimization case, and Table 5.19 also shows the mean and 99% value of the total ΔV. The time series of the standard deviation of true position and velocity at the optimization of both timing using GPS is illustrated in Figs. 5.31 and 5.32. Figures 5.33 and 5.33 and Table 5.20 show the ratio of the standard deviation of position and velocity and the mean of ΔV compared to the Monte Carlo results at the optimization of both timings using SQP.

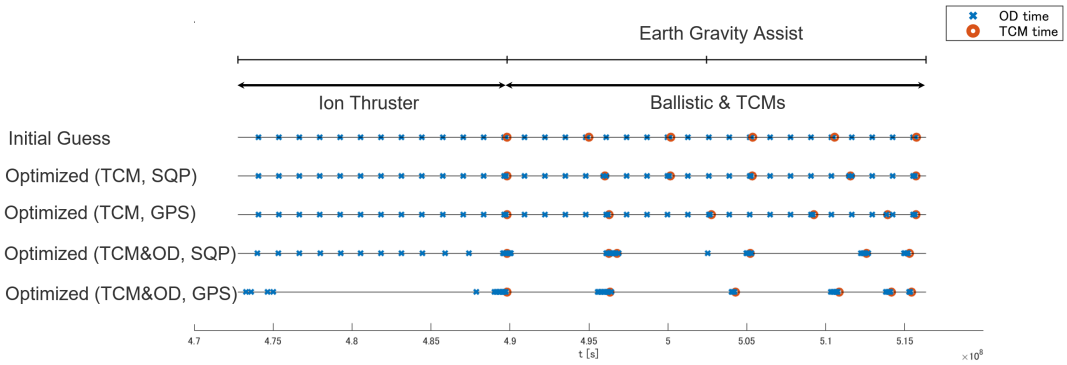

Figure 5.28: Timing of trajectory correction and orbit determination of the initial guess and optimized values.

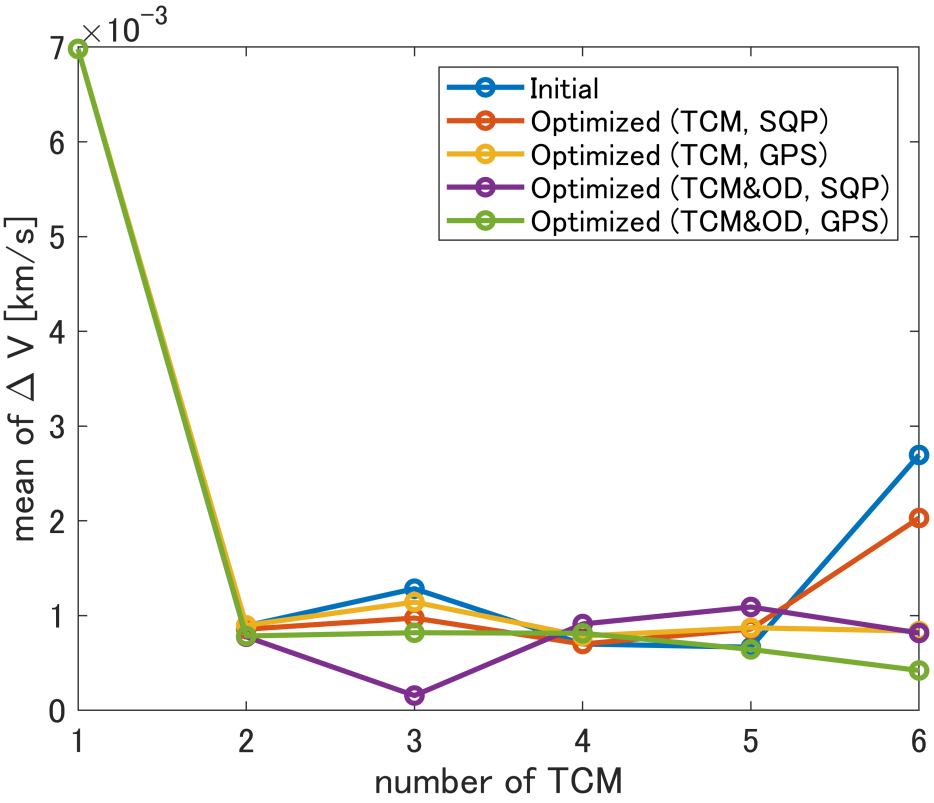

Figure 5.29: Mean of ΔV of each trajectory correction of the initial guess and optimized values.

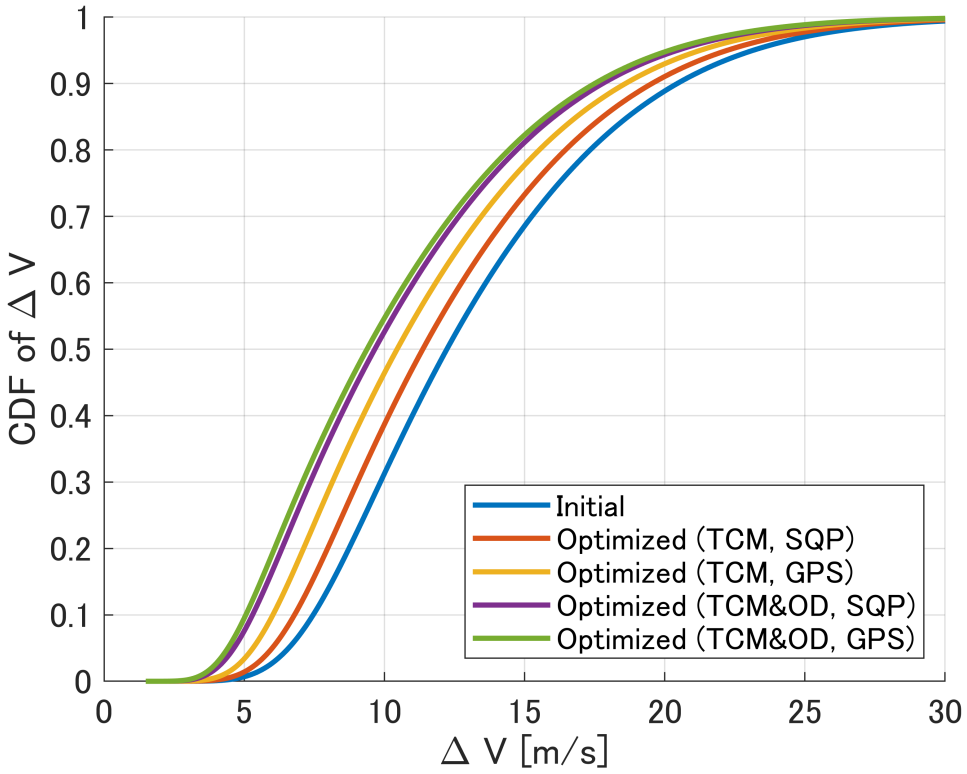

Figure 5.30: Cumulative distribution function of total ΔV of the initial guess and optimized values.

Table 5.19: Mean of ΔV and 99% ΔV of the initial guess and optimized values [m/s].

	Mean	99%
Inital Guess	13.2	28.4
Optimized (TCM, SQP)	12.4	27.5
Optimized (TCM, GPS)	11.5	26.5
Optimized (TCM&OD, SQP)	10.7	25.7
Optimized (TCM&OD, GPS)	10.5	25.4

5.4.3 Discussion

From the simulation results, as with the optimization in the two-body problem, a better solution was obtained by optimizing both times than by optimizing only the TCM time. In addition, although the objective function in this simulation is the mean of ΔV, the value of 99% ΔV was also reduced by the optimization, and the result was

Table 5.20: Ratio of ΔV mean compared with Monte Carlo for the optimized solution of the optimization of both timing.

TCM1	TCM2	TCM3	TCM4	TCM5	TCM6
0.9897	0.9978	1.0034	0.9939	1.0070	0.9934

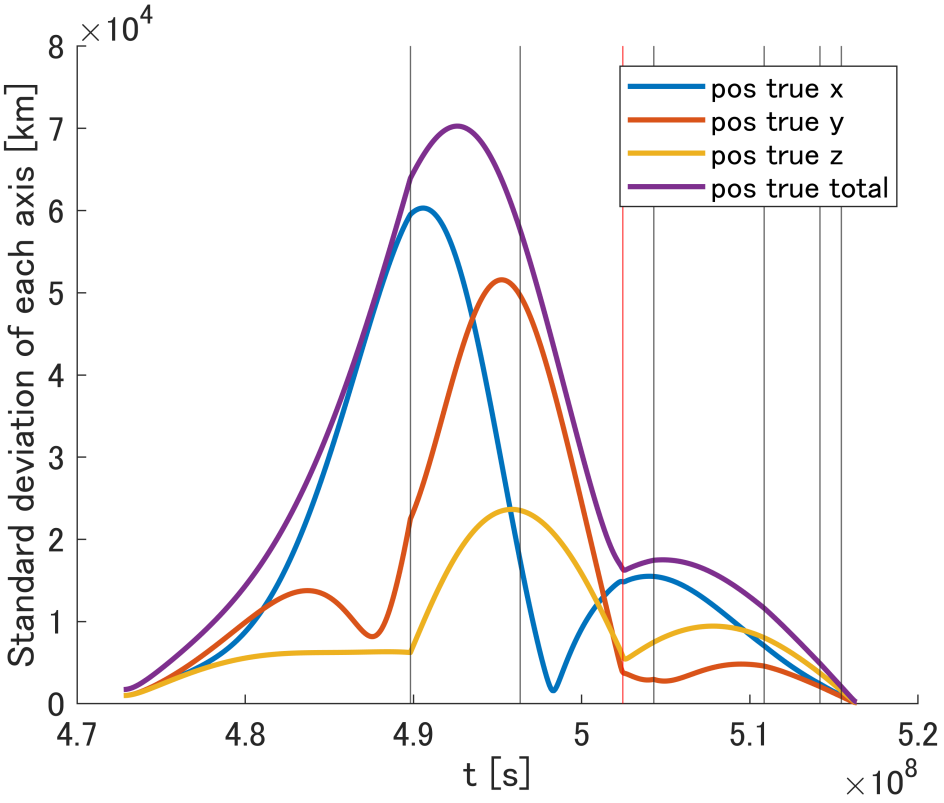

Figure 5.31: Standard deviation of true position for the optimized solution of the optimization of both timing using GPS. Black and red vertical lines represent the time of TCMs and Earth gravity assist respectively.

not such as to cause a practical problem where the value of 99% ΔV was increased instead of the mean of Δ V being reduced.

In the case of optimizing only the TCM time, the optimized solution using SQP does not result in overcoming the orbit determination time; in the case of using GPS, it does result in overcoming the orbit determination time and a better solution is reached. This result really shows the difference in the characteristics of optimization methods.

When both the TCM time and the orbit determination time are optimized, TCM2 and TCM3 are combined when SQP is used. On the other hand, when GPS is used, TCM3 is performed after Earth gravity assist. This is probably because it is difficult to overcome sensitive dynamics such as Earth gravity assist when using SQP, and as a result, TCM2 and TCM3 converge to the optimal time before Earth gravity assist. In the case of GPS, it is possible to change TCM and orbit determination time under the presence of sensitive dynamics, and at the present simulation conditions, GPS gives a better solution than SQP.

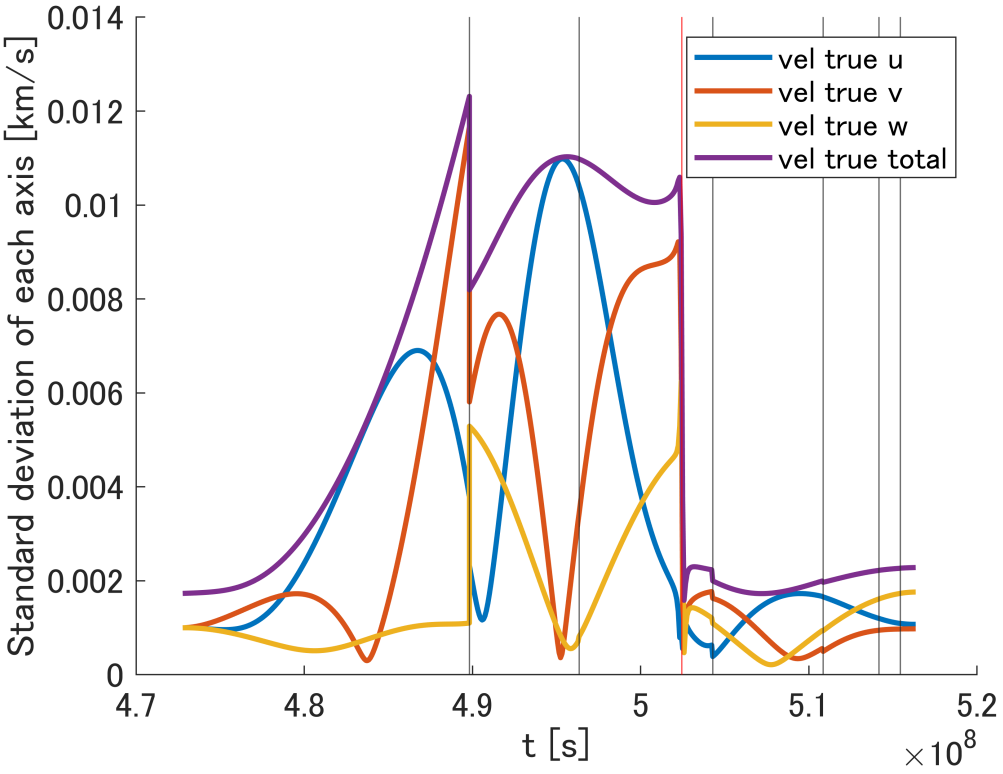

Figure 5.32: Standard deviation of true velocity for the optimized solution of the optimization of both timing using GPS. Black and red vertical lines represent the time of TCMs and Earth gravity assist respectively.

In the case of optimizing only the TCM time, the trajectory correction was always done immediately before or after the orbit determination. In the case of optimization for both times, there was a tendency for the orbit determination to be concentrated just before the trajectory correction. This is because if a correction is planned based on an inaccurate estimate, the guidance error at the final time will be large and the ΔV required for the succeeding maneuvers will increase in order to cancel that error increase. Therefore, the orbit determination was concentrated just before the trajectory correction to improve the accuracy of the orbit determination during the correction.

According to the Figs. 5.31 and 5.32, the movement of the probability distribution changed precipitously at the time of the TCMs and the Earth gravity assist. In particular, at the total covariance of the positions, the trend of decreasing standard deviation changed before and after the Earth swing-by, and the nature of the problem seems to separate before and after this. At the final time, the covariance was converged and the constraint on the guidance accuracy was satisfied.

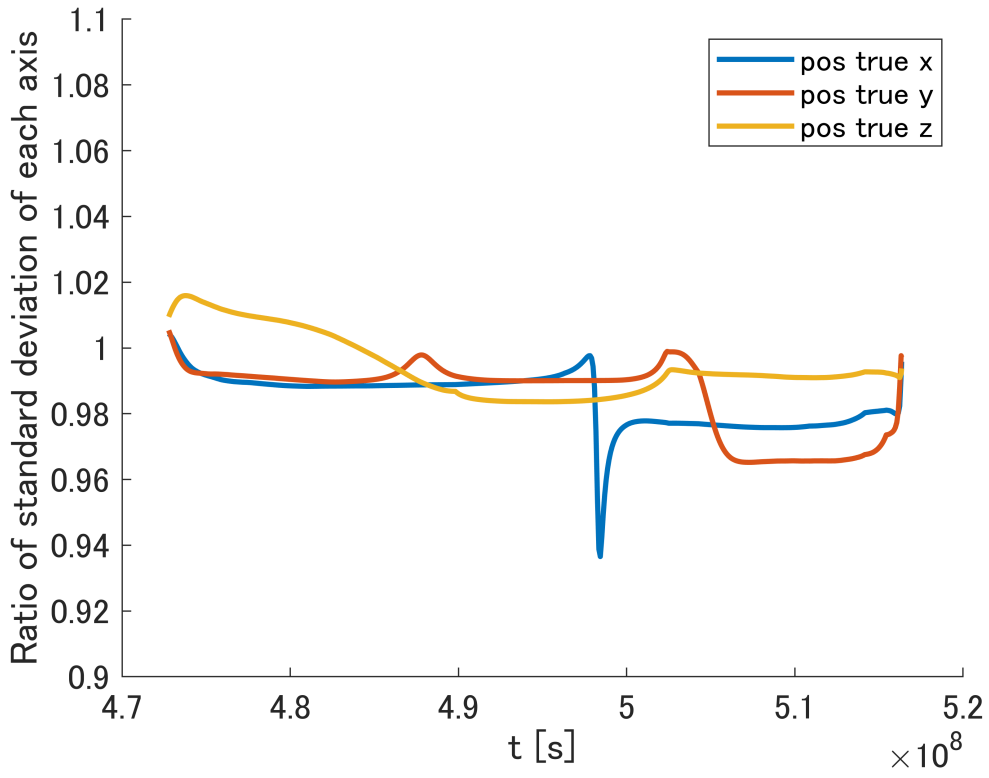

Figure 5.33: Ratio of the standard deviation of true position compared to normal Monte Carlo for the optimized solution of the optimization of both timing using GPS.

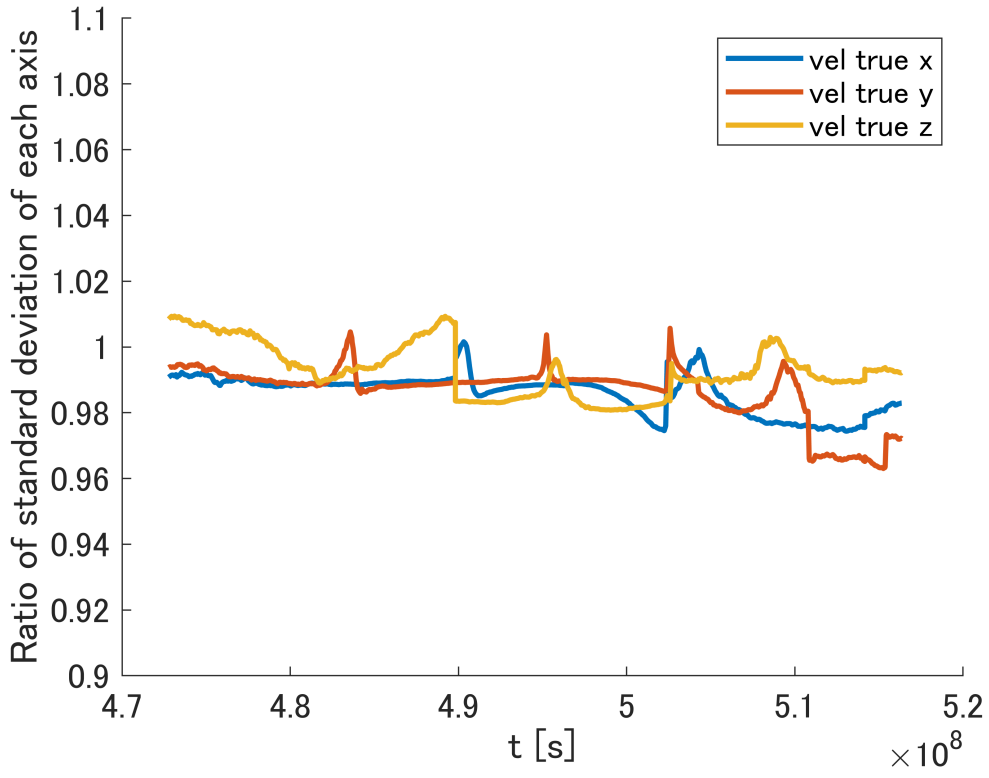

Figure 5.34: Ratio of the standard deviation of true velocity compared to normal Monte Carlo for the optimized solution of the optimization of both timing using GPS.

In Figs. 5.33 and 5.34 and Table 5.20, the error between the linear approximation and the Monte Carlo method was within a few percent, and for the objective function, it was less than approximately 1%, which indicates that the linear approximation is sufficient for this simulation.

In order to investigate the effect of each orbit determination time on the objective function, the objective function was evaluated by deleting one of each orbit determination time from the optimal solution to see how much the amount of ΔV changes in each TCM. The simulation was conducted for the optimized results of both timing optimization using GPS. the results are shown in Fig. 5.35. From the results, it can be seen that ODs at times closer to each TCM time have a greater impact on ΔV than those at the farther time except for those near TCM time once before the TCM. This is because the ΔV of the TCM increases to correct the increase of the guidance error due to the deterioration of the OD accuracy at TCM once before the TCM. Taking this effect into account, it can be inferred that the orbit determination closer to each TCM time has a larger impact than those that do not.

According to the above discussion, it seems that all the orbit determination should be placed just before the trajectory correction, but the simulation results do not necessarily show this. This may be because the time of orbit determination which is less sensitive to the objective function than the accuracy of the objective function cannot be optimized in the numerical optimization algorithm. In particular, the orbit determination up to the fourth time, whose effect was almost non-existent less than 10^{-6}, was performed at a timing that was not immediately before the trajectory correction in Fig. 5.28.

In conventional deep space missions, orbit determination is performed with high accuracy by taking a long arc and using the information on dynamics. In the simulation results of this study, the accuracy of the orbit determination is improved by concentrating the orbit determination, which seems to be counter-intuitive. The reason for this seems to be that the observability of the observation equations in this study is extremely high, and the nature of the system is different from that of an estimation system where the orbit determination is based on partial observations and dynamics

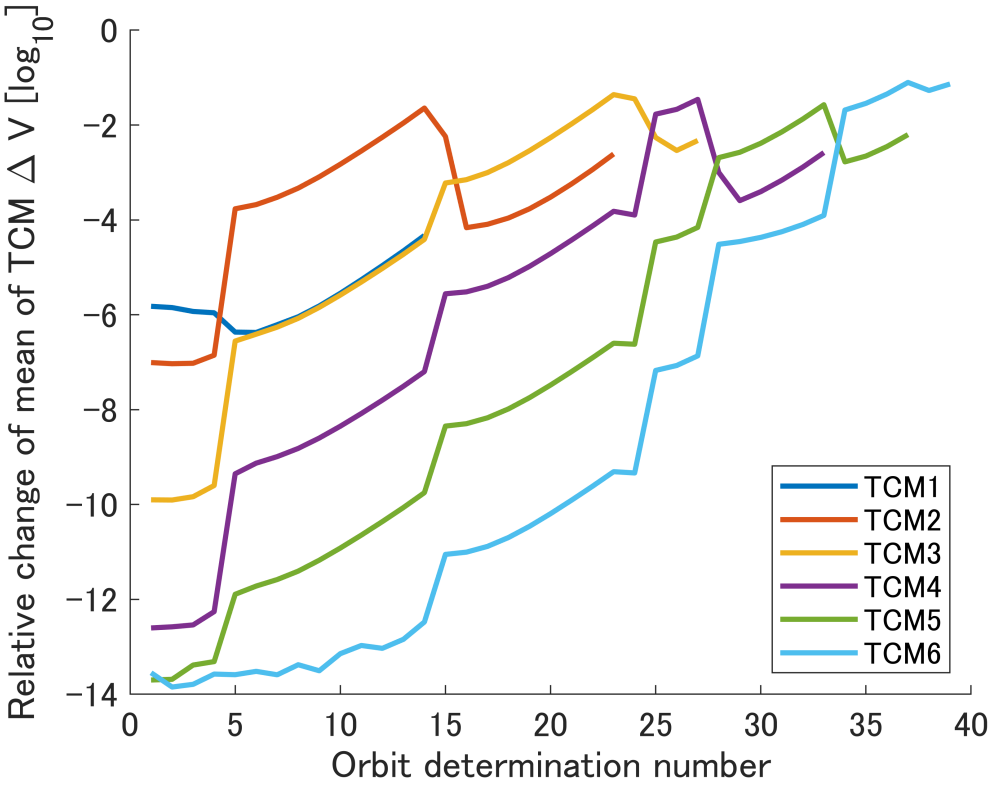

Figure 5.35: Effect on the objective function of each orbit determination. Orbit determination after each trajectory correction is not shown because their effect is zero.

information. In addition, the dynamics error is set to be large in this study, and the larger the observation interval, the more the dynamics error accumulates. Therefore, it is thought that the orbit determination is concentrated in order to suppress the dynamics error. Based on the discussion in Chapter 2 and the simulation results of this chapter, it is important to reduce the orbit determination error at the TCM time, and that the result with long orbit determination intervals will be obtained from the optimization if the problem is such that the orbit determination accuracy can be improved by increasing the time interval of the orbit determination.

From the above discussion, it can be basically concluded that the trajectory correction time is determined to minimize ΔV, and that the orbit determination is planned to sufficiently increase the orbit determination accuracy at the TCM time. At the optimization of the TCM time only, the possible TCM time is limited due to the fixed orbit determination time, and thus optimization of both trajectory correction and orbit determination time can generate superior results. In addition, the proposed method

does not seem to be able to optimize the orbit determination time which has low sensitivity to the objective function, and this point is left as a future problem. Although the number of TCMs or ODs is not changed in this study, a method to reduce the operational cost by removing the orbit determination time with low sensitivity would be a future work.

Chapter 6

Conclusion

That's all.

Momo Asakura

In deep space exploration by micro/nano-spacecraft, the fuel required for trajectory correction and the cost required for orbit determination are important problems. In this study, in order to solve these problems, a method is proposed to optimize the scheduling of the trajectory correction maneuver (TCM) and the orbit determination to minimize the ΔV required for TCM.

The TCM is formulated, and it is shown that the factors affecting the magnitude of the TCM include various uncertainties and the sensitivity of the control depending on the dynamics. The factors include the orbit determination error, and it is shown that the ΔV required for the TCM can be reduced by optimization of the orbit determination.

The optimization problem is formulated by using stochastic trajectory optimization formulation. The propagation of the probability distribution of the true and estimated states is formulated as the propagation of the parameters of the probability distribution. The true and estimated states are combined as the augmented state because of the coupling effect of the true and estimated states. It is proved that the objective function and constraints of the optimization problem can be calculated from the parameters, and that they can be calculated once the trajectory correction time and orbit determination time are determined. The optimization problem is formulated to

be solved numerically by using numerical optimization algorithms.

The validity of the proposed method has been confirmed by numerical simulations. The Hohmann transfer trajectory in the two-body problem was taken as an example and optimized by various optimization methods. The results show that optimizing both the TCM time and the orbit determination time gives better results than optimizing only the TCM time. Also, assuming that the orbit determination is conducted just before the TCM, an optimization method is proposed in which the TCM time and the number of orbit determination are varied, and it gives the best results. Sensitivity analysis was performed by changing the magnitude of various uncertainties, and it was confirmed that the magnitude of uncertainty has a significant impact on the objective function, optimal TCM time, and orbit determination strategy.

Taking the nominal trajectory of PROCYON as an example, a more practical problem was optimized. It is also shown that the ΔV required for TCM is smaller when both times are optimized than when only the TCM time is optimized. In addition, in order to improve the accuracy of orbit determination at the TCM time, the orbit determination time tends to be gathered just before the TCM, but this is not always the case for the orbit determination time with low sensitivity to the objective function because of the limitation of the numerical algorithm.

Through the analysis and numerical simulation in this study, it is shown that not only control but also navigation plays a significant role in stochastic trajectory design that considers uncertainty, especially orbit determination error, and that optimization of not only control but also navigation is important. In this study, the analysis is focused on the optimization of TCM, but the future work is to apply it to a broader range of trajectory planning, including the optimization of nominal trajectories.

Appendix A

Derivation of Uncertainty Propagation in Linear Approximation Method

When the state, observation, and control are linearized around a reference trajectory, the propagation equations of states are as follows.

For the true state, Eqs.(4.13), (4.15), and (4.16) are linearized as

$$\boldsymbol{x}_k = \Phi_{k,l(k)}\boldsymbol{x}_{l(k)} + B\left(\boldsymbol{u}_k + \delta\boldsymbol{U}_k\right) + \Gamma\delta\boldsymbol{w}_{k,l(k)} \tag{A.1}$$

$$\boldsymbol{u}_k = \left.\frac{\partial \boldsymbol{M}_k}{\partial \boldsymbol{X}_k}\right|_{\boldsymbol{F}_{k,l(k)}\left(\boldsymbol{X}^*_{l(k)}\right)} \Phi_{k,l(k)}\widehat{\boldsymbol{x}}_{l(k)} \tag{A.2}$$

$$\boldsymbol{x}_l = \Phi_{l,l-1}\boldsymbol{x}_{l-1} + \Gamma\delta\boldsymbol{w}_{l,l-1}, \tag{A.3}$$

and for the estimated state, Eqs.(4.22), (4.25), (4.26), and (4.27) are linearized as

$$\widehat{\boldsymbol{x}}_k = \Phi_{k,l(k)}\widehat{\boldsymbol{x}}_{l(k)} + B\boldsymbol{u}_k \tag{A.4}$$

$$\widehat{\boldsymbol{x}}_l = \Phi_{l,l-1}\widehat{\boldsymbol{x}}_{l-1} + K_l\left(\boldsymbol{y}_l - \widehat{\boldsymbol{y}}_l\right) \tag{A.5}$$

$$\boldsymbol{y}_l = H_l\boldsymbol{x}_l + \boldsymbol{\varepsilon}_l \tag{A.6}$$

$$\widehat{\boldsymbol{y}}_l = H_l\widehat{\boldsymbol{x}}_l. \tag{A.7}$$

Thus, the mean and covariance matrices of the augmented state are propagated as follows.

At the control time,

$$\boldsymbol{\mu}_{\mathbf{Z}_k} = \begin{bmatrix} I & C_k \\ O & I + C_k \end{bmatrix} \begin{bmatrix} \Phi_{k,l(k)} & O \\ O & \Phi_{k,l(k)} \end{bmatrix} \boldsymbol{\mu}_{\mathbf{Z}_{l(k)}} \tag{A.8}$$

$$\begin{aligned} \Sigma_{\mathbf{Z}_k} = & \begin{bmatrix} I & C_k \\ O & I + C_k \end{bmatrix} \begin{bmatrix} \Phi_{k,l(k)} & O \\ O & \Phi_{k,l(k)} \end{bmatrix} \Sigma_{\mathbf{Z}_{l(k)}} \begin{bmatrix} \Phi_{k,l(k)} & O \\ O & \Phi_{k,l(k)} \end{bmatrix}^{\mathsf{T}} \begin{bmatrix} I & C_k \\ O & I + C_k \end{bmatrix}^{\mathsf{T}} \\ & + \begin{bmatrix} B \\ O \end{bmatrix} S_k \begin{bmatrix} B \\ O \end{bmatrix}^{\mathsf{T}} + \begin{bmatrix} \Gamma \\ O \end{bmatrix} Q_{k,l(k)} \begin{bmatrix} \Gamma \\ O \end{bmatrix}^{\mathsf{T}} \end{aligned} \tag{A.9}$$

$$C_k = B \frac{\partial \boldsymbol{M}_k}{\partial \boldsymbol{X}_k}\bigg|_{\boldsymbol{F}_{k,l(k)}\left(\boldsymbol{X}^*_{l(k)}\right)}, \tag{A.10}$$

and at the orbit determination time,

$$\boldsymbol{\mu}_{\mathbf{Z}_l} = \begin{bmatrix} I & O \\ K_l H_l & I - K_l H_l \end{bmatrix} \begin{bmatrix} \Phi_{l,l-1} & O \\ O & \Phi_{l,l-1} \end{bmatrix} \boldsymbol{\mu}_{\mathbf{Z}_{l-1}} \tag{A.11}$$

$$\begin{aligned} \Sigma_{\mathbf{Z}_l} = & \begin{bmatrix} I & O \\ K_l H_l & I - K_l H_l \end{bmatrix} \begin{bmatrix} \Phi_{l,l-1} & O \\ O & \Phi_{l,l-1} \end{bmatrix} \Sigma_{\mathbf{Z}_{l-1}} \begin{bmatrix} \Phi_{l,l-1} & O \\ O & \Phi_{l,l-1} \end{bmatrix}^{\mathsf{T}} \begin{bmatrix} I & O \\ K_l H_l & I - K_l H_l \end{bmatrix}^{\mathsf{T}} \\ & + \begin{bmatrix} \Gamma \\ O \end{bmatrix} Q_{k,l(k)} \begin{bmatrix} \Gamma \\ O \end{bmatrix}^{\mathsf{T}} + \begin{bmatrix} O \\ K_l \end{bmatrix} R_l \begin{bmatrix} O \\ K_l \end{bmatrix}^{\mathsf{T}}. \end{aligned} \tag{A.12}$$

References

[1] Funase, R., Inamori, T., Ikari, S., Ozaki, N., Nakajima, S., Koizumi, H., Tomiki, A., Kobayashi, Y., and Kawakatsu, Y.,, ”One-year Deep Space Flight Result of the World’s First Full-scale 50kg-class Deep Space Probe PROCYON and Its Future Perspective,” 30th Annual AIAA/USU Conference on Small Satellite, Logan, UT, SSSC16-III-05, 2016.

[2] Klesh, A, Clement, B., Colley, C., Essmiller, J., Forgette D., Krajewski, J., Marinan A., Martin-Mur, T., Steinkraus, J., Sternberg, D., Werne, T., and Young, B., ”MarCO: Early Operations of the First CubeSats to Mars,” Small Satellite Conference, 32nd Annual AIAA/USU Conference on Small Satellites, Logan, UT, SSC18-WKIX-04, 2018.

[3] Funase, R., Ikari, S., Miyoshi, K., Kawabata, Y., Nakajima, S., Nomura, S., Funabiki, N., Ishikawa, A., Kakihara, K., Matsushita, S., Takahashi, R., Yanagida, K., Mori, D., Murata, Y., Shibukawa, T., Suzumoto, R., Fujiwara, M., Tomita, K., Aohama, H., Iiyama, K., Ishiwata, S., Kondo, H., Mikuriya, W., Seki, H., Koizumi, H., Asakawa, J., Nishii, K., Hattori, A., Saito, Y., Kikuchi, K., Kobayashi, Y., Tomiki, A., Torii, W., Ito, T., Campagnola, S., Ozaki, N., Baresi, N., Yoshikawa, I., Yoshioka, K., Kuwabara, M., Hikida, R., Arao, S., Abe, S., Yanagisawa, M., Fuse, R., Masuda, Y., Yano, H., Hirai, T., Arai, K., Jitsukawa, R., Ishioka, E., Nakano, H., Ikenaga, T., and Hashimoto, T., ”Mission to Earth–Moon Lagrange Point by a 6U CubeSat: EQUULEUS,” *IEEE Aerospace and Electronic Systems Magazine*., Vol. 35, No. 3, 2020, pp. 30–44.

[4] Oguri, K., Oshima, K, Campagnola, S., Kakihara, K., Ozaki, N., Barasi, N., Kawakatsu, Y., and Funase, R., ”EQUULEUS Trajectory Design,” *The Journal of the Astronautical Sciences*., Vol. 67, 2020, pp. 950–976.

[5] Campagnola, S., Hernando-Ayuso, J., Kakihara, K., Kawabata, Y., Chikazawa, T., Funase, R., Ozaki, N., Baresi, N., Hashimoto, T., Kawakatsu, Y., Ikenaga, T., Oguri, K., Oshima, K., “Mission analysis for the EM-1 CubeSats EQUULEUS and OMOTENASHI,” 69th International Astronautical Congress, Bremen, Germany, October, 2018.

[6] Oguri, K., Kakihara, K., Campagnola, S., Ozaki, N., Oshima, K., Yamaguchi, T., and Funase, R., “EQUULEUS Mission Analysis: Design of the Science Orbit Phase,” 31st International Symposium on Space Technology and Science, ISTS-2017-d-072, Matsuyama, Japan, June, 2017.

[7] Oshima, K., Campagnola, S., Yam, C. H., Kayama, Y., Kawakatsu, Y., Ozaki, N., Verspieren, Q., Kakihara, K., Oguri, K., and Funase, R. “EQUULEUS Mission Analysis: Design of Transfer Phase,” 31st International Symposium on Space Technology and Science, ISTS-2017-d-159, Matsuyama, Japan, June, 2017.

[8] Campagnola, S., Ozaki, N., Hernando-Ayuso, J., Oshima, K., Yamaguchi, T., Oguri, K., Ozawa, Y., Ikenaga, T., Kakihara, K., Takahashi, S., Funase, R., Kawakatsu, Y., Hashimoto, T., “Mission Analysis for EQUULEUS and OMOTENASHI,” 31st International Symposium on Space Technology and Science, ISTS-2017-f-044, Matsuyama, Japan, June, 2017.

[9] Campagnola, S., Ozaki, N., Oguri, K., Verspieren, Q., Kakihara, K., Yanagida, K., Funase, R., Yam, C. H., Ferella, L., Yamaguchi, T., Kawakatsu, Y., Kayama, Y., Suda, S., Yarnoz, D. G., “Mission Analysis for EQUULEUS, JAXA’s Earth-Moon Libration Orbit Cubesat”, 67th International Astronautical Congress, IAC-16-B4.8.1, Guadalajara, Mexico, September, 2016.

[10] Breakwell, J., ”Fuel Requirements for Crude Interplanetary Guidance,” *Advances in Astronautical Science*., Vol. 5, 1960, pp. 53–65.

[11] Breakwell, J., ”The Optimum Spacing of Corrective Thrusts in Interplanetary Navigation,” *Mathematics in Science and Engineering*., Vol. 5, 1962, pp. 333–375.

[12] Kawaguchi, J. and Matsuo, H., ”Low-Thrust Flyby Guidance and an Extended Optimal Spacing Rule,” *Journal of Guidance, Control, and Dynamics*., Vol. 19, No.2, 1996, pp. 347–354.

[13] Serban, R. Koon, W., Lo, M., Marsden, J., Petzold, L., Ross, S., and Wilson, R., ”Halo orbit mission correction maneuvers using optimal control,” *Automatica*., Vol. 38, No. 4, 2002, pp. 571–583.

[14] Gomez, G., Marcote, M., and Masdemont, J., ”Trajectory correction manoeuvres in the transfer to libration point orbits,” *Acta Astronautica*., Vol. 56, No.7, 2005, pp. 652–669.

[15] Kakihara, K, Ozaki, N., Ishikawa, A., Chikazawa, T., and Funase, R., ”Tube Stochastic Optimal Control with Imperfect Information:Application to Navigation and Guidance Analyses,” AIAA Scitech 2020 Forum, AIAA 2020-0961, Orlando, FL, January, 2020.

[16] Gentile, L., Graco, C., Minisci, E., Bartz-Beielestein, T., and Vasile, M., ”An optimization approach for designing optimal tracking campaigns for low-resources deep-space missions,” 70th International Astronautical Congress, Washington, USA, IAC–19–B4,IP,20,x52943, 2019.

[17] Ozaki, N., ”Tube Stochastic Differential Dynamic Programming and Application to Robust-Optimal Spacecraft Trajectory Design,” Ph.D. Thesis.

[18] Ozaki, N., Campagnola, S., and Funase, R., ”Tube Stochastic Optimal Control for Nonlinear Constrained Trajectory Optimization Problems,” *Journal of Guidance, Control, and Dynamics*., Vol.43, No.4, 2020, pp. 645–655.

[19] Oguri, K. and McMahon, J., "Robust Spacecraft Guidance Around Small Bodies Under Uncertainty: Stochastic Optimal Control Approach," *Journal of Guidance, Control, and Dynamics*., Vol. 44, No. 7, 2021, pp. 1295–1313.

[20] Oguri, K. and McMahon, J., "Risk-aware Mission Design for In situ Asteroid Exploration under Uncertainty," 2021 IEEE Aerospace Conference, Big Sky, MT, March, 2021.

[21] Ridderhof, J., Pilipovsky, J., and Tsiotras, P., "Chance-constrained Covariance Control for Low-Thrust Minimum-Fuel Trajectory Optimization," 2020 AAS/AIAA Astrodynamics Specialist Conference, AAS 20-618, Online, 2020.

[22] Zavoli, A. and Federici, L., "Reinforcement Learning for Robust Trajectory Design of Interplanetary Missions," *Journal of Guidance, Control, and Dynamics*., Vol. 44, No. 8, 2021, pp. 1440–1453.

[23] Greco, C., Campagnola, S., and Vasile, M., "Robust Space Trajectory Design using Belief Stochastic Optimal Control," AIAA Scitech 2020 Forum, AIAA 2020-1471, Orlando, FL, January, 2020.

[24] A. Mesbah, " Stochastic Model Predictive Control, "An Overview and Perspectives for Future Research, " *IEEE Control Systems*, Vol. 36, No. 6, 2016, pp. 30–44.

[25] Geller, D., K., "Linear Covariance Techniques for Orbital Rendezvous Analysis and Autonomous Onboard Mission Planning," *Journal of Guidance, Control, and Dynamics*., Vol. 29, No. 6, 2006, pp. 1404–1414.

[26] Geller, D., K., Rose, M., B., and Woffinden, D., C., "Event Triggers in Linear Covariance Analysis with Applications to Orbital Rendezvous," *Journal of Guidance, Control, and Dynamics*., Vol. 32, No. 1, 2009, pp. 102–111.

[27] Jin, K., Geller, D., K., and Luo, J., "Development and Validation of Linear Covariance Analysis Tool for Atmospheric Entry," *Journal of Spacecraft and Rockets*., Vol. 56, No. 3, 2019, pp. 854–864.

[28] Jin, K., Geller, D., K., and Luo, J., "Robust Trajectory Design for Rendezvous and Proximity Operations with Uncertainties," *Journal of Guidance, Control, and Dynamics*., Vol. 43, No. 4, 2020, pp. 741–753.

[29] Fleming, W., and Rishel, R., "Deterministic and Stochastic Optimal Control," Springer, New York, 1975.

[30] Tapley, B. D., Schutz, B. E., and Born, G. H., "Statistical Orbit Determination," Elsevier, Amsterdam, The Netherlands, 2004.

[31] Julier, S. and Uhlmann, J., "A General Method for Approximating Nonlinear Transformations of Probability Distributions," University of Oxford, Tech. Rep., 1996.

[32] Julier, S., Uhlmann, J., and Durrant-Whyte, H., "A New Method for the Nonlinear Transformation of Means and Covariances in Filters and Estimators," *IEEE Transactions on Automatic Control*, Vol. 45, No. 3, 2000, 477–482.

[33] Julier, S., "The Scaled Unscented Transformation," 2002 American Control Conference, Anchorage, AK, May, 2002.

[34] Arasaratnam, I. and Haykin, S., "Cubature Kalman Filters," *IEEE Transactions on Automatic Control*., Vol. 54, No. 6, 2009, pp. 1254–1269.

[35] Jones, B. A., Doosta, A., and Born, G. H., "Nonlinear Propagation of Orbit Uncertainty Using Non-Intrusive Polynomial Chaos," *Journal of Guidance, Control, and Dynamics*., Vol. 36, No. 2, 2013, pp. 430–444.

[36] Jones, B. A., Parrish, N., and Doostan, A., "Postmaneuver Collision Probability Estimation Using Sparse Polynomial Chaos Expansions," *Journal of Guidance, Control, and Dynamics*, Vol. 38, No. 8, 2015, pp. 1425–1437.

[37] Vittaldev, V., Russell, R. P., and Linares, R., "Spacecraft Uncertainty Propagation Using Gaussian Mixture Models and Polynomial Chaos Expansions,"

Journal of Guidance, Control, and Dynamics, Vol. 39, No. 12, 2016, pp. 2615–2626.

[38] Park, R. S., and Scheeres, D. J., "Nonlinear Mapping of Gaussian Statistics: Theory and Applications to Spacecraft Trajectory Design," *Journal of Guidance, Control, and Dynamics*, Vol. 29, No. 6, 2006, pp. 1367–1375.

[39] Fujimoto, K., Scheeres, D. J., and Alfriend,K. T., "Analytical Non-Linear Propagation of Uncertainty in the Two-Body Problem," *Journal of Guidance, Control and Dynamics*, Vol. 140, No. 2, 2011, pp. 1439–1457.

[40] Gates, C. R., "A Simplified Model of Midcourse Maneuver Execution Errors," JPL Technical Report, 32-504, Pasadena, CA, 1963.

[41] Goodson, T. D., "Execution-Error Modeling and Analysis of the Grail Spacecraft Pair," AAS/AIAA Spaceflight Mechanics Meeting, AAS Paper 13-268, San Diego, CA, 2013.

[42] K. Okamoto, M. Goldshtein, and P. Tsiotras, "Optimal Covariance Control for Stochastic Systems Under Chance Constraints," *IEEE Control Systems Letters*, Vol. 2, No. 2, 2018, pp. 266–271.

[43] van Hessem, D., and Bosgra, O., "A Conic Reformulation of Model Predictive Control Including Bounded and Stochastic Disturbances Under State and Input Constraints," 41st IEEE Conference on Decision and Control, Las Vegas, NV, Dec., 2002.

[44] Ono, M., Williams, B. C., and Blackmore, L., "Probabilistic Planning for Continuous Dynamic Systems Under Bounded Risk," *Journal of Artificial Intelligence Research*, Vol. 46, 2013, pp. 511–577.

[45] A. Prekopa, "Boole-Bonferroni Inequalities and Linear Programming," *Operations Research*, Vol. 36, No. 1, 1988, pp. 145–162.

[46] L. Blackmore, H. X. Li, and B. C. Williams, “A Probabilistic Approach to Optimal Robust Path Planning with Obstacles,” American Control Conference, Minneapolis, MN, June, 2006.

[47] Nemirovski, A., and Shapiro, A., “Convex Approximations of Chance Constrained Programs,” *SIAM Journal on Optimization*, Vol. 17, No. 4, 2006, pp. 969–996.

[48] Blackmore, L., and Ono, M., “Convex Chance Constrained Predictive Control Without Sampling,” AIAA Guidance, Navigation, and Control Conference, AIAA Paper 2009-5876, 2009.

[49] Audet, C. and Dennis, J. E., ”Analysis of generalized pattern searches,” *SIAM Journal on optimization*., Vol. 13, No. 3, 2002, pp. 889–903.

[50] Campagnola, S., et al., ”Low-Thrust trajectory design and operations of PROCYON,” the first deep-space micro-spacecraft, 25th International Symposium on Space Flight Dynamics, Munich, Germany, 2015.

[51] Kakihara, K., “Navigation Analysis of Autonomous Orbit Determination with Satellite-to-Satellite Tracking Using Resonant Flybys in Three-Body System,” 32nd International Symposium on Space Technology and Science, 2019-d-118s, Fukui, Japan, June, 2019.

[52] C. Van Loan, “Computing Integrals Involving the Matrix Exponential,” *IEEE Transactions on Automatic Control*, Vol. 23, No. 3, 1978, pp. 395–404.